

National Defense Academy
Doctoral Dissertation

**A Study on Antennas for Small Terminals
with Wideband Characteristic**

(広帯域特性を有する小型端末用アンテナに関する研究)

A Thesis in
Electronics Engineering
Electronics and Information Engineering
Graduate School of Science and Engineering

by
Tsutomu Ito

March, 2015

Abstract

Mobile communication continues to grow due to the increase of the number of small terminals for the internet access such as smartphones and tablet devices. In addition, the mobile data traffic as well as transmission rate is drastically increasing in recent years because of the high demand for large-capacity contents. On the other hand, wideband operation and miniaturization of the terminal antenna are highly required since a lot of wireless applications are installed, while the space for the antennas inside the small terminal is quite limited. Also, multi-antenna system is getting in common so as to deal with today's high speed communication. Furthermore, human body in the vicinity of the terminal antenna is also important factor to be considered since antenna performances are deteriorated, especially antenna radiation.

This dissertation focuses on folded dipole antenna with feed line (FDAFL), which has more than twice the bandwidth compared with folded dipole antenna (FDA) when the characteristic impedance of FDA is transformed to $300\ \Omega$. However, the study on application of FDAFL to a small terminal has not yet been conducted in detail. Thus, the objective of dissertation is to apply FDAFL to a small terminal and present indications for enhancing antenna performances with consideration of antenna requirements for a small terminal.

Chapter 1 introduces the background, motivation, and objective of this dissertation.

In Chapter 2, an overview of FDAFL as well as fundamental characteristics and operation principle of FDA are presented. FDA is the most fundamental antenna with folded structure. Due to the structure, the current flow on the antenna element is varied, which generates distinctive antenna properties. On the other hand, FDAFL shows wider bandwidth than FDA, led by two resonant operation, while current distribution and radiation characteristic are equivalent to FDA.

Chapter 3 presents the way to miniaturize the feed line of FDAFL without utilizing meandered structure, then FDAFL is applied to a small terminal. Impedance matching of FDAFL can be obtained by altering the width of antenna element and feed lines, which results in low-profile antenna configuration and broadband property of FDAFL. In addition, FDAFL is applied to various sizes of the ground plane, but wideband characteristics are maintained despite of the different ground sizes. When the

antenna parameters are properly adjusted on the ground plane of $50 \times 80 \text{ mm}^2$, antenna height is reduced to 12 mm, which is 43% compared with the initial length. Relative bandwidth ($\text{VSWR} \leq 3$) is about 65%. Thus, FDAFL can be applied to a small terminal with wideband characteristic.

In Chapter 4, two different 3D FDAFL are proposed for miniaturizing the antenna system. Model-A is bent over the ground plane, and Model-B is bent outside of the ground plane. In both cases, since impedance transformation is possible by changing the width of antenna element and feed lines, the relative bandwidth over 74% is obtained when antenna height h is greater than 7 mm in Model-A. As for Model-B, very broadband characteristics over 86% are achieved even $h=1$ mm. It is also confirmed that the prominence w can be decreased from 12 mm to 6 mm with the bandwidth over 83% when $h=4$ mm. Thus, these 3D models can show wider bandwidth than planar FDAFL proposed in Chapter 3.

In Chapter 5, multiband folded monopole antenna (FMA) array derived from FDAFL is proposed, and its wideband characteristics and a suitable configuration for MIMO (Multiple-Input Multiple-Output) antenna are presented. FMA has wider bandwidth (58.0%) compared with planar inverted-F antenna (PIFA) (34.8%) which has the same physical volume. In order to obtain a frequency resonance, a parasitic element (PE) is introduced for multiband antenna. Proposed antenna can almost cover WiMAX 2.5/3.5/5.5 GHz bands and WLAN 2.4/5 GHz bands. The antenna efficiency of between 70% to 96% and very low correlation coefficient of less than 0.02 are observed.

Chapter 6 presents the application of a quarter-wavelength additional element (AE) to multiband FMA array and wire inverted-F antenna (WIFA) in order to reduce the current on the ground plane. Then, the effect of AE on a human hand is analyzed in hand-held condition. $\lambda/4$ and higher structure of AE from the ground are more effective for current suppression. In addition, the hand model is taken into consideration, then antenna efficiency and radiation characteristics are improved by the installation of AE. Thus, AE is very easy and effective to reduce the current on the ground plane and enhance antenna performances with user's hand. Also, it is found that AE can work with other different antennas.

Finally, this dissertation is concluded in Chapter 7 including the summary of each chapter.

Contents

Chapter 1 Introduction

1.1	Background	1
1.2	Requirements for Antenna Design in Small Terminals	3
1.2.1	Wideband Characteristic	3
1.2.2	Miniaturization	4
1.2.3	MIMO Antenna	5
1.2.4	Current Reduction on the Terminal	5
1.3	Terminal Antennas with Wideband Characteristic	6
1.4	Objective and Organization of the Dissertation	8

Chapter 2 Fundamental Characteristics of FDA and FDAFL

2.1	Introduction	10
2.2	Main Features and Operation Principle of FDA	11
2.2.1	High Input Impedance and Step-up Ratio	11
2.2.2	Wideband Characteristic	15
2.3	Basic Property of FDAFL and Comparison with FDA	16
2.3.1	Two Resonant Operation	16
2.3.2	Equivalent Circuit of Feed Line	18
2.3.3	Wideband Characteristic	19
2.3.4	Current Distribution	20
2.3.5	Radiation Characteristic	21
2.4	Summary	22

Chapter 3 Miniaturization of FDAFL and Application to Small Terminal

3.1	Introduction	24
3.2	Parametric Analysis Contributing to Low-profile Antenna	25
3.2.1	Antenna Configuration	25
3.2.2	Impedance Characteristic by the Change of Antenna Parameters	26

3.3	Miniaturization of Feed Line and Wider Bandwidth	28
3.3.1	Technique for Obtaining Impedance Matching	29
3.3.2	Bandwidth Change by the Antenna Parameters	31
3.3.3	Current Distribution and Radiation Characteristic	33
3.3.4	Consideration Points for Miniaturization	35
3.4	Antenna Characteristics with Ground Plane	36
3.4.1	Antenna Configuration	36
3.4.2	Characteristic Change with respect to Size of Ground Plane	37
3.4.3	Miniaturization of Antenna Height with Ground Plane	39
3.5	Summary	42

Chapter 4 Wideband Characteristic of 3D-FDAFL

4.1	Introduction	43
4.2	Antenna Configuration	44
4.3	Change of VSWR Characteristic according to the Models	46
4.4	Analysis of Model-A	46
4.4.1	Relative Bandwidth	46
4.4.2	VSWR Characteristic	48
4.5	Analysis of Model-B	49
4.5.1	Relative Bandwidth	49
4.5.2	VSWR Characteristic	50
4.6	Measured Results and Comparisons	52
4.6.1	VSWR Characteristic	53
4.6.2	Radiation Characteristic and Current Distribution	54
4.7	Summary	59

Chapter 5 MIMO Antenna Derived from FDAFL with Parasitic Element

5.1	Introduction	60
5.2	Wideband Characteristic of FMA	61
5.2.1	Antenna Configuration	61
5.2.2	VSWR Characteristic and Current Distribution	63
5.2.3	Bandwidth Comparison with PIFA	64

5.3	Suitable FMA Array for MIMO	65
5.3.1	S-parameter Characteristic and Electric Near-field Distribution	65
5.3.2	Antenna Efficiency	69
5.4	Multiband FMA Employing Parasitic Element	70
5.4.1	Antenna Configuration	70
5.4.2	Parametric Analysis and Distribution of Cover Ratio	71
5.4.3	Radiation Characteristic and Current Distribution	74
5.4.4	Characteristic Change with respect to Size of Ground Plane	75
5.5	Fundamental Characteristics of FMA Array with Parasitic Elements	76
5.5.1	S-parameter Characteristic	76
5.5.2	Envelope Correlation Coefficient and Antenna Efficiency	77
5.5.3	Radiation Characteristic	78
5.6	Summary	80
 Chapter 6 Current Reduction on the Ground Plane using Quarter-wavelength Additional Element		
6.1	Introduction	81
6.2	Parametric Analysis Contributing to Current Reduction	83
6.2.1	Antenna Configuration	83
6.2.2	Length and Height of AE	83
6.2.3	Location of AE	86
6.2.4	Current Distribution and Radiation Characteristic	89
6.3	Effect of a Human Hand on Antenna Characteristics	91
6.3.1	Antenna Configuration	91
6.3.2	Antenna Efficiency and Current Distribution	91
6.3.3	Radiation Characteristic	93
6.4	Application of AE to a Different Antenna	96
6.4.1	Antenna Configuration	96
6.4.2	Location of AE	97
6.4.3	Fundamental Characteristics	99
6.5	Summary	101
 Chapter 7 Conclusion		 102

Acknowledgments	104
Bibliography	105
List of Publications and Awards	113
Journal Papers	113
International Conferences	113
Technical Reports and Other Conferences	115
Awards	118
Other Research Activities	118
Internship	118
Technical Presentation	118

Chapter 1

Introduction

1.1 Background

Many wireless access systems have been significantly developed in the past few decades, such as WPAN (Wireless Personal Area Network), WLAN (Wireless Local Area Network), WMAN (Wireless Metropolitan Area Network), and WWAN (Wireless Wide Area Network) [1]-[3]. These systems can be classified depending on the communication distance. Figure 1.1 shows the relation between service area size and wireless systems (based on [1]). It is obvious that the range of each area size varies from several centimeters to several tens of kilometers in order to increase the coverage area. Bluetooth, UWB (Ultra Wide Band), Wi-Fi (Wireless Fidelity), WiMAX (Worldwide Interoperability for Microwave Access), the second, third, and forth generation (2G, 3G, 4G) services are representative examples of the wireless networks. Also mobile

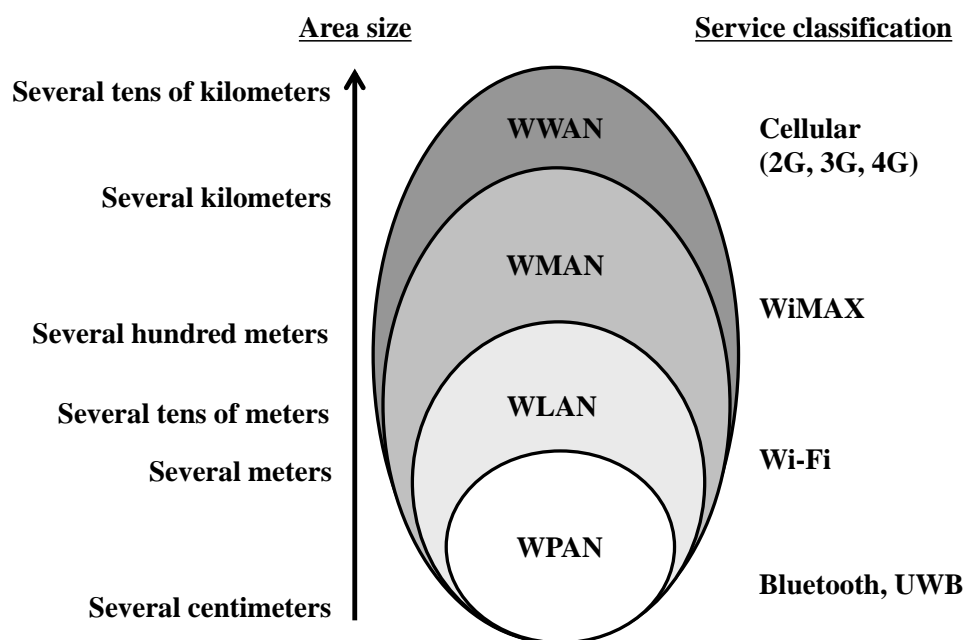


Figure 1.1: Relation of service area size and wireless systems.

communication continues to grow due to the increase of the number of small terminals for internet access such as cellular phones (especially smartphones) and tablet devices. For example, the total enrollment of cellular phones in Japan is reported as 147,535,025 by the end of September, 2014 [4]. In addition, the mobile data traffic is annually expanding about 60% in recent years [4] due to the high demand for large-capacity contents and the increase of M2M (Machine-to-Machine) networks [5]. Then, it is estimated that mobile data traffic of 2015 will become from 20.8 to 39.1 times as much as that of 2010. Thus, a variety of wireless systems and mobile terminals have affected our lifestyles significantly in the short term.

The second thing to be mentioned here is about the communication speed. Transmission rate has been drastically enhanced as well. Figure 1.2 shows the transmission speed of the wireless systems, especially focusing on the mobile communication services and WiMAX/WLAN services (based on [6]). As for LTE-Advanced (Long Term Evolution-Advanced) and WiMAX2 (WMAN-Advanced), which are respectively the enhancement of LTE and WiMAX, these are categorized into IMT-Advanced (International Telecommunications-Advanced) or 4G service by ITU-R (International Telecommunication Union-Radiocommunication Sector) in 2012 [7]-[8]. The peak data rate requirements for 4G are set to 100 Mbps for high and low mobility,

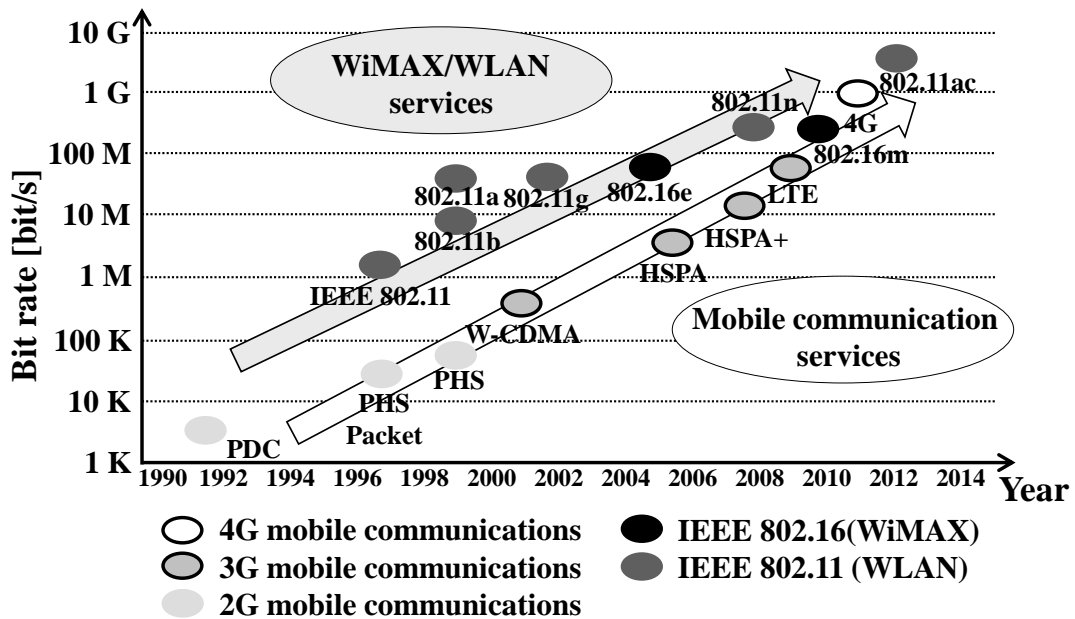


Figure 1.2: Enhancement of the transmission speed.

respectively [9]. On the other hand, the discussion on the fifth generation service (5G) has already been started [10]-[13]. Also, IEEE 802.11ax standardization activities are in progress as the next generation following IEEE 802.11ac [14]. These developments are realized by the enhancement of many factors, such as wireless access technology, network architecture, radio communication module (e.g. receiver, synthesizer, transceiver), baseband processor (e.g. modulator, coder, error corrector), CPU (e.g. communication protocol, signal processing), and antenna technology [15]-[16].

Antenna technology is one of the important factors affecting the QoS (Quality of Service) which includes the system throughput and SN (Signal-to-Noise) ratio [17]-[19]. For the mobile communication, needless to say, the development of both base station antennas and terminal antennas is required. However, the contents required for the antenna enhancement are not necessarily the same, since the usage environment of each antenna type is different [20]-[21]. Compared with base station antennas, the design of terminal antennas has some distinctive difficulties due to the small chassis and the presence of a human body near the antenna [22]-[23]. Thus, the terminal antenna will be focused on in this dissertation.

1.2 Requirements for Antenna Design in Small Terminals

This section describes the requirements for antennas in small terminals. First of all, wideband characteristic and miniaturization of every terminal antenna are always highly required. This is because a lot of wireless applications as mentioned above are utilized simultaneously in one terminal, while the space for each antenna inside the terminal is quite limited. On the other hand, multi-antenna system is becoming in common because of the demands for high speed communication and improvement of QoS. Furthermore, considering the effect of human body in the vicinity of terminal antennas is also very significant since antenna performances, especially radiation characteristic, are deteriorated in actual use. Thus, these requirements are discussed in detail below.

1.2.1 Wideband Characteristic

Due to the progress of wireless communication, a number of wireless systems, such as Wi-Fi, WiMAX, Bluetooth, and GPS (Global Positioning System), are highly in use on

a daily basis. Also, the recent small terminals including smartphones and tablets require these several systems in one terminal. In order to cover the frequency bands of these applications, wideband operation of antennas is highly required [24]-[25]. Furthermore, each wireless system requires a relatively wide frequency bandwidth. Particularly, the frequency bandwidth of UWB system is between 3.1 GHz and 10.6 GHz [26], which means the relative bandwidth is over 100%. In addition, the frequency band of the cellular systems in Japan operates across a broad range of frequencies from 700 MHz band to 2 GHz band. Not only that, due to the recent increase of the system traffic, the frequency band between 3.4 GHz and 3.6 GHz is under review for 4G service [27]. Thus, wideband antenna including multiband antenna is highly required in wireless communication.

1.2.2 Miniaturization

As well as the wideband characteristic of the terminal antenna, antenna miniaturization is necessary along with changes of the size of the small terminals. In cellular system, for example, although a representative cellular phone in 1984 had 600 cc in volume and 850 g in weight, its volume and weight were reduced to 60 cc and 60 g, respectively in 1999 [28]. Thus, size and weight reduction of the cellular phones have been promoted due to the usage itself. Recently, because the smartphones are very popular and these have big screens, their volume and weight of major products are not so small (110 cc, 130 g). However, since the multi-antenna system (explained in the following section) and a number of applications are highly required, further antenna miniaturization should be conducted.

Not only the cellular phones but also various small terminals have become reduced in size, such as USB keys, mobile routers, wireless mice, and even watches, which have wireless network connection. Furthermore, wearable terminals have been addressed as a recent interest. For instance, glasses [29], belts [30], and rings [31], which are used with a short distance between the device and human body (wearable antenna), they operate at UHF (Ultra High Frequency) band including 2.4 GHz band of WLAN. Thus, since the small terminal itself is becoming small and the space for antennas is very limited, the size of each antenna element should also be downsized.

1.2.3 MIMO Antenna

From a historical point of view, the terminal antenna of the cellular system is changed from single-antenna system to multi-antenna system, such as diversity antenna, adaptive array antenna, and MIMO (Multiple-Input Multiple-Output) antenna [21], in order to increase the communication speed and improve the communication reliability. As shown in Fig. 1.2, the transmission data rate is enhanced, and one of the most effective techniques for this enhancement is MIMO technology [32]-[33]. MIMO technology enables the system to create parallel data streams on a single channel, which increases the channel capacity and data throughput. For example, the maximum transmission rate of IEEE 802.11ac is theoretically about 6.9 Gbs, namely 11.5 times faster than IEEE 802.11n by utilizing double number of antennas and other technologies [34]. Also, LTE/LTE-Advanced and WiMAX/WiMAX2 introduce MIMO system [15], [35]-[36]. Thus, MIMO technology is necessary in today's wireless communication.

On the other hand, since multi-antenna system takes more space inside the small terminals, miniaturization of each antenna element is strongly required. Otherwise, the distance between the antenna elements becomes too close, which results in large pattern/spatial correlation and strong mutual coupling. When strong mutual coupling exists, a large part of the input power fed into one port will be coupled to the other ports rather than radiating to free space. Thus, the SN ratio and radiation efficiency degrade, which eventually leads to the deterioration of channel capacity and data throughput [37]-[39]. Since these degradations negate the beneficial effect of multi-antenna system, mutual coupling between the antenna elements should be carefully considered.

1.2.4 Current Reduction on the Terminal

Characteristics of an antenna are very susceptible to a nearby object. Especially, the performances of cellular phone's antennas are highly affected, generally deteriorated by human body such as a user's hand and head [40]-[43]. According to [42], degradation of radiation efficiency is larger by user's hand rather than by user's head. In addition, assuming that antennas are mounted on a Wi-Fi router and usually it is put on the wall, ceiling, or floor in actual use, then the antenna characteristics might be altered due to the adjacent effect [44]-[46]. Thus, antenna characteristics are always affected by surrounding environments.

It has been reported that the currents flow on both the antenna element and the terminal (or ground plane) when power is fed to a terminal antenna, and these currents contribute to the antenna characteristics such as radiation patterns and gain [47]. However, the current variation on the ground plane occurs in actual use, which is generated by adjacent effect, then the current variation on the ground plane will cause the degradation of antenna performances. Thus, the current reduction on the ground plane is highly required in order to mitigate the effect of nearby objects.

1.3 Terminal Antennas with Wideband Characteristic

In 1990s, the initial cellular phone had an external antenna, such as a helix, a monopole (whip), or a helix-plus-whip combination. A monopole antenna has the length of $\lambda/4$ and excellent performances, especially bandwidth and radiation efficiency. However, an external antenna generally has a high SAR (Specific Absorption Rate) and single polarization. Thus, approximately 3 dB drop in received power was observed, while internal antennas like a microstrip antenna have multiple polarizations. Consequently, external antennas replaced internal antennas. According to [48], which surveyed internal antennas in cellular phones from 1997 to 2010, there are mainly two types of internal antennas; PIFA (Planar Inverted-F Antenna) and PMA (Planar Monopole Antenna). PIFA is regarded as a microstrip antenna. Basically, both PIFA and PMA are the same monopole antenna which requires quarter-wavelength, but the difference is whether there is the ground plane directly under the antenna or not.

Figure 1.3 shows the relative bandwidth ($VSWR \leq 4$) versus ka of PIFA and PMA based on [48], where k is the wavenumber ($k=2\pi/\lambda$) and a is the radius of a sphere enclosing the maximum dimension of the antenna. As for the radius a in [48], since PMA generates significant currents on the ground plane that acts as the other radiator, the ground plane must be regarded as part of the antenna's dimension when calculating ka . Thus, a is half the maximum length of the entire ground plane. On the other hand, the current on the ground plane of PIFA is smaller than that of PMA. That's why the radius a is set to the maximum length of the PIFA in Fig. 1.3, which indicates that the achievable performance would shift to the left in the figure. For the comparison, FDA (Folded Dipole Antenna) and FMA (Folded Monopole Antenna) are also plotted in Fig.

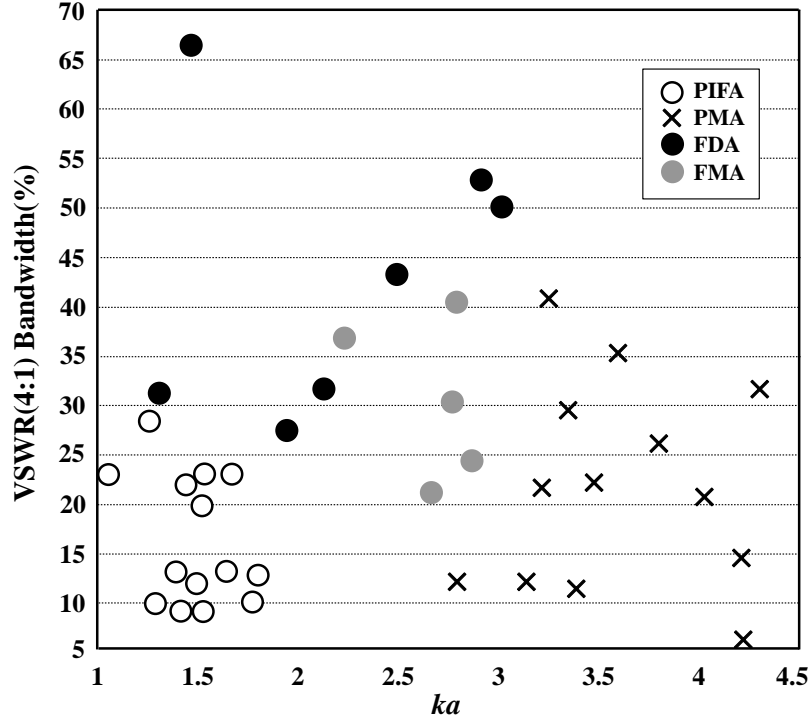


Figure 1.3: Relative bandwidth ($VSWR \leq 4$) versus ka .

1.3 [49]-[61]. As its name mentions, FDA and FMA have folded structure, which is discussed in Chapt. 2. In both cases, the radius a is considered as half the length of the whole ground plane assuming the strict condition. It can be seen in the figure that FDA and FMA have the wideband characteristic with relatively small value of ka . Actually, the value ka highly depends on the size of the ground plane, but Figure 1.3 indicates that wider bandwidth is possible even with similar size of the ground plane. Thus, the antennas that have the folded structure show wideband characteristic.

As a wideband antenna, FDAFL (Folded Dipole Antenna with Feed Line) has been reported in [62]. Two parallel quarter-wavelength feed lines are added to FDA, and each input impedance of FDA and FDAFL is about 50Ω and 300Ω , respectively. The most important property to be mentioned is that FDAFL exhibits more than twice the bandwidth compared with FDA when the characteristic impedance is transformed to 300Ω . This is because one more resonant frequency is generated by the feed lines, while FDA has only a single resonance. Thus, FDAFL is able to achieve further broadband operation. However, the study on application of FDAFL to a small terminal has not yet been conducted in detail.

1.4 Objective and Organization of the Dissertation

The objective of dissertation is to apply the FDAFL to a small terminal and present indications for enhancing antenna performances with consideration of requirements for a terminal antenna as mentioned in Sect. 1.2.

The organization of this dissertation is illustrated in Fig. 1.4. This dissertation consists of seven major chapters, and each chapter and antenna requirements for a small terminal are linked as described in the figure. Chapter 1, the present chapter, has introduced the background, motivation, and objective. Chapter 2 presents an overview of the fundamental characteristics of FDA and FDAFL.

Chapter 3 presents how to miniaturize the FDAFL in order to apply it to a small terminal. Original FDAFL requires the length of $\lambda/4$ for the feed lines, but impedance matching is deteriorated when the feed lines are shortened. In this chapter, important antenna parameters are indicated to obtain impedance matching, and fundamental characteristics of FDAFL which is mounted to a ground plane are analyzed.

Chapter 4 proposes two different 3D-FDAFLs which have a very wideband characteristic. The first antenna model is mounted over the ground plane, and the second model antenna is outside of the ground plane so that the antenna itself does not protrude from the ground plane as much as possible. Then, the mechanism of wideband operation is investigated. Also, the distributions of relative bandwidth with respect to antenna parameters are shown in detail.

In Chapter 5, MIMO antenna derived from FDAFL is proposed. Four different antenna configurations of FMA are analyzed in order to achieve MIMO antenna. So, fundamental properties, such as S-parameter characteristics, antenna efficiency, and envelope correlation coefficient are presented. Also, parasitic elements are installed for the multiband antenna operating in WiMAX/WLAN frequency bands. Thus, the parametric analysis of the parasitic element is conducted in detail.

Chapter 6 presents the application of a quarter-wavelength additional element to the vicinity of FMA array in order to suppress the current on the ground plane. Also, the effect of the current reduction is analyzed utilizing nearby object, such as user's hand for the case of a handset assuming the hand-held condition. Furthermore, the additional element is applied to a different type of antenna in order to confirm the effectiveness. In this dissertation, WIFA (Wire Inverted-F Antenna) is selected as a reference antenna,

and fundamental characteristics after applying the additional element are analyzed.

Finally, Chapter 7 concludes this dissertation.

In the analysis, the electromagnetic simulator FEKO [63] is used for calculations, and the adequateness of calculated results will be verified by measured results of several fabricated antenna prototypes.

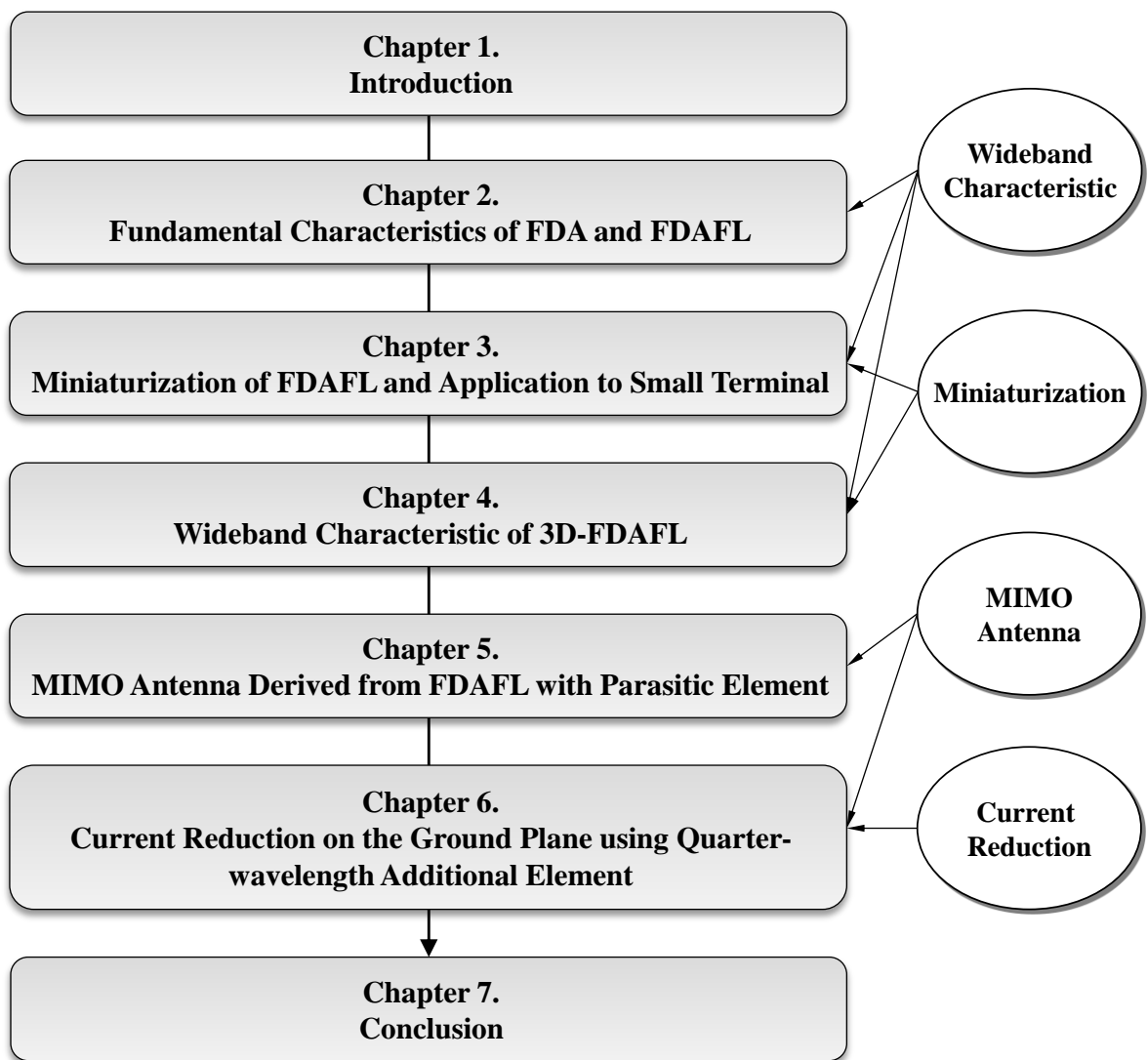


Figure 1.4: Organization of the dissertation.

Chapter 2

Fundamental Characteristics of FDA and FDAFL

2.1 Introduction

Folded dipole antenna (FDA) is the most fundamental antenna with folded structure, consisting of two parallel dipole antennas (DA) connected at the both ends. Therefore, current paths between FDA and DA are different from each other, which create several changes in the antenna properties. For instance, FDA itself can eliminate the unbalanced current on the feed line; that is, FDA has a self-balanced structure when the antenna length is $\lambda/2$ [64]. Also, impedance transformation can be readily achieved by altering the ratio of two dipole widths. Since these features cannot be seen in DA, many kinds of folded antennas for a small terminal were proposed by taking advantage of distinctive characteristics [65]-[67].

Recently, as an antenna with folded structure and broadband property, folded dipole antenna with feed line (FDAFL) has been proposed [62]. This antenna is composed of FDA and two parallel quarter-wavelength feed lines. One of the most significant features of FDAFL is that this antenna has more than twice the bandwidth compared with FDA when the characteristic impedance is transformed to $300\ \Omega$. Thus, this dissertation focuses on FDAFL, and an overview of FDA and FDAFL is shown in this chapter.

First, this chapter presents fundamental characteristics and operation principle of FDA in Sect. 2.2. Sect. 2.3 provides an overview of basic properties of FDAFL and comparison between FDA and FDAFL. Finally, Sect. 2.4 gives the conclusion.

2.2 Main Features and Operation Principle of FDA

2.2.1 High Input Impedance and Step-up Ratio

Figure 2.1 shows the two parallel wire conductors whose radii are respectively r_1 and r_2 with the central distance d which is much smaller than a wavelength. Assume that the out-of-phase currents flow on the wires presented in Fig. 2.1(a), then the complex potential of each location on the wires are expressed as

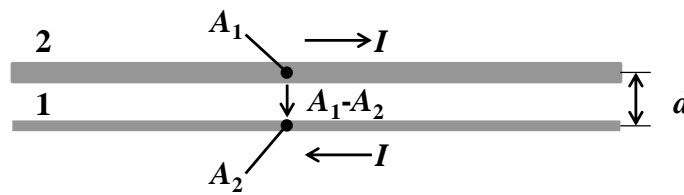
$$\text{Conductor 1: } A_1 = KI \ln \frac{d}{r_1} \quad (2.1)$$

$$\text{Conductor 2: } A_2 = -KI \ln \frac{d}{r_2} \quad (2.2)$$

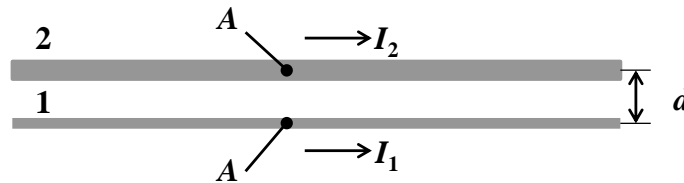
where K is a constant. v_p is the ratio of the complex potentials which is given by

$$v_p = \frac{A_1}{A_1 - A_2} = \frac{1}{2} \frac{\log \frac{d}{r_1}}{\log \frac{d}{\sqrt{r_1 r_2}}}. \quad (2.3)$$

Also, assume that the in-phase currents flow and the complex potentials on the wires are the same at an arbitrary point as can be seen in Fig. 2.1(b), which gives the following equation:



(a) Out-of-phase current



(b) In-phase current

Figure 2.1: Two parallel wire conductors and complex potential.

$$I_1 \log r_1 + I_2 \log d = I_2 \log r_2 + I_1 \log d, \quad (2.4)$$

and therefore

$$\frac{I_1}{I_2} = \frac{\log \frac{d}{r_2}}{\log \frac{d}{r_1}}. \quad (2.5)$$

ν_i is defined as the ratio of the currents on the conductors as below.

$$\nu_i = \frac{I_1}{I_1 + I_2} = \frac{1}{2} \frac{\log \frac{d}{r_2}}{\log \frac{d}{\sqrt{r_1 r_2}}} \quad (2.6)$$

In Eq. (2.3) and (2.6), $\nu_p = \nu_i = 1/2$ when $r_1 = r_2$.

Furthermore, the following equation can be obtained by Eq. (2.3) and (2.6).

$$\nu_p + \nu_i = 1 \quad (2.7)$$

Thus, this relation is always satisfied regardless of the cross-section shape of the conductor.

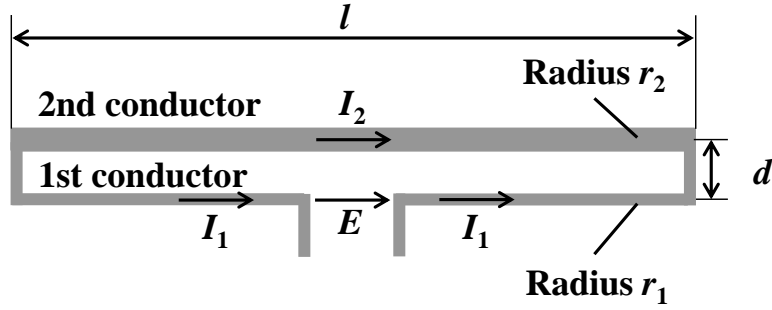
Figure 2.2 shows a FDA which consists of two parallel wire dipoles connected at the ends. Each radius of wire dipole is respectively r_1 and r_2 , and the distance of the dipoles is d with much smaller than l and a wavelength. The side with the feed point is defined as the 1st conductor of r_1 , and the other side is the 2nd conductor of r_2 . The feed point is located at the center of the 1st conductor. Assume a voltage E is applied to the FDA. Then, its current is divided into two distinct modes, an antenna mode and a transmission-line mode [39],[64], [68]-[72].

When the current flows in the same direction on the conductors as seen in Fig 2.2(b), which is called the antenna mode, the fields from the currents on each dipole reinforce in the far-field. Thus, the impedance is regarded as a cylindrical dipole antenna with an equivalent radius r_0 given by

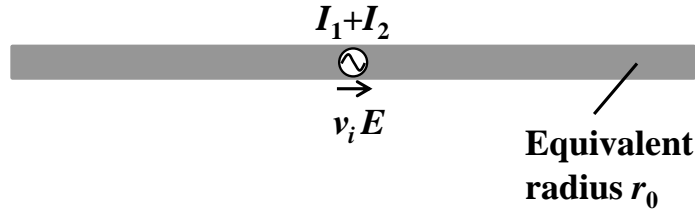
$$\nu_i E = (I_1 + I_2) Z_u. \quad (2.8)$$

On the other hand, the currents on each conductor flow in the opposite direction in Fig. 2.2(c), which is called the transmission line mode. The currents in the transmission line mode have the fields that tend to cancel in the far-field because d is small, and the impedance is obtained by

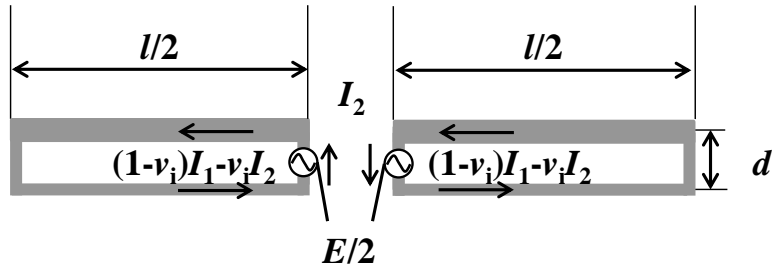
$$\frac{E}{2} = [(1 - \nu_i)I_1 - \nu_i I_2] \cdot 2Z_b. \quad (2.9)$$



(a) Folded dipole antenna



(b) Antenna mode



(c) Transmission line mode

Figure 2.2: Equivalent models of folded dipole antenna.

From Eq. (2.8) and (2.9), I_1 and I_2 are calculated as

$$I_1 = E \left(\frac{v_i^2}{Z_u} + \frac{1}{4Z_b} \right) \quad (2.10)$$

$$I_2 = E \left[\frac{(1-v_i)v_i}{Z_u} - \frac{1}{4Z_b} \right]. \quad (2.11)$$

Since the input impedance of FDA is given by $Z_{in}=E/I_1$, Z_{in} can be obtained as follows by substituting Eq. (2.10).

$$Z_{in} = \frac{4Z_u Z_b}{4Z_b v_i^2 + Z_u} \quad (2.12)$$

When l is half wavelength, then $Z_b=\infty$. Therefore, Eq. (2.12) is

$$Z_{in} = \frac{Z_u}{v_i^2}. \quad (2.13)$$

Furthermore, when the radius of each conductor is the same ($r_1=r_2$), then $v_i=1/2$.

$$Z_{in} = 4Z_u \quad (2.14)$$

Thus, the input impedance of FDA is four times greater than that of DA which has the same length and radius. $1/v_i^2$ in Eq. (2.13) is called step-up ratio of FDA. The term a is

introduced here, and a is the ratio of currents on the two conductors in the antenna mode; that is, $a = I_2/I_1$. Therefore, the step-up ratio with respect to a is also expressed as follows using Eq. (2.6).

$$\frac{1}{v_i^2} = (1+a)^2 \quad (2.15)$$

The value of a can be obtained by

$$a = \frac{\cosh^{-1} \left(\frac{\gamma^2 - \mu^2 + 1}{2\gamma} \right)}{\cosh^{-1} \left(\frac{\gamma^2 + \mu^2 - 1}{2\mu\gamma} \right)} \cong \frac{\ln \gamma}{\ln \gamma - \ln \mu} \quad (2.16)$$

where $\mu = r_2/r_1$, $\gamma = d/r_1$, which means that the step-up ratio depends on r_1 , r_2 and d . Thus, step-up ratio is theoretically more than 1 from Eq. (2.15). Figure 2.3 shows the step-up ratio. When $r_1=r_2$, the step-up ratio becomes four, and more than four of the step-up ratio can be obtained with the larger radius of the 2nd conductor compared with the 1st conductor. One of the most significant features of FDA is that the input

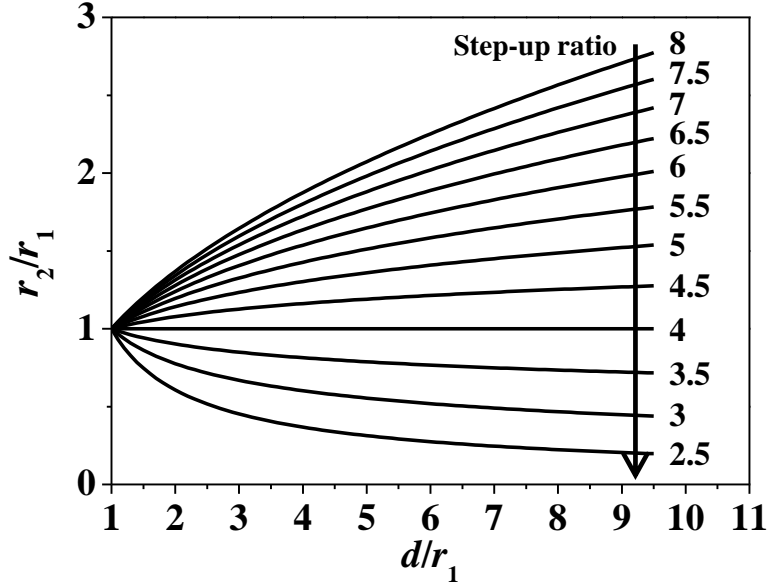


Figure 2.3: Step-up ratio of FDA.

impedance is readily changed depending on the step-up ratio which consists of the distance and each radius of antenna conductors.

2.2.2 Wideband Characteristic

The equivalent radius of FDA (r_0) in antenna mode is calculated by

$$\log r_0 \cong \frac{1}{(r_1 + r_2)^2} (r_1^2 \log r_1 + r_2^2 \log r_2 + 2r_1 r_2 \log d). \quad (2.17)$$

When $r_1 = r_2 = r$, Eq. (2.17) can be approximated by

$$r_0 = \sqrt{rd}. \quad (2.18)$$

Thus, FDA works as DA which has a larger radius (r_0) in antenna mode as Fig. 2.2(b) indicates. Therefore, the more current paths are created, then wideband characteristic can be obtained since the excitation of more modes is generated [73]. Figure 2.4 shows the VSWR characteristic of DA and FDA, which have the same radius of r . Also, the characteristic impedance of the feed line for DA and FDA is $75 \, \Omega$ and $300 \, \Omega$, respectively. When the bandwidth ($\text{VSWR} \leq 2$) is compared, about 1.5 times wider bandwidth can be obtained by FDA.

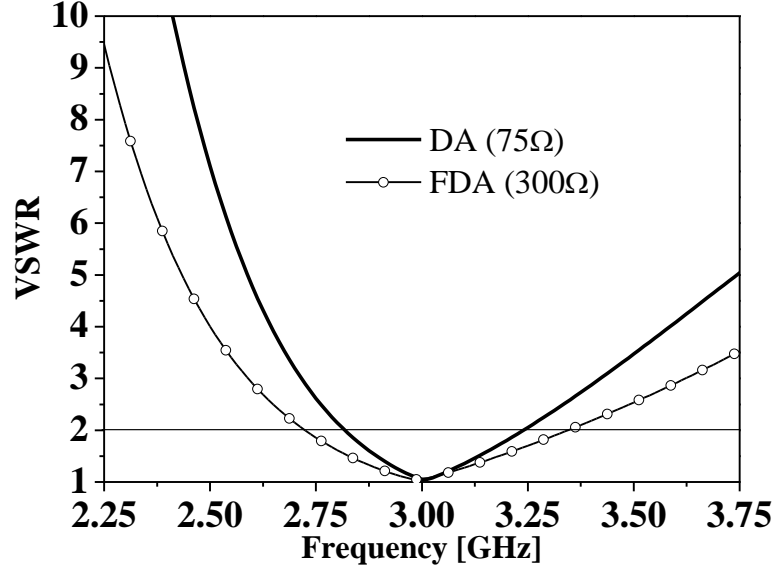


Figure 2.4: VSWR characteristics of DA and FDA.

2.3 Basic Property of FDAFL and Comparison with FDA

2.3.1 Two Resonant Operation

Figure 2.5 shows the structure of FDAFL, which consists of FDA and quarter-wavelength feed lines. In this study, the target frequency is 3 GHz. Then, the antenna length l is 50 mm and the feed line length lf is 25 mm. Also, the width of the antenna elements and feed line are defined as w_1 , w_2 , and w_f , respectively. All the element widths and gaps are 1 mm.

Figure 2.6 shows the variations of input impedance when lf is changed from 25 mm to 0 mm. In Fig. 2.6(a), the locus rotates counterclockwise on the Smith chart with decreasing the length of the feed lines, and the impedance is transformed to higher value. Also, it is found that the locus rotates by π comparing $lf=25$ mm and 0 mm. In addition, it can be seen that there are two resonant frequencies by adding the feed lines. The characteristic impedance of the feed lines is calculated by

$$Z_c = \frac{377}{\pi} \ln \left(\frac{D}{d} + \sqrt{\left(\frac{D}{d} \right)^2 - 1} \right). \quad (2.19)$$

where d is the equivalent wire diameter of the feed line and D is the distance between the centers of the wire feed lines [74]. When the thickness of the element is sufficiently small compared with the width wf , d is obtained as follows from [39]

$$d = 0.5wf . \quad (2.20)$$

Thus, $d=0.5$ mm because $wf=1$ mm. Since $D=2$ mm, the characteristic impedance of the feed lines is approximately 248Ω using Eq. (2.19). This value is approximately the same as the rotation center of the locus, which is about 250Ω . In Fig. 2.6(b), the VSWR characteristic corresponding to the Smith chart is shown. The VSWR is well improved with the quarter-wavelength feed line. In other cases, two resonant frequencies separate with each other, and impedance matching cannot be obtained with 50Ω characteristic impedance. Also, it is found that the 1st resonant frequency does not change so much compared with the 2nd resonance.

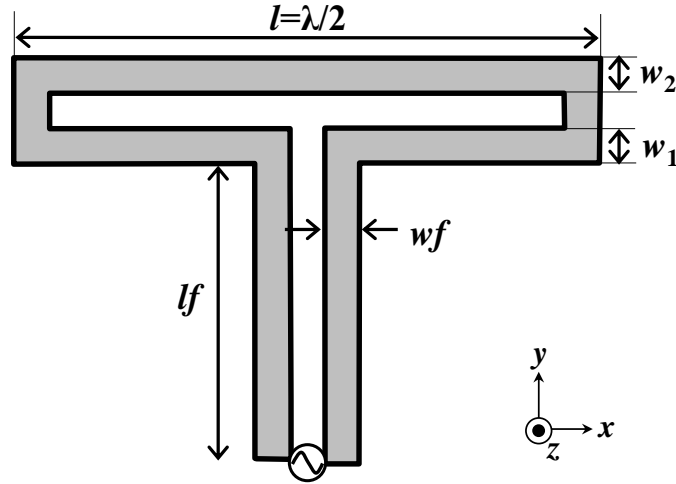
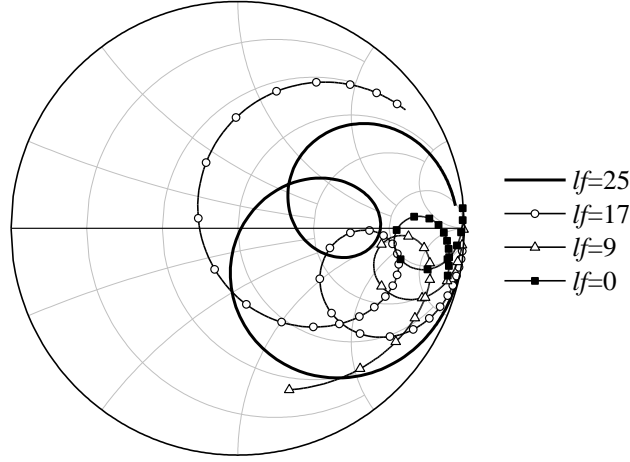
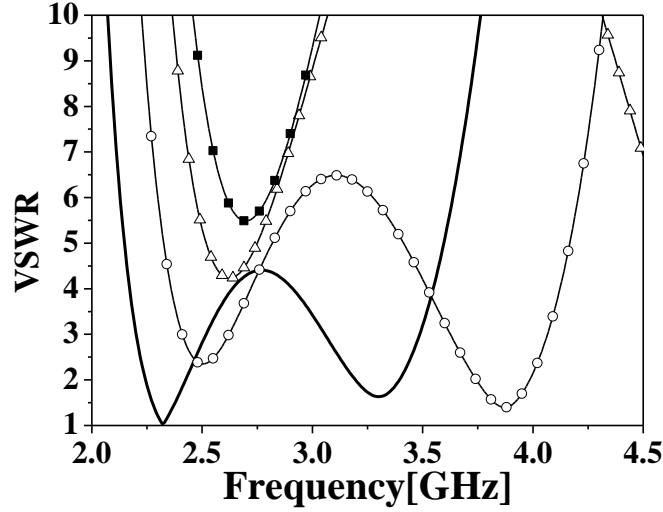


Figure 2.5: Folded dipole antenna with feed line.



(a) Smith chart



(b) VSWR characteristics

Figure 2.6: Impedance characteristics when the parameter lf is varied.

2.3.2 Equivalent Circuit of Feed Line

Figure 2.7 shows FDA and the equivalent circuit of the feed lines. The circuit is composed of a serial inductor L and a parallel capacitor C , which are connected to FDA as can be seen in the figure. The variations of input impedance are shown in Fig. 2.8 when L and C are varied. The loci of impedance characteristics in Fig. 2.8 are quite similar to those of the impedance characteristics in Fig. 2.6(a). Thus, it is confirmed that the variation of the length lf is equivalent to the changes of L and C as seen in Fig. 2.7.

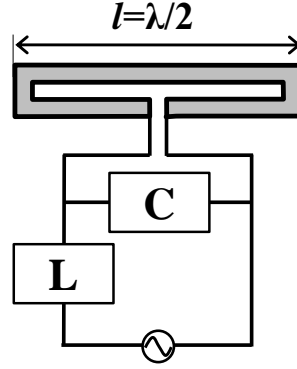


Figure 2.7: Equivalent circuit of the feed lines.

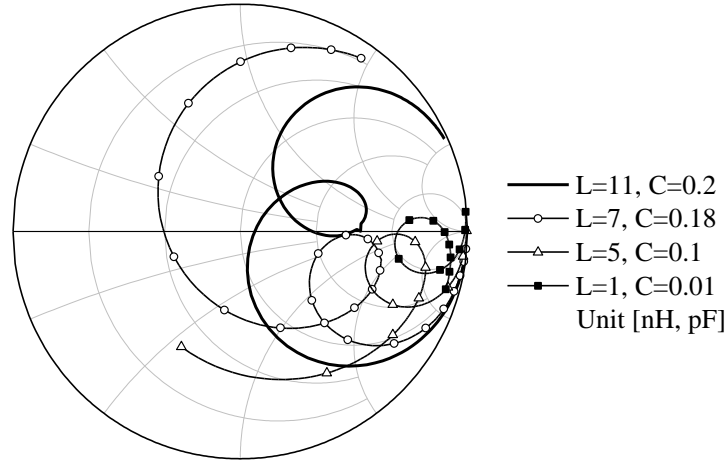


Figure 2.8: Impedance characteristics when L and C are varied.

2.3.3 Wideband Characteristic

Figure 2.9 shows the comparison of VSWR characteristic between FDA ($lf=0$) and FDAFL ($lf=\lambda/4$). The characteristic impedance of the feed line for FDA and FDAFL is $300\ \Omega$ and $50\ \Omega$, respectively since the input impedance of FDAFL is transformed to lower value due to the length of the feed lines, which is $\lambda/4$. Initial value of width of antenna elements and the gap between the elements are 1 mm. Here, the width and the spacing of the feed lines are changed to 3 mm and 0.5 mm, respectively so that the FDAFL acts in wideband operation. In the figure, the relative bandwidth ($VSWR \leq 2$) of FDA and FDAFL are respectively 20.0% and 32.7%, so approximately 1.6 times wideband operation is possible by FDAFL.

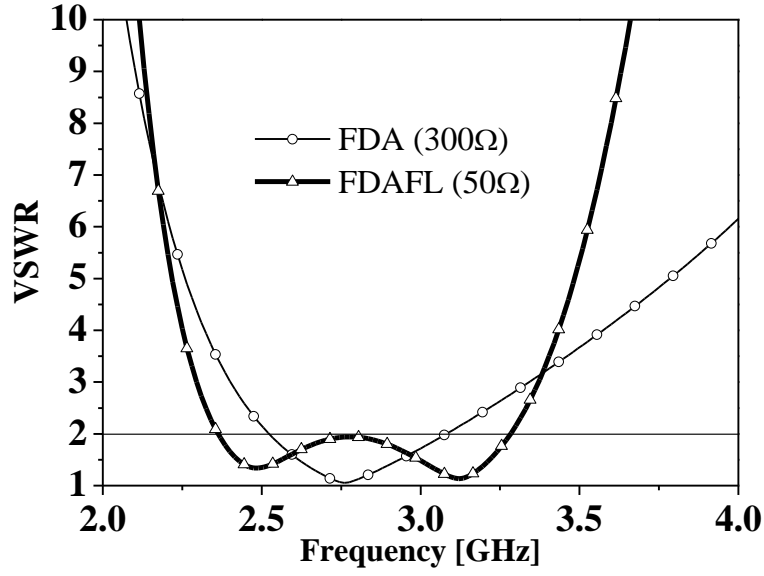


Figure 2.9: VSWR characteristics of FDA ($l_f=0$) and FDAFL ($l_f=\lambda/4$).

2.3.4 Current Distribution

Current distributions of FDA and FDAFL are shown in Fig. 2.10. The arrows in the figure indicate the vector of the current flow. The evaluated frequencies are 2.3 GHz, 2.7 GHz and 3.3 GHz, which are the resonant frequencies of FDA and FDAFL.

It can be seen in Fig. 2.10(a) and Fig. 2.10(b) that the current distributions on the antenna elements and the directions of the current flow are almost the same between $l_f=0$ mm and $l_f=\lambda/4$, so the existence of the feed line itself does not affect the current flow. Also, the larger current is observed on the different antenna element at each resonant frequency in Fig. 2.10(c) and Fig. 2.10(d). For instance, the upper element is dominant at 2.3 GHz, and the lower element is dominant at 3.3 GHz. Thus, the operating antenna element varies depending on the resonant frequency. In addition, current distributions without feed lines are presented in Fig. 2.10(e) and Fig. 2.10(f) for comparison with the case of $l_f=\lambda/4$. Similarly, it is found that the current on FDA is independent from the presence of the feed lines.

As for the currents on the feed lines, they flow in the opposite direction each other at all the frequencies in the figure. Therefore, it is more likely that the radiation patterns are not affected by the feed lines. In order to confirm that, radiation patterns are investigated in the following subsection.

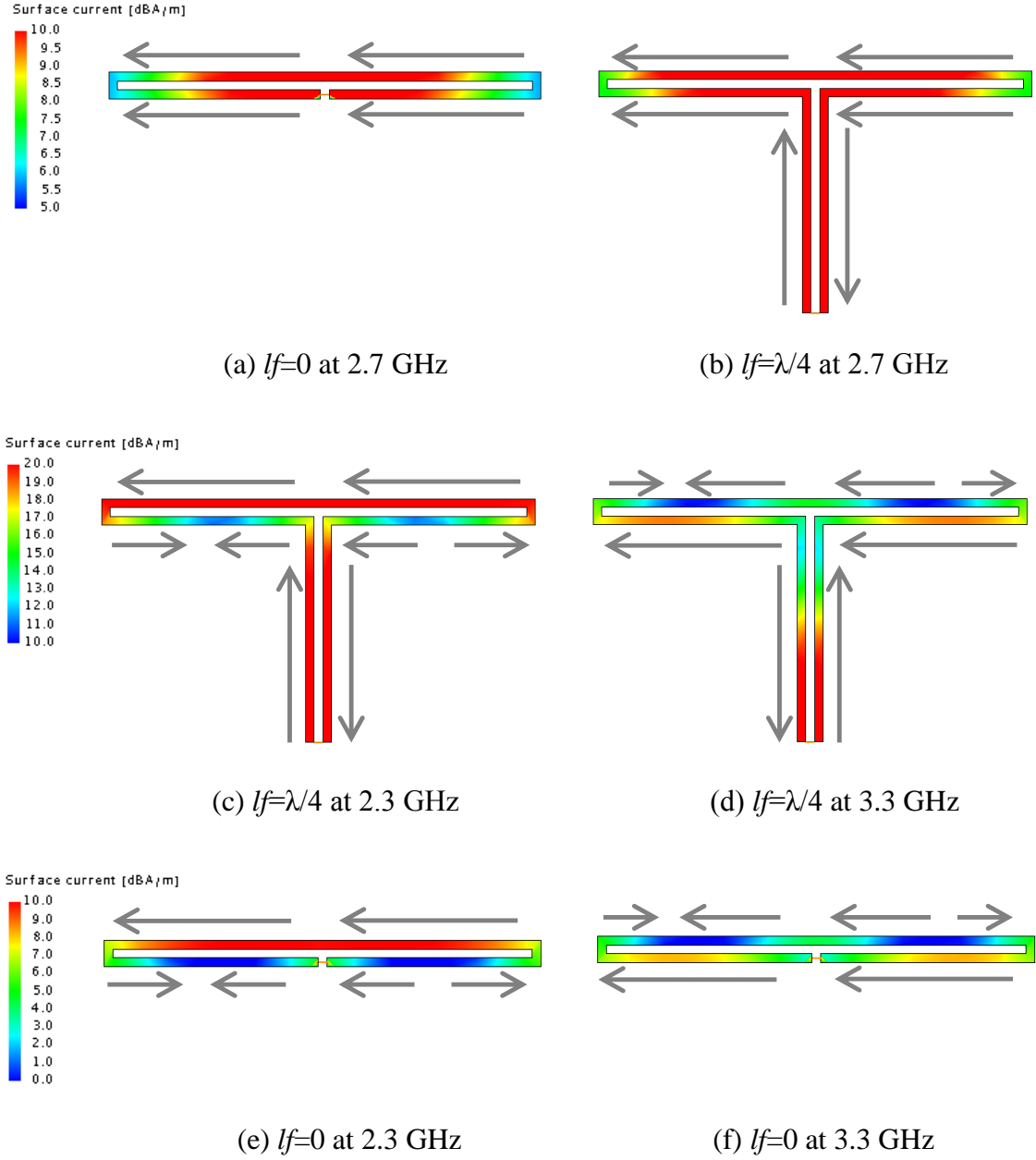


Figure 2.10: Current distributions of FDA and FDAFL at each resonant frequency.

2.3.5 Radiation Characteristic

Figure 2.11 shows the radiation patterns of FDAFL with $lf=\lambda/4$ at 2.3 GHz and 3.3 GHz. At both frequencies, the main polarization components depict the shape of figure eight and omnidirectional pattern. Also, it can be seen in the figures that the cross polarization components of FDAFL are very small in spite of the existence of the feed lines. This is because the currents on the feed lines flow in the opposite direction, which

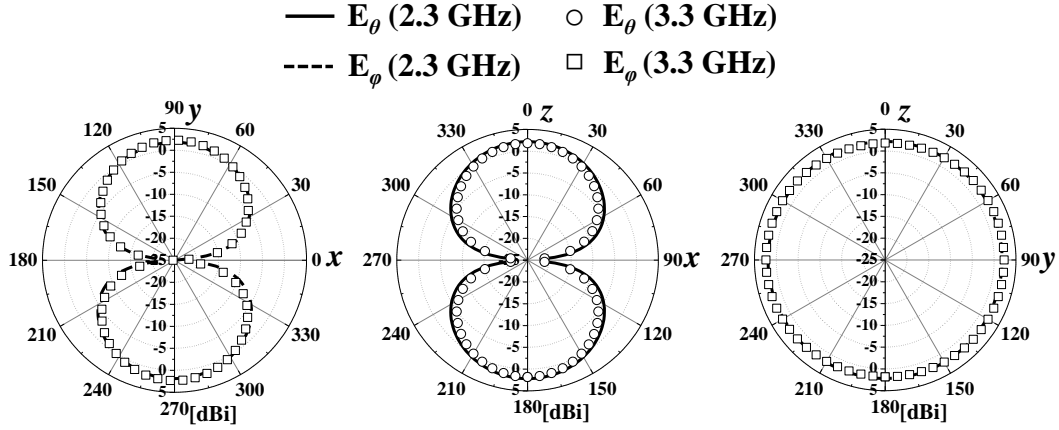


Figure 2.11: Radiation patterns of FDAFL at each resonant frequency.

is observed in the previous subsection. Thus, these currents are cancelling each other, and there is little radiation from the feed lines.

Moreover, the radiation patterns remain unchanged by the frequency shift about 1 GHz, which indicates the range between 2.3 GHz and 3.3 GHz. In addition, the gains of FDAFL at 2.3 GHz and 3.3 GHz are approximately 2.18 dBi and 2.33 dBi, which are nearly identical to the gain of FDA. Therefore, it can be explained that the feed lines do not affect the radiation patterns and gains.

2.4 Summary

This chapter presents an overview of FDAFL as well as fundamental characteristics and operation principle of FDA. FDA is the most fundamental antenna with folded structure, consisting of two parallel dipoles. Due to the structure, the current flow on the antenna element is varied, which generates distinctive antenna properties. The summary of this chapter is described below.

➤ Higher input impedance and wideband characteristic

Since step-up ratio is theoretically more than 1, input impedance of FDA is higher than that of DA. Also, the input impedance is easily altered according to the step-up ratio which consists of the distance and each width of antenna elements. Moreover, FDA shows wideband characteristic because more current paths are created, which acts as thick DA.

- Two resonant operation of FDAFL
By adding the feed lines, there are two resonant frequencies, which cannot be seen in FDA's characteristic. When the length is $\lambda/4$, the impedance matching can be mostly obtained at both resonant frequencies, which means that FDAFL's input impedance is about $50\ \Omega$, while FDA shows $300\ \Omega$.
- Wideband characteristic of FDAFL
Impedance transformation of FDA can be conducted by varying the characteristic impedance of the feed line. Thus, the width and gap of the feed lines are adjusted based on Eq. (2.19), then FDAFL shows around 1.6 times wideband characteristic compared to FDA when the width of feed lines element is 3 mm, and the gap between them is 0.5 mm.
- Similar radiation patterns
Radiation patterns between FDAFL and FDA are equivalent since currents on the feed lines flow in the opposite direction, causing the currents to cancel each other. Thus, there is little radiation from the feed lines, and similar antenna patterns are observed.

Chapter 3

Miniaturization of FDAFL and Application to Small Terminal

3.1 Introduction

In order to deal with today's increase in demand for high-speed large-capacity wireless communication, various systems such as WiMAX, WLAN, and UWB have been significantly progressed in the past few decades. Consequently, wideband operation including multiband operation of the antennas is highly required, especially in mobile communication [75]-[81]. In addition to that, since the wireless terminal itself is becoming small and the space for the antennas is very limited, the size of the antenna element should also be miniaturized and low-profile, while maintaining its bandwidth and gain characteristics. As a small and low-profile antenna for instance, a patch antenna fed by microstrip transmission line and a strip antenna have been widely proposed for portable devices [82]-[83].

Chapter 1 and 2 indicated that the antenna with folded structure is able to show wideband operation, and overview of FDAFL has been presented. Originally, FDAFL requires the length of $\lambda/4$ for the feed lines in order to obtain impedance matching. However, the feed line is too long for mounting to the small terminal, which means the length of the feed line must be decreased in somehow. In general, meandered structure is effective to decrease the size of the element without reducing the current path length, which does not cause a major alteration in impedance characteristics [62]. On the other hand, meandered elements make antenna structure much more complicated. Therefore, in this chapter, the technique for miniaturizing the feed line of FDAFL is investigated without utilizing meandered structure. Then, FDAFL is applied to a ground plane, and antenna characteristics are analyzed.

First, this chapter shows parametric analysis of FDAFL contributing to low-profile in Sect. 3.2. Sect. 3.3 presents miniaturization and wideband characteristics

of FDAFL. Characteristics of FDAFL with ground plane are analyzed in Sect. 3.4, then Sect. 3.5 gives the conclusion.

3.2 Parametric Analysis Contributing to Low-profile Antenna

In this chapter, important antenna parameters which contribute to low-profile antenna configuration are presented. As can be seen in Sect. 2.3, impedance characteristics of FDAFL are deteriorated with decreasing the length of the feed lines. Thus, in order to obtain impedance matching, two antenna parameters are discussed here.

3.2.1 Antenna Configuration

Figure 3.1 shows the antenna configuration of FDAFL (Basic model). The antenna length is la , and the antenna element widths are wa_1 , wa_2 and wa_3 . Also, the length and width of the feed line are lf and wf , respectively. The spacing of antenna elements and feed lines are respectively sa and sf . The target bandwidth is from 2.3 GHz to 3.8 GHz, which is 2.5 GHz band and 3.5 GHz band of WiMAX. Since the central frequency is about 3 GHz, $la=50\text{ mm}=\lambda/2$, $lf=25\text{ mm}=\lambda/4$. Other parameters are initially set to 1 mm. Thus, when the antenna height is defined as H , the height H of basic model is 28 mm.

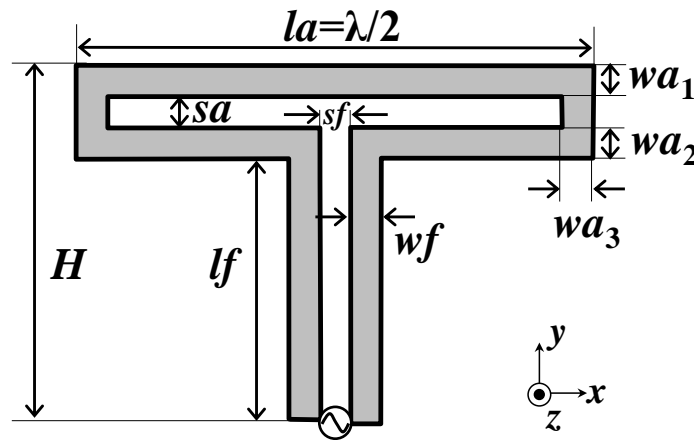
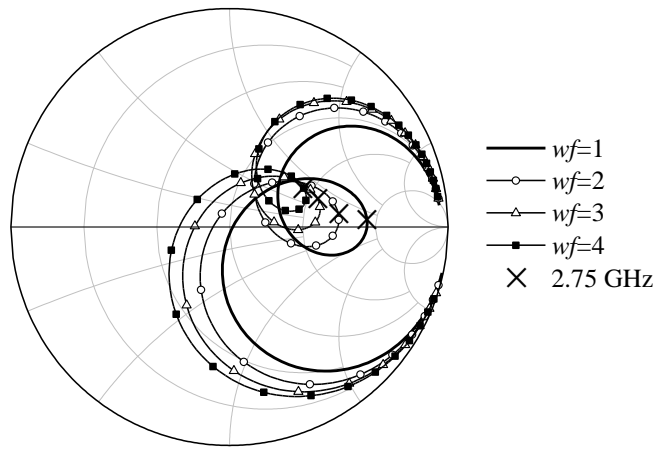


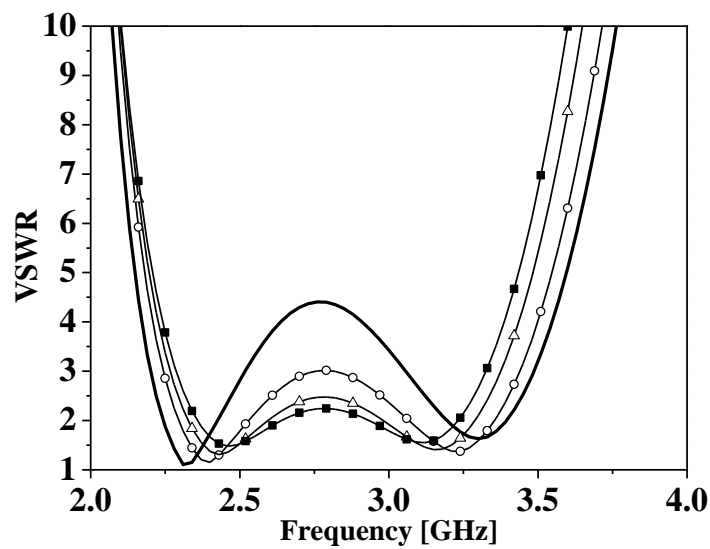
Figure 3.1: Antenna configuration of FDAFL (Basic model).

3.2.2 Impedance Characteristic by the Change of Antenna Parameters

Figure 3.2 shows the impedance variations when wf is varied from 1 mm to 4 mm. The locus of the input impedance shift to the left with increasing wf , which means the impedance is transformed to lower values. The characteristic impedance of the feed lines is calculated by Eq. (2.19). Again, d is the equivalent wire diameter of the feed line and D is the distance between the centers of the wire feed lines. Since d is obtained by Eq. (2.20), the relation between D/d , Z_c , and wf is described as Fig. 3.3. With increasing

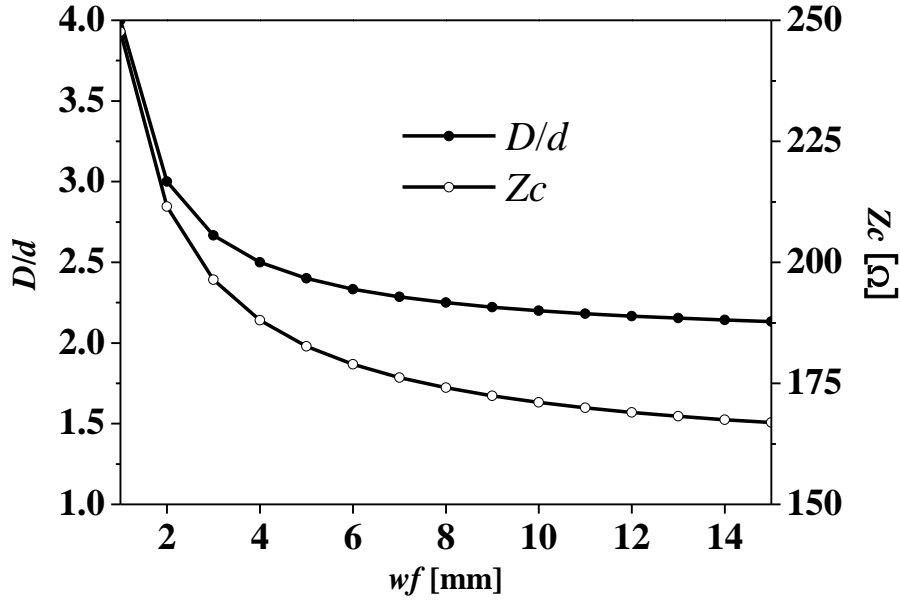


(a) Smith chart



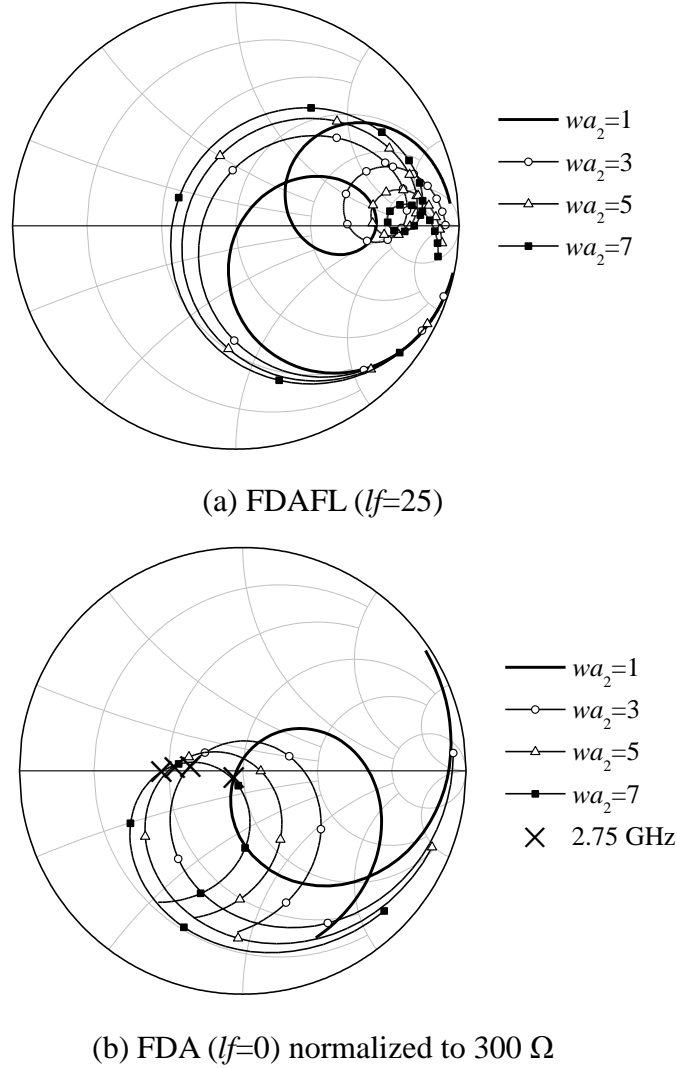
(b) VSWR characteristics

Figure 3.2: Impedance characteristics when wf is varied.

Figure 3.3: D/d and Z_c versus wf .

wf , D/d is decreased, and in the end, Z_c of the feed line also decreases as can be seen in the figure. Therefore, the entire impedance of FDAFL decreases as well, causing the locus on Smith chart to shift to the left. In Fig. 3.2(b), the VSWR around 2.75 GHz is improved with increasing wf since the kink moves to the center on Smith chart.

The next important antenna parameters contributing to low-profile antenna is wa_2 . Figure 3.4 shows the impedance variations when wa_2 is varied from 1 mm to 7 mm. In Fig. 3.4(a), the loci of the impedance characteristics rotate clockwise with increasing wa_2 . This is because the step-up ratio of FDA is changed based on Figure 2.3, then input impedance of FDAFL is also varied. Figure 3.4(b) shows the impedance variation of FDA which is normalized to 300 Ω . When 2.75 GHz is focused on, the impedance shifts to a lower value since the step-up ratio becomes less than 4 with $wa_2 > 1$ mm. Since the locus rotates by π with the quarter-wavelength feed lines, therefore the loci of FDAFL look like rotating clockwise in Fig. 3.4(a).

Figure 3.4: Impedance characteristics when wa_2 is varied.

3.3 Miniaturization of Feed Line and Wider Bandwidth

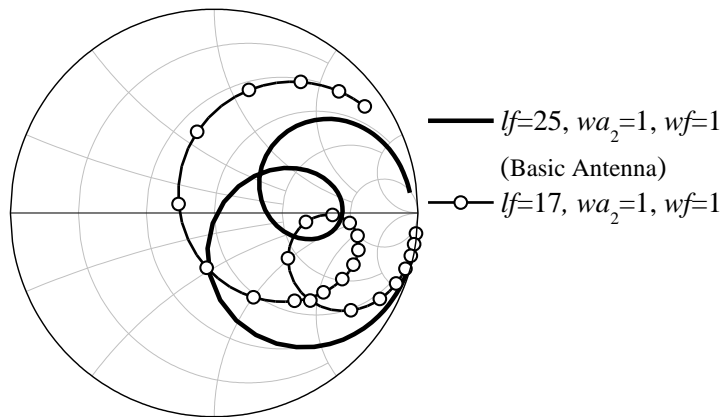
In order to apply FDAFL to a small terminal, the length of the feed line lf should be shortened and antenna height H should be miniaturized. However, VSWR characteristic degrades because the input impedance is transformed to higher value according to the miniaturization of lf . In this section, the method to obtain impedance matching utilizing parametric analysis mentioned in the previous study is shown. Also, the wideband characteristic of FDAFL is discussed.

3.3.1 Technique for Obtaining Impedance Matching

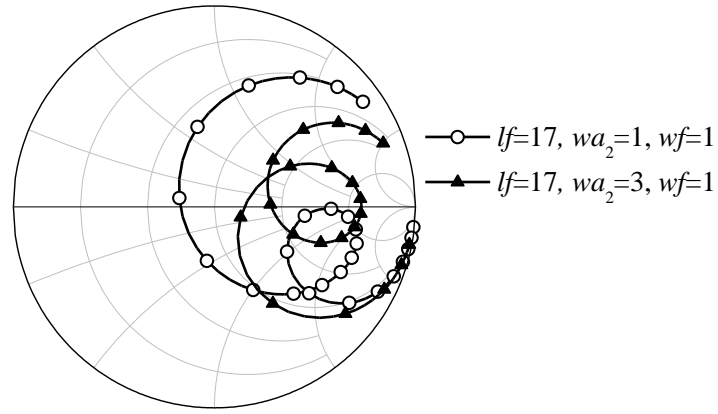
It is possible to miniaturize H by adjustment of wa_2 and wf . This is because impedance matching can be obtained even though lf is shortened.

As an example, Figure 3.5 shows the input impedance variations when lf is changed to 17 mm. Firstly, lf is shortened from 25 mm to 17 mm (Step 1). Then, the locus rotates counterclockwise as can be seen in Fig. 2.6(a). Secondly, wa_2 is adjusted from 1 mm to 3 mm so that the locus returns mostly to original position (Step 2). Finally, wf is altered from 1 mm to 5 mm in order to move the locus to the center of the Smith chart and obtain impedance matching (Step 3). By following three steps above, relative bandwidth is approximately 52% ($VSWR \leq 3$) shown in Fig. 3.5(d). Furthermore, H can be miniaturized from 28 mm to 22 mm, which is approximately 21% reduction. This is because the amount of change of wa_2 is smaller than that of lf ($|\Delta lf| = |17 \text{ mm} - 25 \text{ mm}| = 8 \text{ mm}$, $|\Delta wa_2| = |3 \text{ mm} - 1 \text{ mm}| = 2 \text{ mm}$).

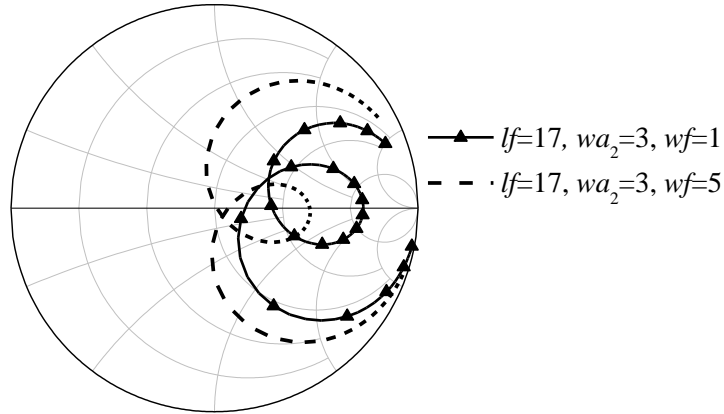
Thus, the antenna height H decreases by the difference between Δlf and Δwa_2 ($|\Delta lf| - |\Delta wa_2| = |8 - 2| = 6 \text{ mm}$). Thus, by adjusting the antenna parameters, wf and wa_2 , not only obtaining impedance matching, but also the miniaturization of H is possible although lf is shortened.



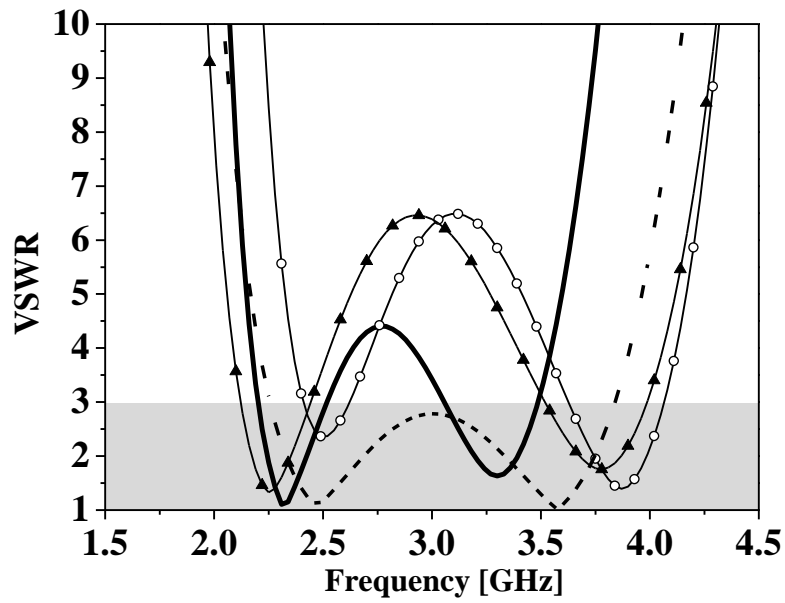
(a) Step 1



(b) Step 2



(c) Step 3



(d) VSWR characteristics

Figure 3.5: Impedance variations when wa_2 and wf are varied.

3.3.2 Bandwidth Change by the Antenna Parameters

In subsection 3.3.1, wider bandwidth characteristic can also be obtained with respect to the miniaturization of antenna height H . To describe this phenomenon in detail, the distributions of relative bandwidth ($VSWR \leq 3$) with lf of 25 mm, 17 mm, 9 mm and 1 mm are shown in Fig. 3.6. wa_2 and wf are respectively changed by 1 mm spacing from 1 mm to 12 mm and from 1 mm to 15 mm. Also, the scale only for the case of $lf=25$ mm is different from other cases due to the consideration for the visibility since the relative bandwidth is small.

It can be seen in Fig. 3.6 that the area where the relative bandwidth is large moves toward the upper right side of the figure as lf decreases. Thus, the bandwidth under $VSWR \leq 3$ is realized with larger wa_2 and wf . Furthermore, when the value of relative bandwidth is focused on, the bandwidth is less than 40% with $lf=25$ mm. On the other

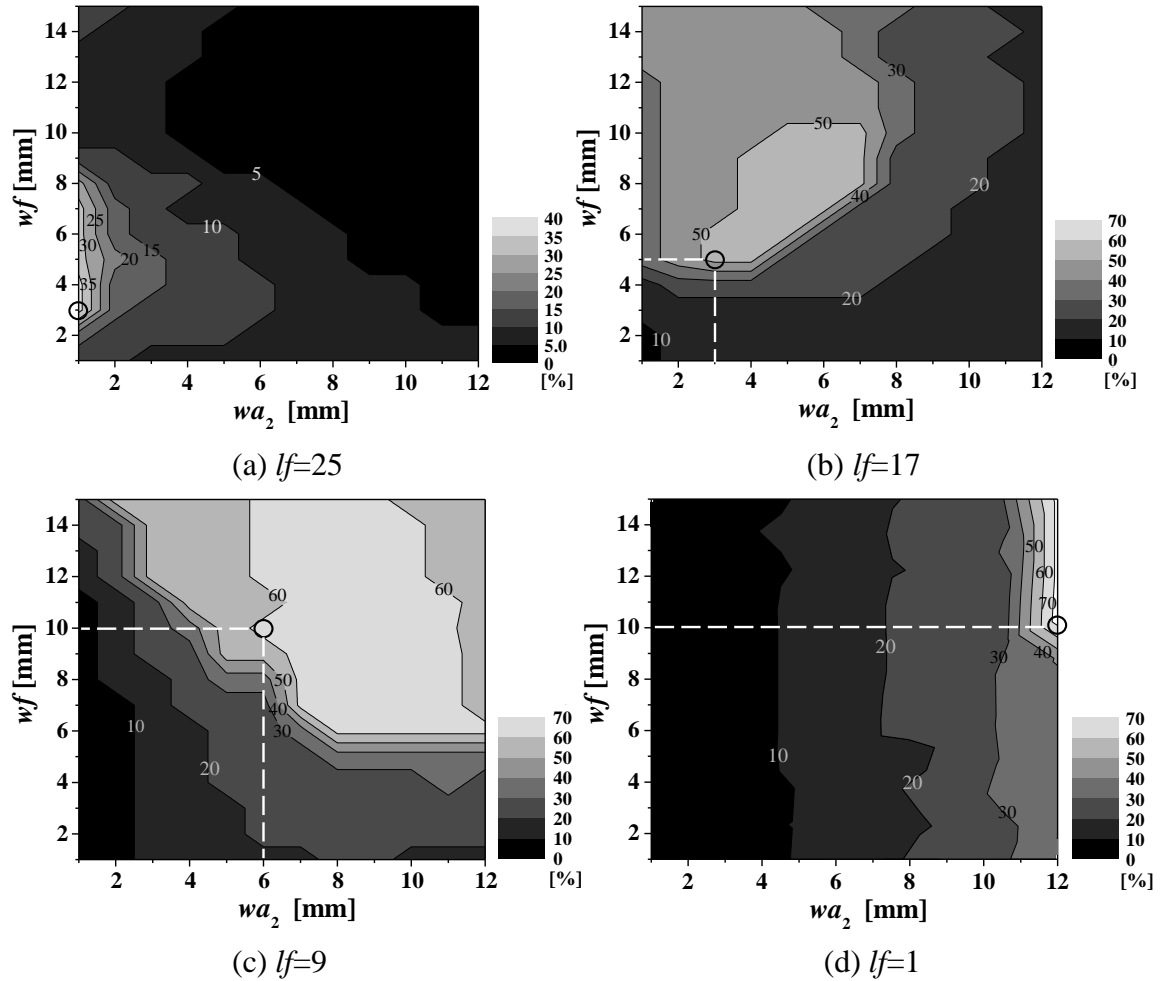
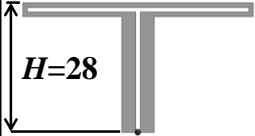
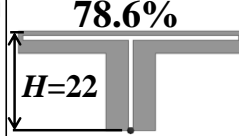
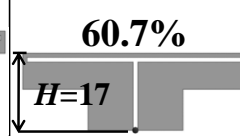
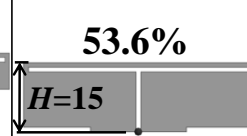


Figure 3.6: Distributions of relative bandwidth.

hand, the bandwidth is enhanced between 50% and 60% with $lf=17$ mm, between 60% and 70% with $lf=9$ mm and more than 70% with $lf=1$ mm. Also, it is reported that FDA with $lf=0$ presents the wideband property [67].

Table 3.1 shows the comparison of physical size and relative bandwidth. Each value of wa_2 and wf is presented by a circle in Fig. 3.6 where broadband characteristic and smallest wa_2 , that is, minimum antenna height H are obtained at each lf . From the table, it is possible to miniaturize lf and H at the same time. For instance, $H=15$ mm with $lf=1$ mm, which is 53.6% height and physical area of basic model. Furthermore, relative bandwidth ($VSWR \leq 3$) is enhanced from 13.5% (basic model) to 73.0% when $lf=1$ mm. Figure 3.7 shows the VSWR characteristics of each antenna height. It can be seen in the figure that the 1st resonant frequency hardly changes since it depends on the antenna length la . On the other hand, the 2nd resonances move to higher frequency as the length of lf is decreased and wa_2 and wf are increased instead. Thus, wa_2 and wf contribute to the 2nd resonant frequency, and these are obvious from the current distribution in Fig. 2.10. Consequently, the wideband operation of FDAFL is achieved by the shift of the 2nd resonant frequencies.

Table 3.1: Comparison of H , relative bandwidth, and metal area.

lf	25 mm	17 mm	9 mm	1 mm
H	 $H=28$	 $H=22$	 $H=17$	 $H=15$
Relative bandwidth [%]	39.4	52.0	61.0	73.0
Metal area [mm ²]	251 (100%)	369 (147%)	526 (210%)	660 (263%)

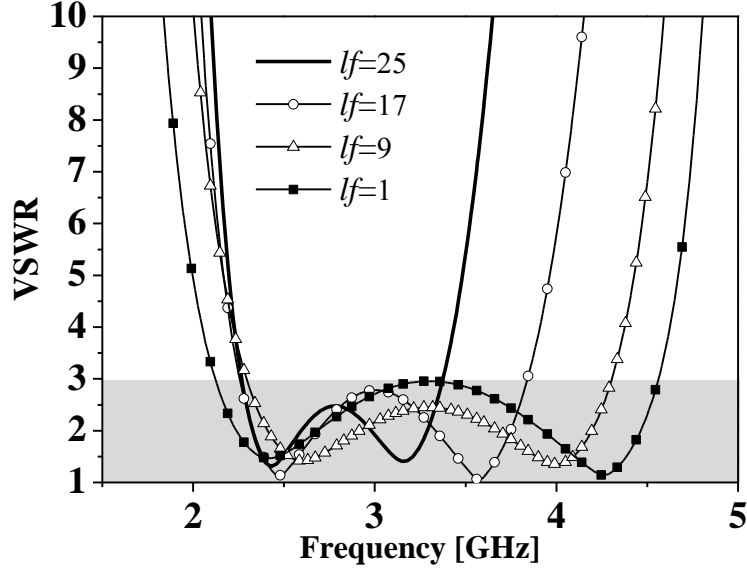


Figure 3.7: VSWR characteristics of each antenna height.

3.3.3 Current Distribution and Radiation Characteristic

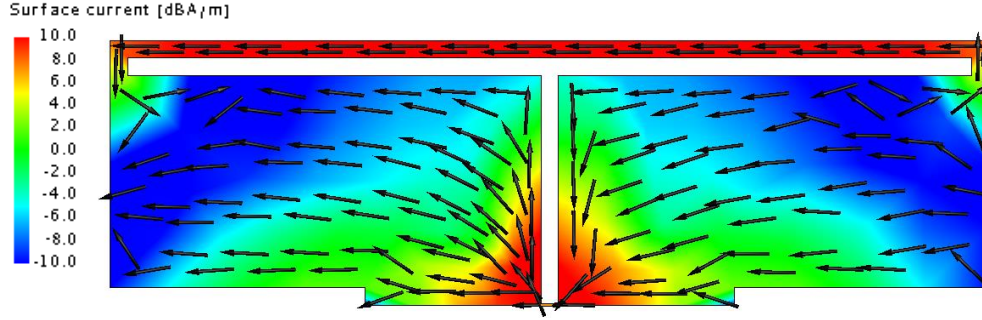
From the figures in Table 3.1, actually the antenna shape significantly changes in aiming for low-configuration and wideband antenna. Thus, the antenna shape itself becomes like a T-shaped slot antenna. In this subsection, the current distribution and radiation pattern are compared, and the principle of operation is discussed.

Figure 3.8 shows the current distributions when $l_f=1$ mm in Table 3.1. The arrows in the figure describe the vector of the current flow. The evaluated frequencies are 2.4 GHz and 4.3 GHz resonances. In Fig. 3.8(a), the directions of current flowing on wa_1 and wa_2 are the same at 2.4 GHz, while opposite direction can be observed along slit between wa_1 and wa_2 at 4.3 GHz. Therefore, it is considered that FDAFL is in antenna mode and transmission line mode at 2.4 GHz and 4.3 GHz, respectively. Furthermore, when comparing with the current distributions in Fig. 2.10, the current directions on antenna element are nearly equivalent. Also, the current distributions are similar, showing that operating elements are different at each resonant frequency, acting with wa_1 in lower frequency and wa_2 in higher frequency.

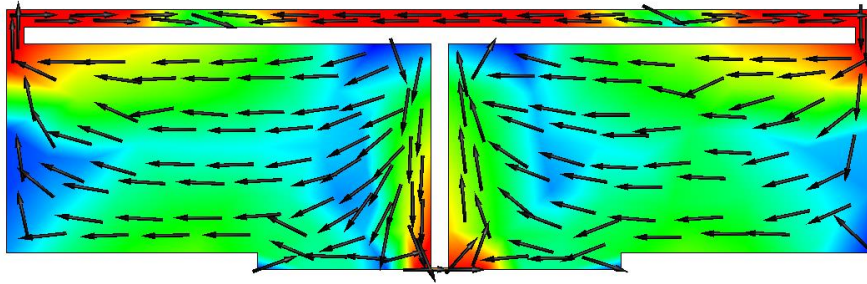
Radiation patterns of each antenna height are presented in Fig. 3.9. At each frequency, the main polarization components draw the shape of figure eight and omnidirectional pattern. Also, the cross polarization components increase in xz -plane with decreasing the

length of lf due to the extension of the width wa_2 , generating the current flowing y direction. However, cross polarization components remain small and overall radiation patterns are maintained.

Considering the discussion above, the principle of operation of FDAFL is unchanged even though the length of the feed lines is shortened to 1 mm.



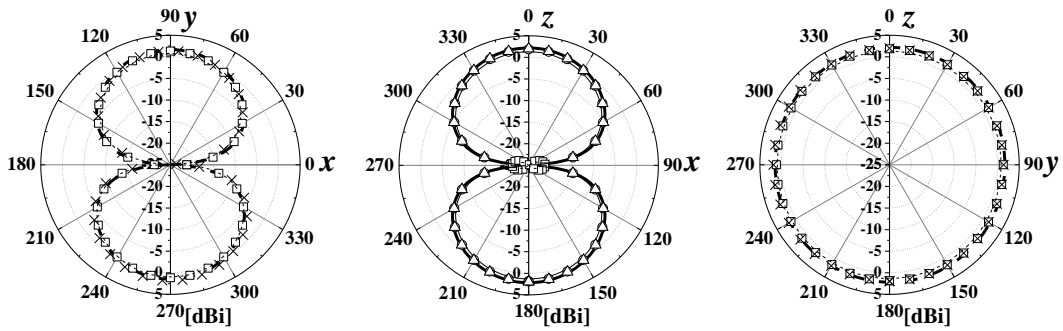
(a) 2.4 GHz



(b) 4.3 GHz

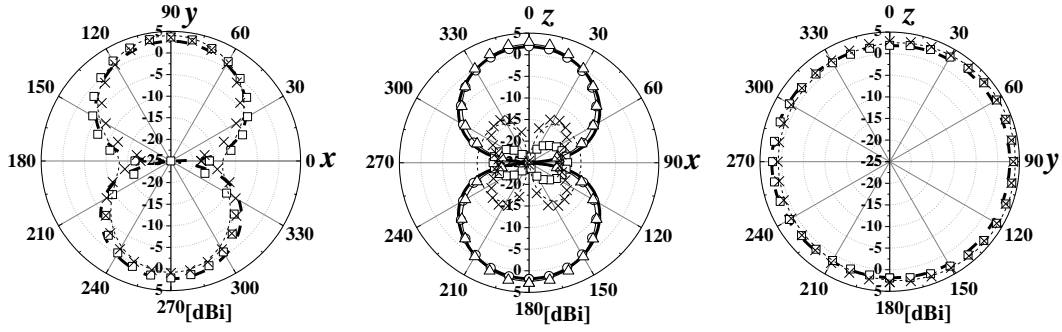
Figure 3.8: Current distributions.

— E_θ ($lf=25_2.4$ GHz) \circ E_θ ($lf=17_2.5$ GHz) — E_θ ($lf=9_2.6$ GHz) \triangle E_θ ($lf=1_2.4$ GHz)
 ---- E_ϕ ($lf=25_2.4$ GHz) \square E_ϕ ($lf=17_2.5$ GHz) E_ϕ ($lf=9_2.6$ GHz) \times E_ϕ ($lf=1_2.4$ GHz)



(a) 1st resonant frequency

— E_θ ($lf=25_3.2$ GHz) \circ E_θ ($lf=17_3.6$ GHz) — E_θ ($lf=9_4.0$ GHz) \triangle E_θ ($lf=1_4.3$ GHz)
 ---- E_ϕ ($lf=25_3.2$ GHz) \square E_ϕ ($lf=17_3.6$ GHz) E_ϕ ($lf=9_4.0$ GHz) \times E_ϕ ($lf=1_4.3$ GHz)



(b) 2nd resonant frequency

Figure 3.9: Radiation patterns of FDAFL at each antenna height.

3.3.4 Consideration Points for Miniaturization

There are several aspects to be considered in the case of short lf . First of all, the metal area of the antenna significantly increases. Table 3.1 shows the metal area as well. While the antenna height H can be reduced, the metal area is over 2 times (263%) with $lf=1$ mm. This might lead to a trouble depending on its application, for example, to the glass window of a car. The glass antenna requires small metal area of the antenna because it blocks the visibility [84].

Secondly, it seems that variation of relative bandwidth due to the manufacturing error increases. In Fig. 3.6 (d), wa_2 shifts by 1 mm from 11 mm to 12 mm, whereas the bandwidth is considerably changes by approximately 20% from 50% to 70%. Also, the area where the relative bandwidth becomes more than 50% is very small compared with the cases of $lf=17$ mm and $lf=9$ mm. Consequently, it should be noticed that the bandwidth variation due to the manufacturing error seems to be large with small lf . Therefore, the antenna parameters of FDAFL should be correctly selected according to its application and required bandwidth.

3.4 Antenna Characteristics with Ground Plane

In this section, FDAFL is mounted to a ground plane in order to apply to a small terminal. Then, fundamental characteristics are analyzed.

3.4.1 Antenna Configuration

Figure 3.10 shows the antenna configuration of FDAFL with a ground plane. In this study, two FDAFLs are mounted to three different sizes of the ground planes. The two FDAFLs are $lf=25$ mm and 1 mm from the circles in Fig. 3.6(a) and Fig. 3.6(d), which are also shown in Table 3.1. The basic size of the ground plane, (Lx, Ly) , is (50 mm, 80 mm), which assumes a small terminal such as mobile router or mobile phone. Other two cases, $(Lx, Ly) = (100$ mm, 160 mm), (25 mm, 40 mm), are assumed to be a tablet device and USB dongle application, respectively. In the analysis, FDAFL is located at the center of Lx side all the time.

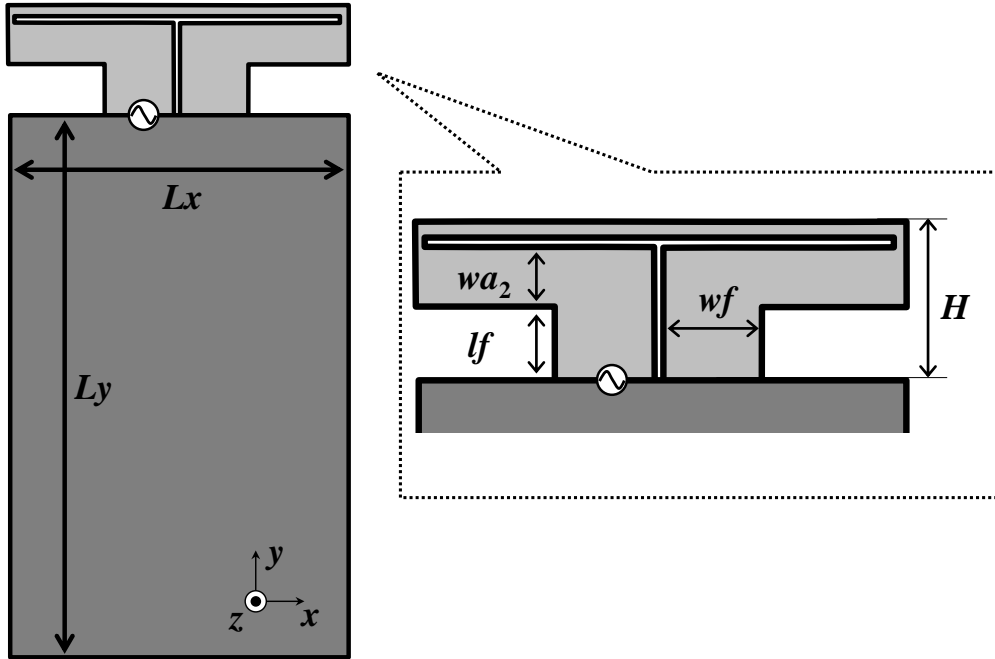
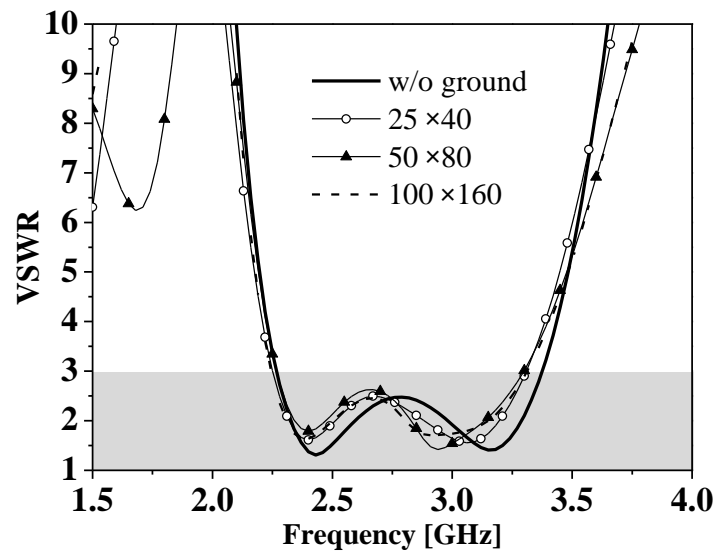


Figure 3.10: Antenna configuration.

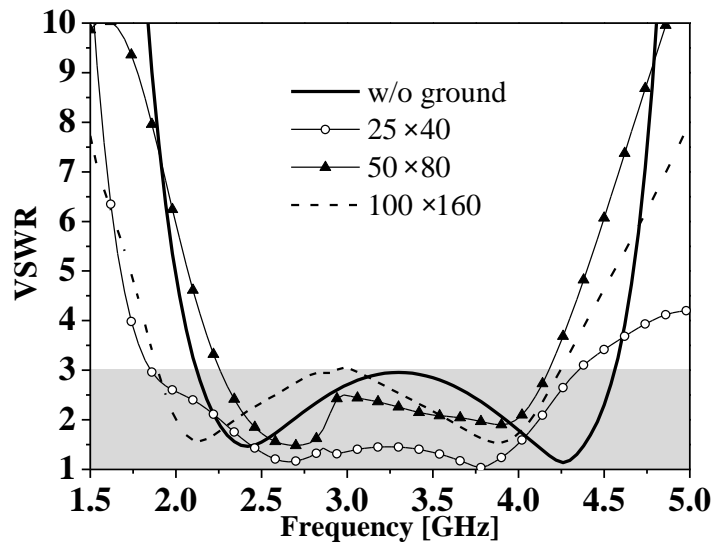
3.4.2 Characteristic Change with respect to Size of Ground Plane

A. VSWR Characteristic

Figure 3.11 shows the VSWR characteristics of FDAFL at $lf=25$ mm and $lf=1$ mm with the three sizes of the ground planes. For the purpose of comparison, the characteristic without ground plane is also presented. In Fig. 3.11(a), it can be seen that the VSWR characteristics hardly changes. Especially, the 1st resonant frequency is almost the same even there is no ground plane.



(a) $lf=25$



(b) $lf=1$

Figure 3.11: VSWR characteristics with respect to the size of the ground plane.

On the other hand, the large variations of the VSWR are observed in Fig. 3.11(b). Thus, the VSWR characteristic is more likely to be affected by the miniaturization of lf . However, the tendency of the VSWR is similar among the different sizes of the ground planes, and wideband property is maintained compared to the case without ground plane. Therefore, the size of the ground plane does not have the large effect on the VSWR characteristics of FDAFL, and it is possible for FDAFL even $lf=1$ mm to be mounted on the ground plane with wideband characteristic.

B. Current Distribution

Figure 3.12 shows the current distributions at the 1st resonant frequency when $(L_x, L_y) = (50 \text{ mm}, 80 \text{ mm})$. It is found that the current on the ground plane is quite small compared with that on antenna element when $lf=25$ mm. On the other hand, the current on the ground plane of $lf=1$ mm is much larger than that of $lf=25$ mm. So, it is considered that the current on the ground plane affect the VSWR characteristics, then the VSWR variation in the case of $lf=25$ mm observed in Fig. 3.11(a) is significantly suppressed regardless of the presence of the ground plane and its size.

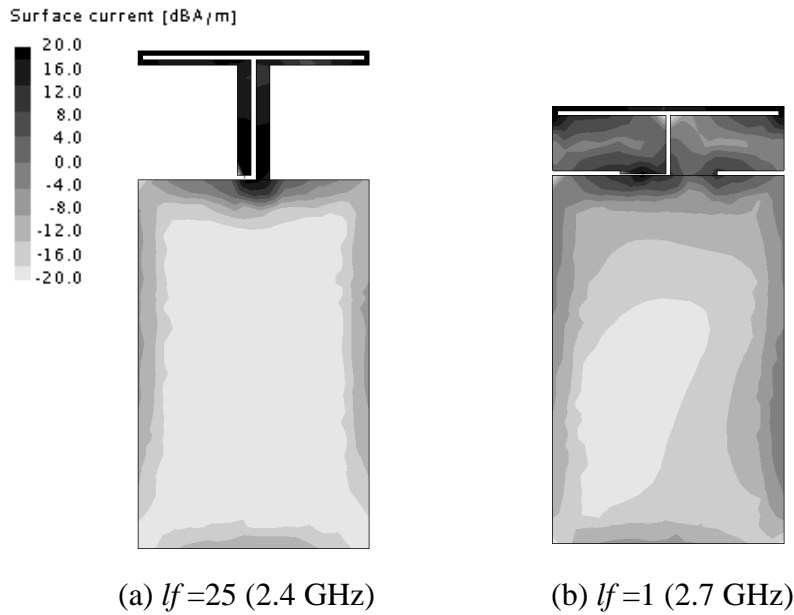


Figure 3.12: Current distributions.

3.4.3 Miniaturization of Antenna Height with Ground Plane

A. Relative Bandwidth and VSWR Characteristic

For the antenna system as a whole, low-profile antenna configuration is required. Figure 3.13 shows the relative bandwidth distribution ($VSWR \leq 3$) of FDAFL with the ground plane of size $50 \times 80 \text{ mm}^2$. This time, wa_2 and lf are respectively changed by 1 mm spacing from 1 mm to 15 mm and from 1 mm to 10 mm in order to minimize the antenna height H . The parameter wf is fixed to 10 mm because wideband characteristic is obtained when wf is more than 10 mm in Fig. 3.6(b) - Fig. 3.6(d).

In Figure 3.13, the bandwidth becomes greater than 65% at the three pairs of parameters of $(wa_2, lf) = (4 \text{ mm}, 8 \text{ mm})$, $(5 \text{ mm}, 6 \text{ mm})$ and $(6 \text{ mm}, 4 \text{ mm})$. From a viewpoint of the miniaturization, the parameters wa_2 and lf should be determined so that the sum of the values is minimized. Thus, the appropriate selection of the parameters is $(wa_2, lf) = (6 \text{ mm}, 4 \text{ mm})$, which is indicated by the circle in Fig. 3.13. In consequence, the antenna height H is reduced to 12 mm, which is approximately 43% of basic model.

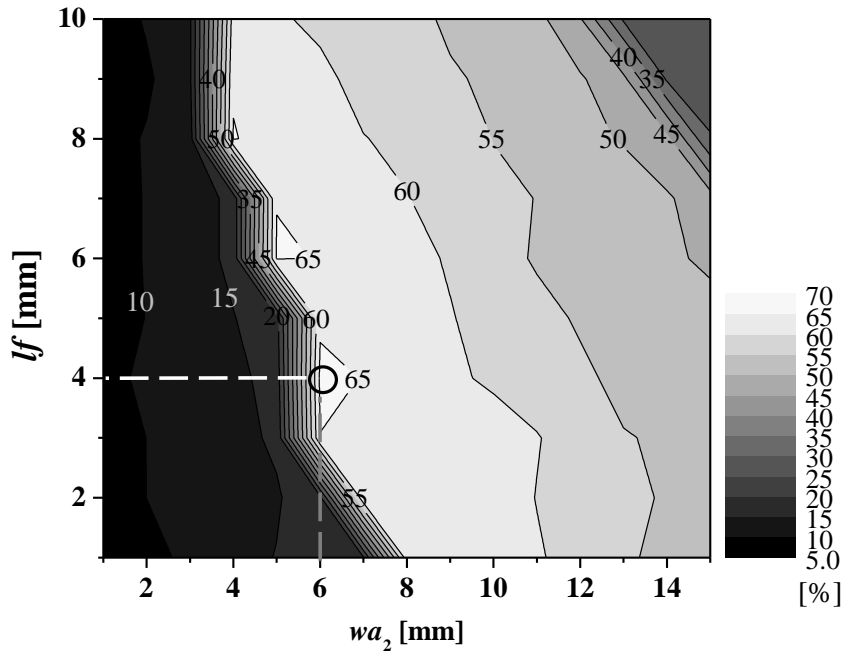


Figure 3.13: Distributions of relative bandwidth.

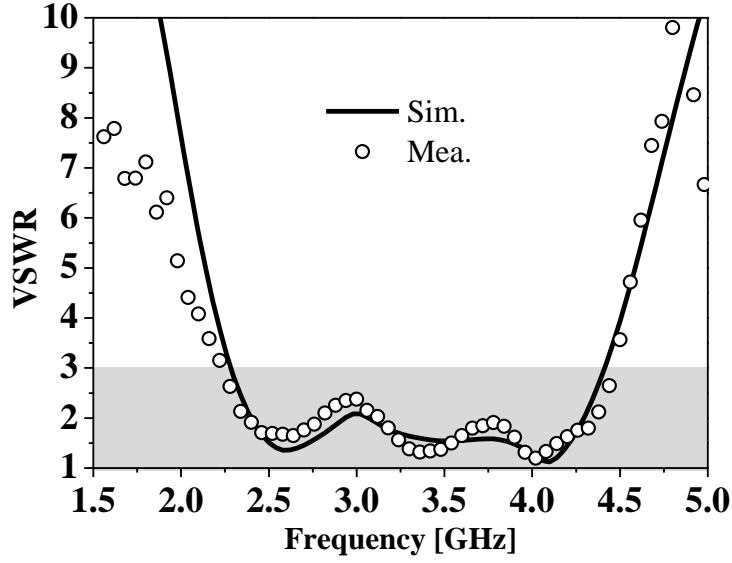


Figure 3.14: VSWR characteristics.

Figure 3.14 shows the VSWR characteristics with the parameters of $(wa_2, lf, wf) = (6 \text{ mm}, 4 \text{ mm}, 10 \text{ mm})$. The measured result is also presented in the figure. In calculation, $VSWR \leq 3$ from 2.26 GHz to 4.44 GHz are observed. Also, $VSWR \leq 3$ from 2.24 GHz to 4.47 GHz are obtained in measurement. Thus, the results show good agreement, and the relative bandwidth in calculation and measurement is 65% and 67%, respectively.

B. Radiation Characteristic

Fig. 3.15 shows the radiation patterns of FDAFL with the parameters of $(wa_2, lf, wf) = (6 \text{ mm}, 4 \text{ mm}, 10 \text{ mm})$. The evaluated frequency is the 1st resonance 2.6 GHz and the 2nd resonance 4.1 GHz. For the purpose of the comparison, the radiation patterns of FDAFL without the ground plane are also displayed in Fig. 3.15(c). Both simulated and measured results are plotted in the same plane, and very good agreement can be obtained.

In xz - and yz - planes, the cross polarization component (E_θ) becomes stronger at both frequencies compared with the case without ground plane, which is caused by the current flows on the ground plane. Thus, the gain in xz -plane at 2.6 GHz is not so high about less than -4 dBi . However, the peak gain is calculated to be 4.1 dBi (θ -component) and to 3.0 dBi (φ -component), respectively.

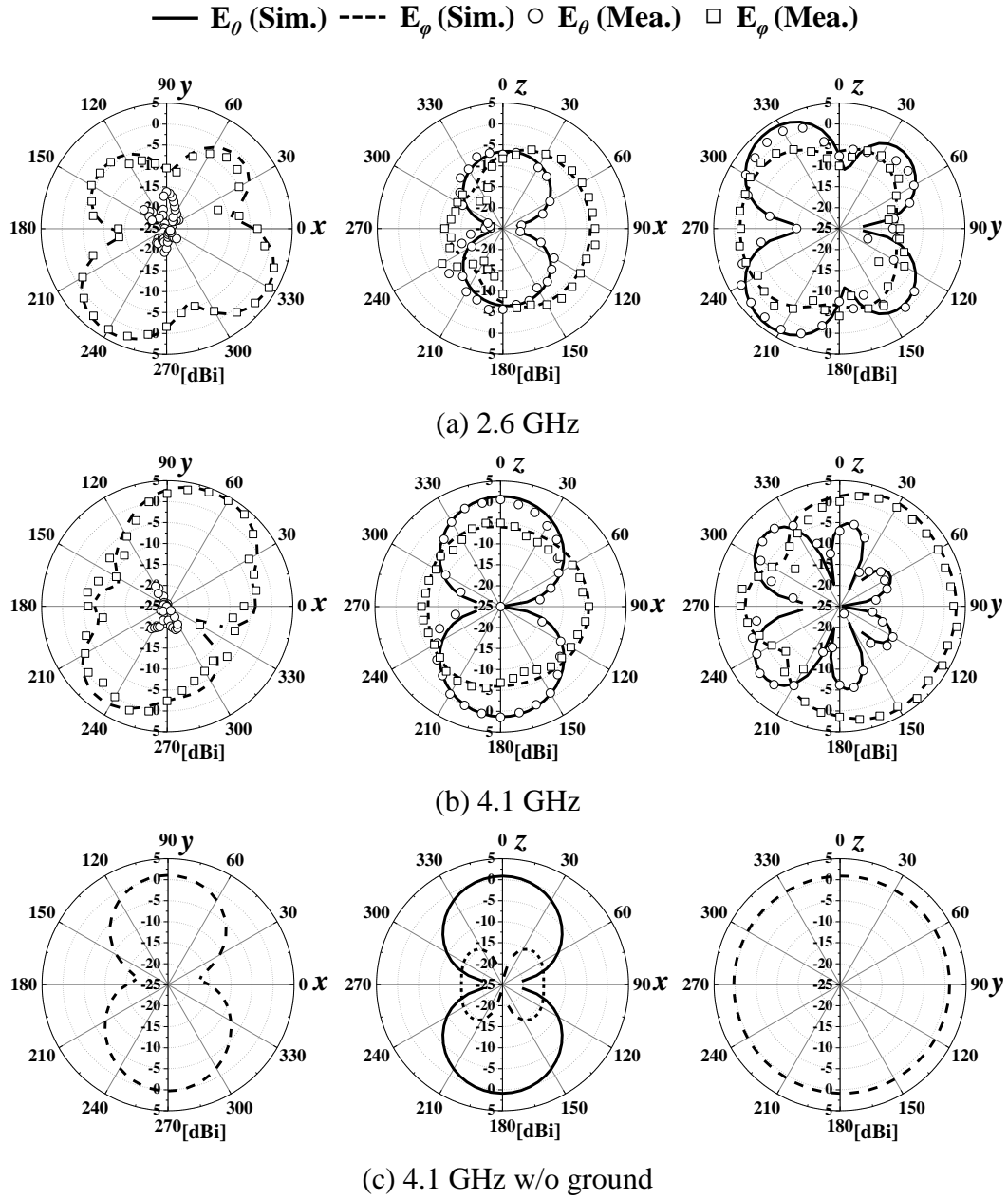


Figure 3.15: Radiation patterns.

3.5 Summary

This chapter has presented the technique for miniaturizing the feed line of FDAFL without employing meandered structure. Then, FDAFL is applied to a ground plane, and antenna characteristics are analyzed.

Impedance characteristic of FDAFL is deteriorated by shorting the length of the feed lines. However, very effective impedance transformation is possible by altering the width of wa_2 and wf , which results in low-profile antenna configuration. Not only that, broadband property of FDAFL is confirmed as the length of lf decreases. This is achieved by the increased antenna surface area. Since parameter ranges for wideband operation are clarified with respect to wa_2 and wf , it will contribute to antenna designing for real applications.

In addition, FDAFL is applied to various sizes of the ground plane assuming wireless devices such as USB dongle, wireless routers, and tablets, but wideband characteristics are maintained regardless of the different ground size. When the antenna parameters are $(lf, wa_2, wf) = (4 \text{ mm}, 6 \text{ mm}, 10 \text{ mm})$ on the ground plane of $50 \times 80 \text{ mm}^2$, it is found that the antenna height H is miniaturized up to 12 mm, which is 43% compared to the initial length. Relative bandwidth ($VSWR \leq 3$) is about 65% in calculation and 67% in measurement, which completely covers the frequency bands of WiMAX 2.5/3.5 GHz bands and WLAN 2.4 GHz band. Thus, it has been confirmed that FDAFL can be applied to a small terminal with wideband characteristic.

Chapter 4

Wideband Characteristic of 3D-FDAFL

4.1 Introduction

A number of methods are proposed for miniaturizing antenna element. The methods are mainly divided into three categories, change of the current paths, loading matching circuits, and use of materials such as dielectric and magnetic materials [85]. Therefore, forming antenna element on dielectric substrate is one of them, taking advantage of the wavelength shortening effect caused by relative permittivity. Moreover, the antenna element can be constituted on both sides of the substrate for further antenna miniaturization, which requires three dimensional (3D) antenna configurations.

In Chapter 3, the feed line of FDAFL is miniaturized by altering the widths of the antenna element and feed lines. Also, FDAFL can be applied to a small terminal, covering the frequency bands of WiMAX 2.5/3.5 GHz bands and WLAN 2.4 GHz band. However, this antenna itself is prominent from the ground plane by 12mm. In general, it is desired that the antenna does not protrude outside of the ground plane as much as possible considering the miniaturization of the antenna system as a whole. In this chapter, 3D geometry of FDAFL is proposed in order to further miniaturize a small terminal, which also assumes the 3D-antenna configuration utilizing the both sides of the substrate. When the new antenna configuration of 3D-FDAFL is considered, two types of models are possible. The first model is bent over the ground plane, and the second one is bent outside of the ground plane. Thus, the purpose of this study is to analyze the 3D antenna configurations using FDAFL so that the antenna itself does not protrude from the ground plane as much as possible. Thus, two types of 3D models are investigated with regard to relative bandwidth, the VSWR characteristics, physical volume and radiation patterns.

This chapter first presents the configurations of FDAFL and two 3D models in Sect. 4.2. In Sect. 4.3, change of the VSWR characteristics according to the different

models is exhibited. In Sect. 4.4, and 4.5, the distribution of relative bandwidth and the VSWR characteristics of each 3D model are analyzed. Then, the relation between the bandwidth, antenna height and physical volume are presented. In Sect. 4.6, measured and simulated results are compared. Finally, Sect. 4.7 draws the conclusion.

4.2 Antenna Configuration

Figure 4.1 shows the configuration of conventional FDAFL for a small terminal (Basic model). FDAFL is composed in 2D and is attached to a rectangular ground plane of size $50 \times 80 \text{ mm}^2$. The antenna parameters are adjusted so that the prominence of the antenna element from the ground becomes a minimum value. Also, the antenna covers 2.5 GHz band and 3.5 GHz band of WiMAX (2.3 GHz-3.8 GHz) with $\text{VSWR} \leq 3$. The antenna length la , lower element width wa_2 , feed line length lf and width wf are 50 mm, 6 mm, 4 mm and 10 mm, respectively. Other parameters are 1 mm. The antenna element and the ground plane are made of copper with thickness of 0.1 mm. As can be seen in Fig. 4.1, FDAFL protrudes outside of the ground plane by 12 mm.

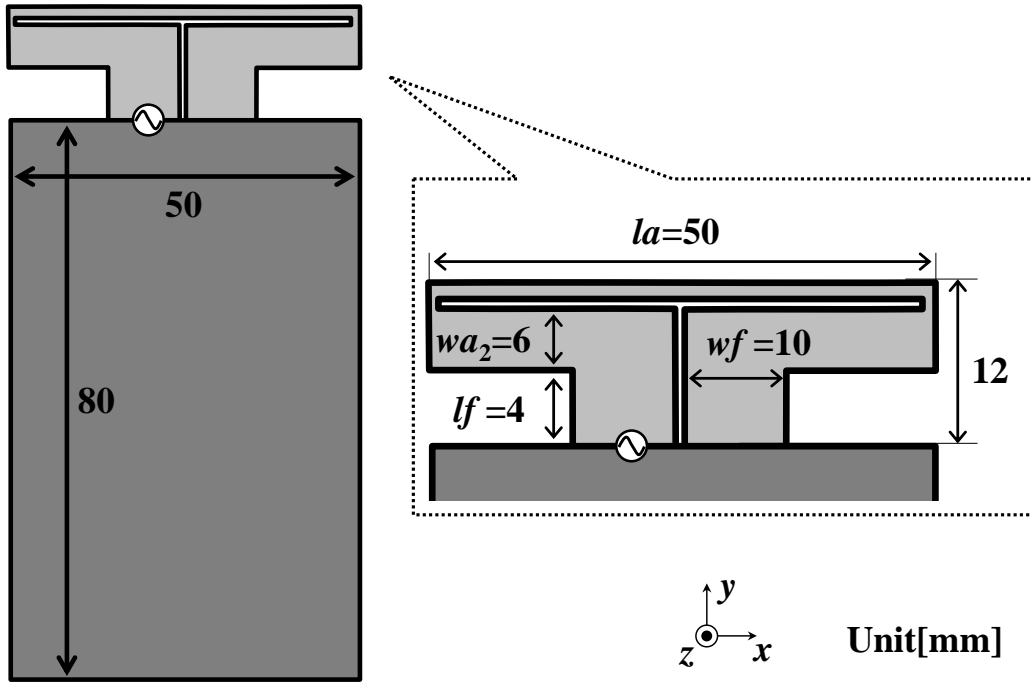


Figure 4.1: Conventional FDAFL (Basic model).

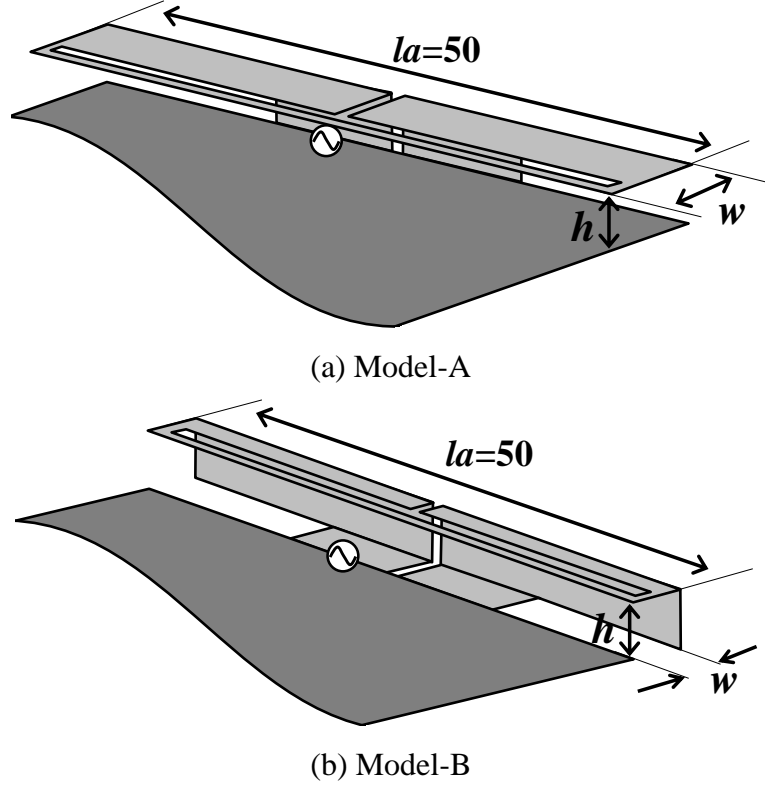


Figure 4.2: 3D models.

The two different types of models which are bent in 3D are shown in Fig. 4.2. In Model-A, Basic model is mounted over the ground plane. On the other hand, Basic model is configured outside of the ground plane in Model-B so that the leading end of the antenna element comes just over the upper edge of the ground plane. These antennas are constructed in 3D by bending Basic model of Fig. 4.1. We define that the antenna height from the ground is h and the antenna width represented in Fig. 4.2 is w . The physical volume (PV) of the antenna, which is also studied in the following sections, is defined as follow.

$$PV = la \times w \times h \quad [mm^3] \quad (4.1)$$

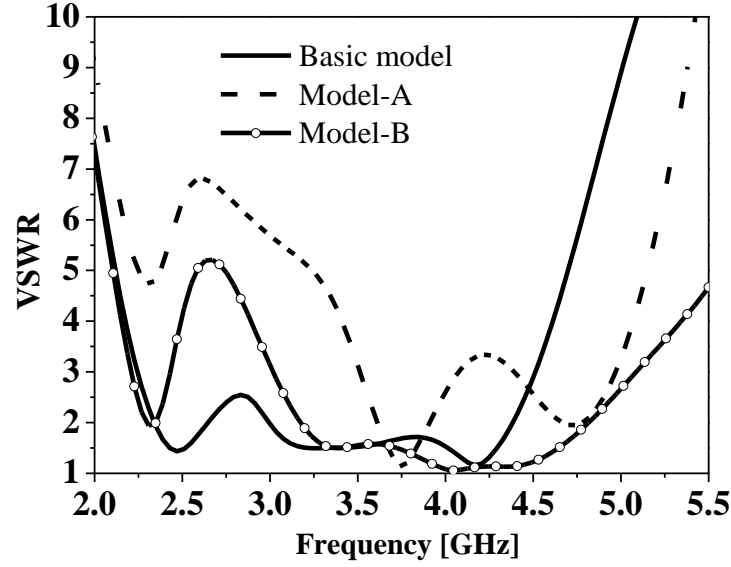


Figure 4.3: VSWR characteristics of three models.

4.3 Change of VSWR Characteristic according to the Models

Figure 4.3 shows the VSWR characteristics of three models; Basic model, Model-A and Model-B when these models have the same shape in 2D as Fig. 4.1. Thus, h and w become 4 mm and 8 mm, respectively in Model-A, and 4 mm for both in Model-B. In Fig. 4.3, Basic model has wideband characteristic, and its relative bandwidth is approximately 65% ($\text{VSWR} \leq 3$). Moreover, it can be seen that the VSWR characteristics of Model-A and Model-B are degraded around 2.5 GHz. However, the broadband characteristic of Model-B is more widely maintained compared to that of Model-A. This is because the input impedance characteristic of the antenna is deteriorated as the antenna approaches to the ground plane. In fact, the input impedance characteristic is improved by trimming the ground plane [86]. Thus, it is considered that it is more difficult for Model-A to obtain a wide band.

4.4 Analysis of Model-A

4.4.1 Relative Bandwidth

Figure 4.4 shows the distributions of the relative bandwidth ($\text{VSWR} \leq 3$) for h values of

8 mm, 7 mm, 6 mm and 5 mm when wa_2 and wf are altered from 2 mm to 11 mm and 5 mm to 14 mm, respectively. Each parameter is changed by 1 mm. In the figure, it is found that when h is greater than 7 mm, relative bandwidth of over 70% is obtained. However, the area of white part, which represents wider bandwidth, is confined to a few combinations of wa_2 and wf . On the other hand, when h is less than 6 mm, the value of relative bandwidth is under 50% mostly. Furthermore, there is a tendency that wider wa_2 is required in order to obtain broadband characteristics as the antenna height becomes large, which means the antenna width w is also becomes large. Thus, it is confirmed that when h is larger than 7 mm, Model-A becomes a more broadband characteristic than Basic model by adjusting the two parameters; wa_2 and wf appropriately.

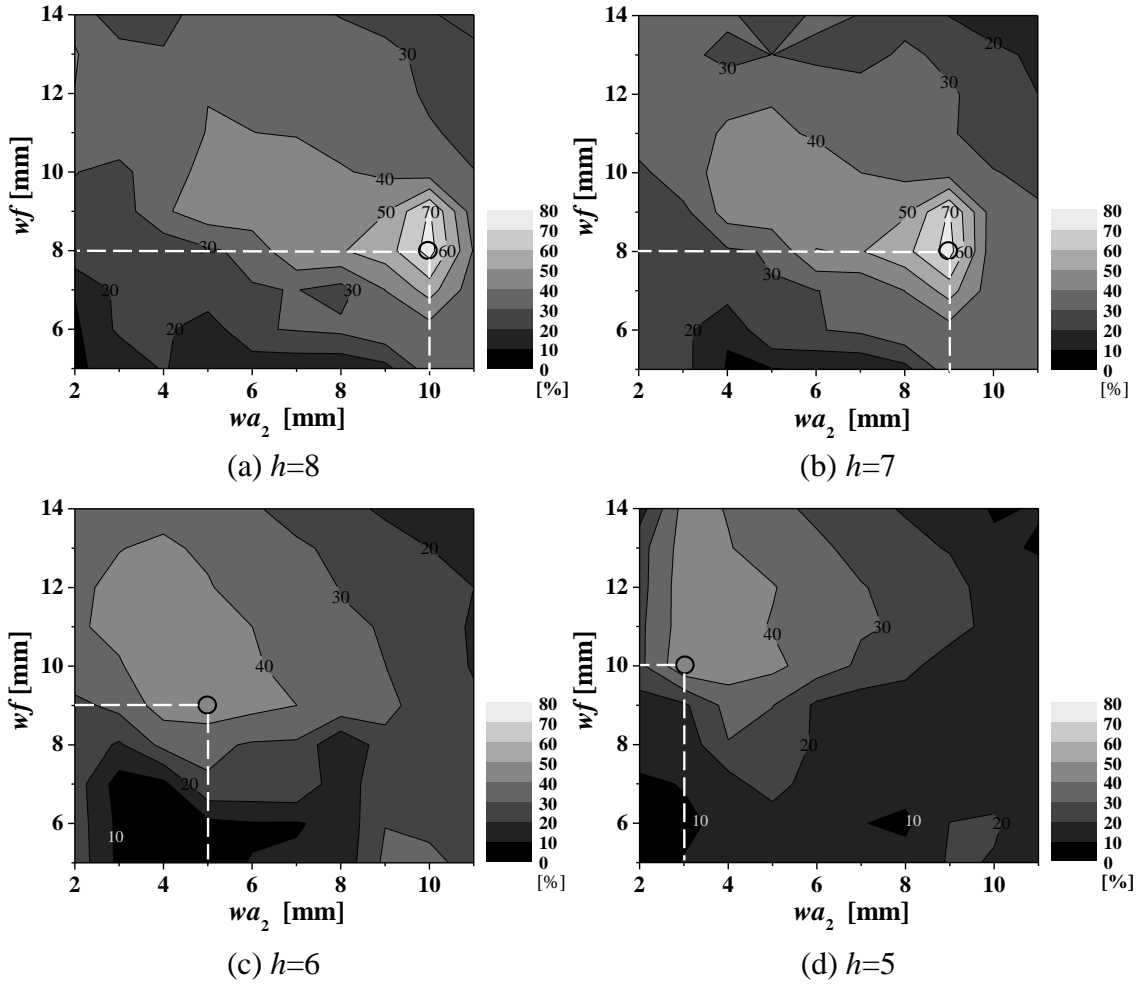


Figure 4.4: Distributions of relative bandwidth (Model-A).

4.4.2 VSWR Characteristic

Figure 4.5 shows the VSWR characteristics with respect to antenna height. Parameters of each antenna height are shown in Fig. 4.4 by the small circle, where the largest value of the relative bandwidth is obtained. In the figure, the minimum operational frequency is about 2.15 GHz, and it does not change so much at each antenna height. However, at the height of 5 mm and 6 mm, the VSWR is considerably degraded between 2.3 GHz and 3.2 GHz, while wideband characteristic is obtained at $h=7$ and 8 mm. This is because the value of wa_2 is quite different between $h=5, 6$ mm and $h=7, 8$ mm in order to find the best antenna parameters showing the widest bandwidth. Thus, broadband characteristics cannot be maintained at small values of h .

Table 4.1 shows the relation between the antenna parameters, relative bandwidth and physical volume of Model-A at each antenna height. In the table, it can be seen that the antenna width w and physical volume of Model-A are increased as the height becomes large. This is because the parameter wa_2 is needed to be large in order to attain the broadband, then w also becomes large at the same time. Therefore, the physical volume increases. It is considered that this broadband characteristic is achieved due to the increased antenna height and surface area caused not by wf , but by wa_2 since wf hardly changes compared to wa_2 in Table 4.1. Thus, even though it is possible for Model-A to obtain the broadband characteristics by adjusting wa_2 and wf , the antenna height, width and physical volume are increased.

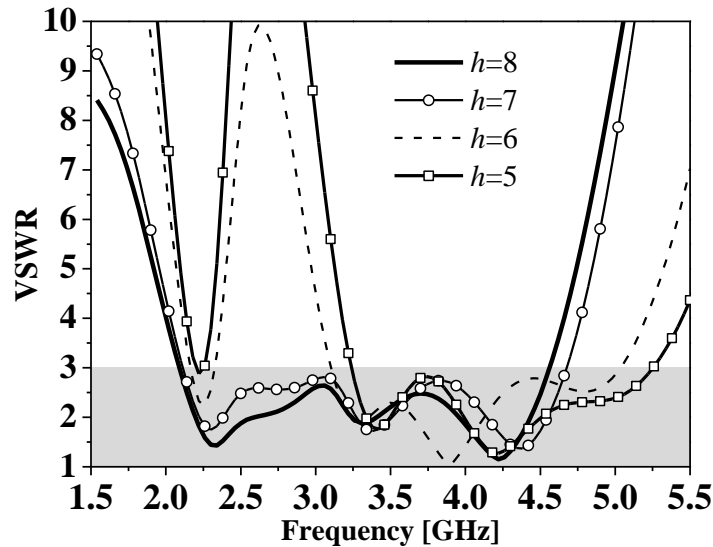


Figure 4.5: VSWR characteristics of Model-A with respect to antenna height h .

Table 4.1: Comparison of H , relative bandwidth, and metal area.

h [mm]	wa_2 [mm]	wf [mm]	w [mm]	Relative bandwidth ($VSWR \leq 3$) [%]	Physical volume [mm ³]
8	10	8	8	74.1	3200 (100%)
7	9	8	8	74.3	2800 (87.5%)
6	5	9	5	47.6	1500 (46.9%)
5	3	10	4	47.4	1000 (31.3%)

4.5 Analysis of Model-B

4.5.1 Relative Bandwidth

Figure 4.6 shows the distributions of the relative bandwidth ($VSWR \leq 3$) for h values of 4 mm, 3 mm, 2 mm and 1 mm. wa_2 and wf are altered from 7 mm to 16 mm and 5 mm to 14 mm, respectively in Figs. 4.6(a), (b), and (c). Only in Fig. 4.6(d), wa_2 are changed from 12 mm to 21 mm. Also, each parameter is changed by 1 mm. As can be seen from each figure, relative bandwidth of over 80% is obtained at each antenna height. However, the area of relative bandwidth over 80% is very limited, and there are only two or three combinations of the parameters at each antenna height. But, the area of relative bandwidth over 60% is widely spread, which cannot be observed in Model-A. Furthermore, there is a tendency that wider wa_2 is required to obtain broadband characteristics as the antenna height becomes low. Thus, it is also clear that Model-B gives a more wideband characteristic than Basic model and Model-A by the proper adjustment of wa_2 and wf .

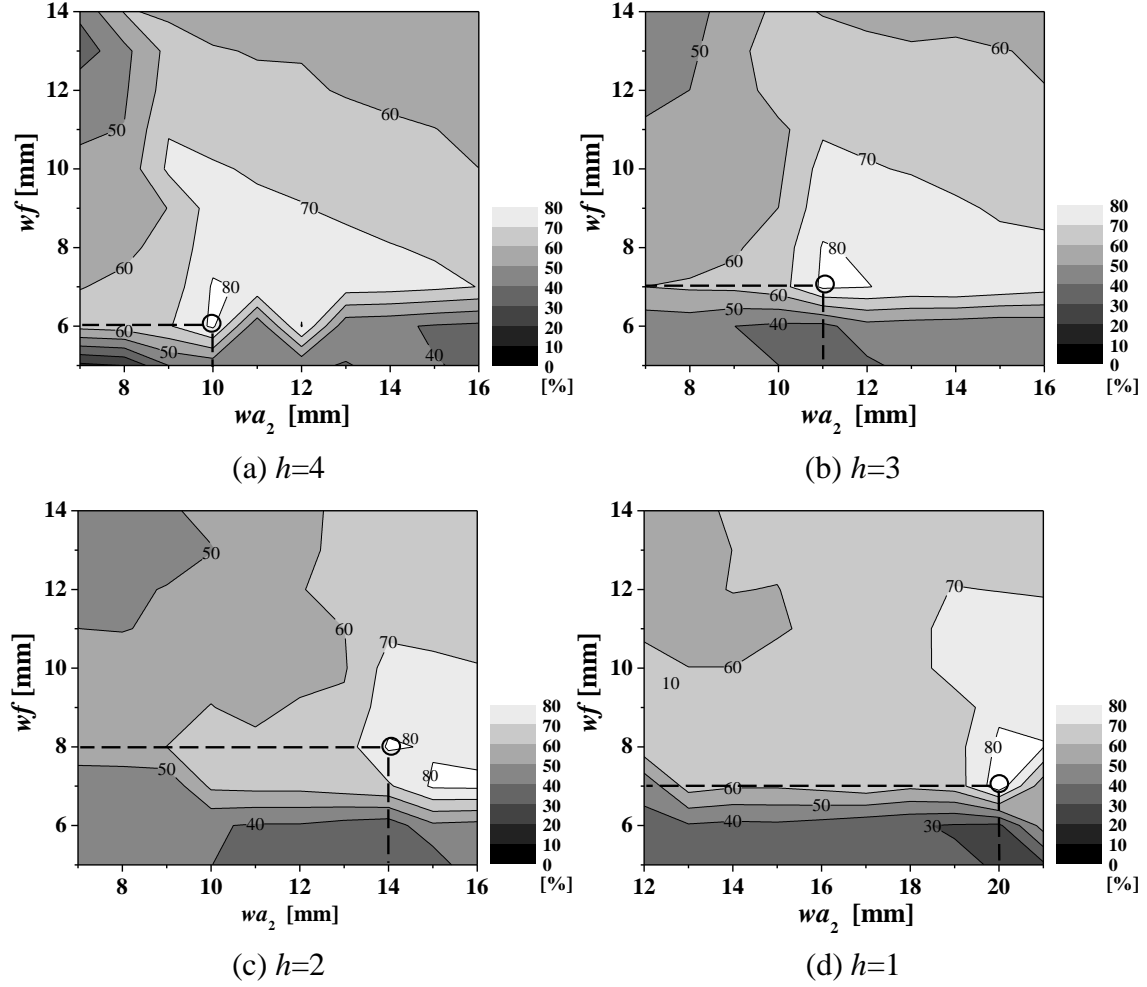


Figure 4.6: Distributions of relative bandwidth (Model-B).

4.5.2 VSWR Characteristic

The VSWR characteristics of each antenna height are shown in Fig. 4.7. In the same way, parameters of each antenna height are indicated in Fig. 4.6 by the small circle, where the largest value of relative bandwidth is obtained. Similar VSWR characteristics are observed in Fig. 4.7, and the minimum operational frequency is approximately 1.9 GHz at $h=4$ mm, 3mm and 2mm. At $h=1$ mm, the frequency is lowered to 1.69 GHz since the total length of the antenna is increased because of the extended width of wa_2 .

Table 4.2 shows the relation between the antenna parameters, relative bandwidth and physical volume of Model-B at each antenna height. From the table, the relative bandwidth does not change so much, and when h is 1 mm, the bandwidth is 86.8%, which is the largest value. Similarly, it is considered that this broadband characteristic is

attained by the increased antenna surface area caused by wa_2 because wf hardly changes. Furthermore, the physical volume is reduced up to 625 mm^3 (52.1%) compared to 1200 mm^3 (100%) of $h=4 \text{ mm}$. These values are highly affected by h and w . In fact, the antenna width w of $h=1 \text{ mm}$ becomes more than twice that of $h=4 \text{ mm}$. Thus, it is difficult to realize the miniaturization of h and w simultaneously, and the combinations of h and w should be selected according to its application.

In Table 4.2, the physical volume of antenna is decreased to 52.1% from $h=4 \text{ mm}$ to 1 mm . Meanwhile, the relative bandwidth are slightly increased to 86.8% at $h=1 \text{ mm}$. It is empirically well known that the bandwidth is also decreased with decreasing the volume of the antenna simultaneously, which can also be seen in Fig. 1.3. In order to analyze the reason for that, the current distributions of each antenna height at the 1st resonant frequency are shown in Fig. 4.8.

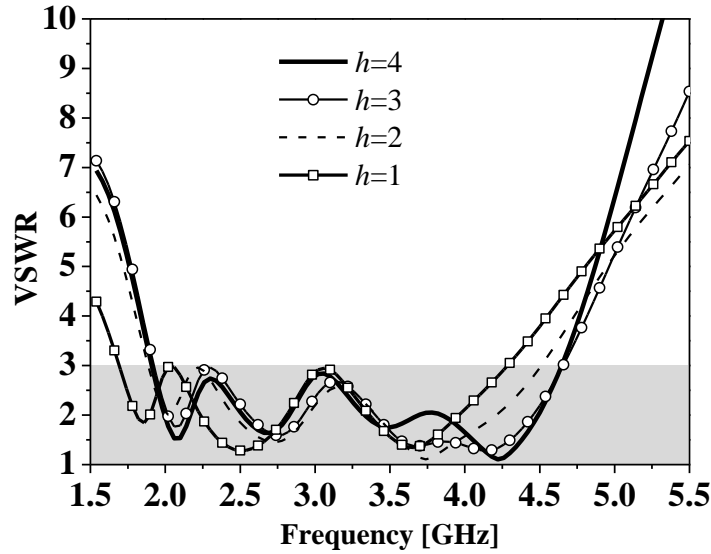


Figure 4.7: VSWR characteristics of Model-B with respect to antenna height h .

Table 4.2: Comparison of H , relative bandwidth, and metal area.

h [mm]	wa_2 [mm]	wf [mm]	w [mm]	Relative bandwidth ($\text{VSWR} \leq 3$) [%]	Physical volume [mm^3]
4	10	6	6	83.5	1200 (100%)
3	11	7	7	83.0	1050 (87.5%)
2	14	8	9	82.1	900 (75.0%)
1	20	7	12.5	86.8	625 (52.1%)

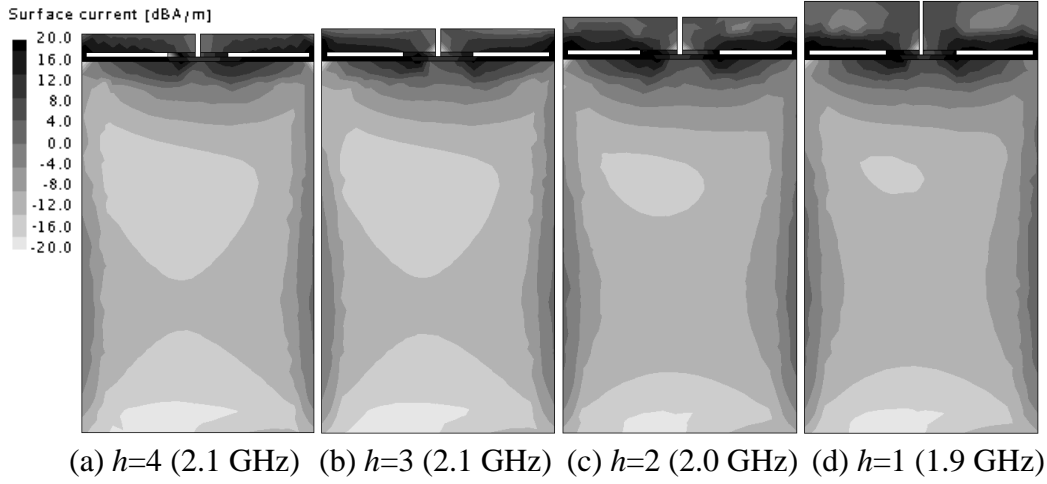


Figure 4.8: Current distributions at the 1st resonant frequency.

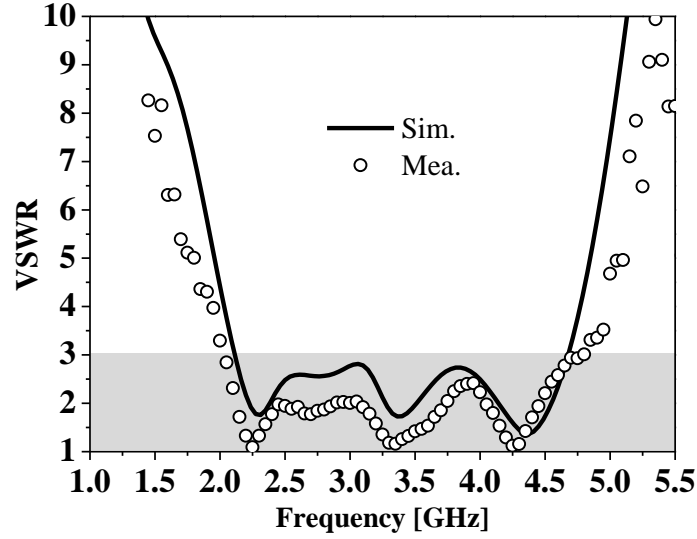
It is obvious in the figure that the current on the ground plane is also slightly increased with decreasing antenna height, and this ground plane can be regarded as part of a radiator because relatively large current is observed compared with the current on the antenna element. Also, since the large current is most widely spread on the ground when $h=1$ mm, it seems that the contribution of the current to the radiation is largest, which means the electrical volume of antenna is also maximum based on the concept of Wheeler. Therefore, although the physical volume of antenna is decreased and the relative bandwidth is slightly increased to 86.8% when $h=1$ mm, this is achieved at the expense of the current on the ground plane, and the electrical volume of antenna is also slightly increased.

4.6 Measured Results and Comparisons

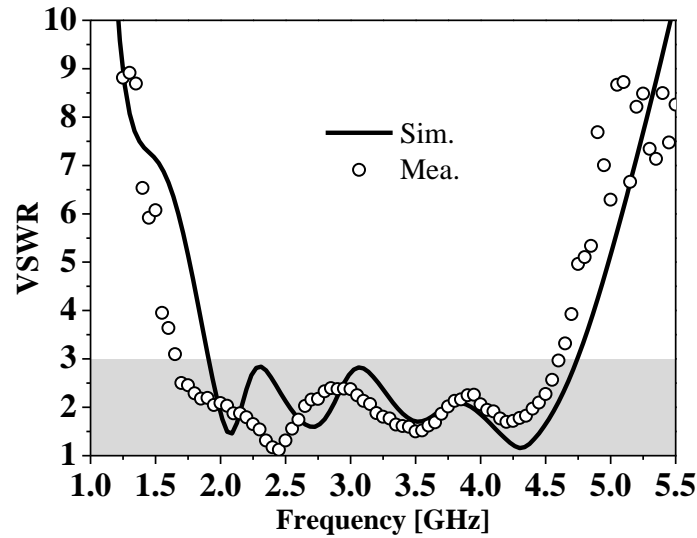
By the analysis described above so far, it is shown that w can be decreased at the expense of the antenna height in Model-B, and the two 3D configurations of FDAFL have wider bandwidth than Basic model. In this section, each antenna from both Model-A and Model-B is fabricated and measured. The parameters are selected in order to minimize the prominence while maintaining wider bandwidth than Basic model. Comparisons between measured and simulated results are conducted. Furthermore, with respect to radiation patterns and current distributions, comparison among three models is also conducted for the further understanding of radiation mechanisms.

4.6.1 VSWR Characteristic

Figure 4.9 shows the comparison between simulated and measured VSWR characteristics of Model-A with $h=7$ and Model-B with $h=4$ mm. The parameters of wa_2 and wf are 9 mm, 8 mm and 10 mm, 6 mm as indicated in Table 5.1 and 5.2, respectively. Good agreement is observed between the simulated and measured results for the both cases. In Model-A, $VSWR \leq 3$ is obtained from 2.05 GHz to 4.65 GHz by the measurement, so the measured bandwidth is about 78%. As for Model-B, $VSWR \leq 3$ is observed from 1.68 GHz to 4.63 GHz. Thus, the measured bandwidth is approximately 93%.



(a) Model-A ($h=7$)



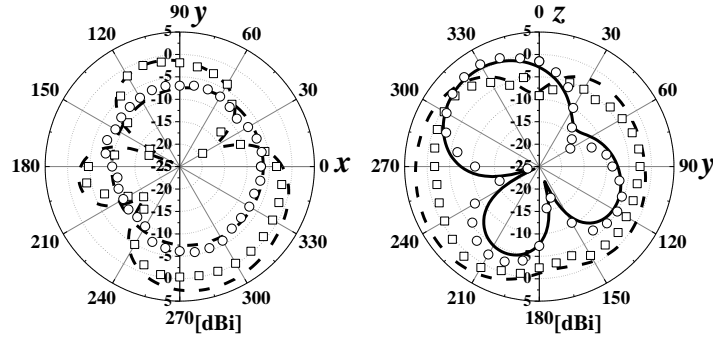
(b) Model-A ($h=4$)

Figure 4.9: Comparison of VSWR characteristics between simulation and measurement.

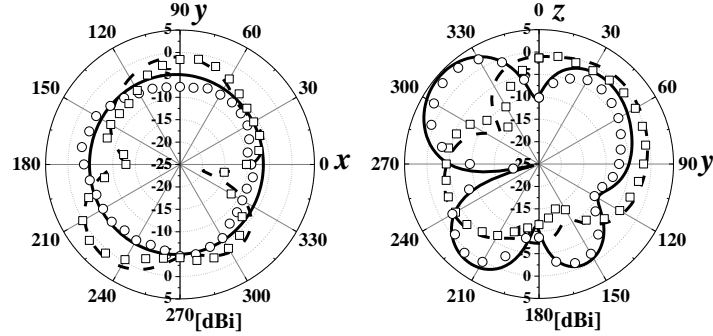
4.6.2 Radiation Characteristic and Current Distribution

Figure 4.10 and 4.11 shows the radiation patterns of Model-A with $h=7$ and Model-B with $h=4$ mm, respectively. The evaluated frequencies are 2.5 GHz and 3.6 GHz, which are the central frequencies of each 2.5/3.5 GHz bands of WiMAX. A good agreement is seen between the simulated and measured results. In xy -plane, larger cross polarization component is observed in Model-A compared to Model-B at both frequencies. Figure 4.12 shows the current distributions of each model at 2.5 GHz. Larger current is observed on the antenna element along z -axis in Model-A. Thus, it is considered that cross polarization component in xy -plane of Model-A is caused by the current along z -axis. Also, in the paper [62], the identical analysis is shown, and the paper reaches the same conclusion.

— E_θ (Sim.) ---- E_ϕ (Sim.) \circ E_θ (Mea.) \square E_ϕ (Mea.)



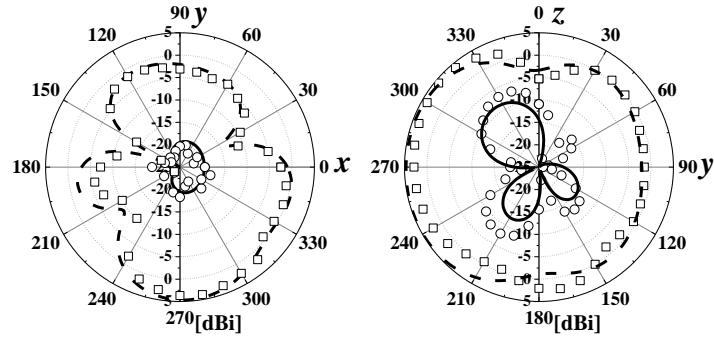
(a) 2.5 GHz



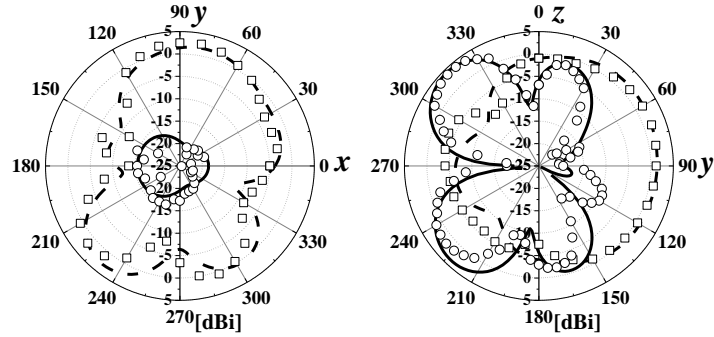
(b) 3.6 GHz

Figure 4.10: Radiation patterns (Model-A, $h=7$).

— E_θ (Sim.) ---- E_ϕ (Sim.) \circ E_θ (Mea.) \square E_ϕ (Mea.)

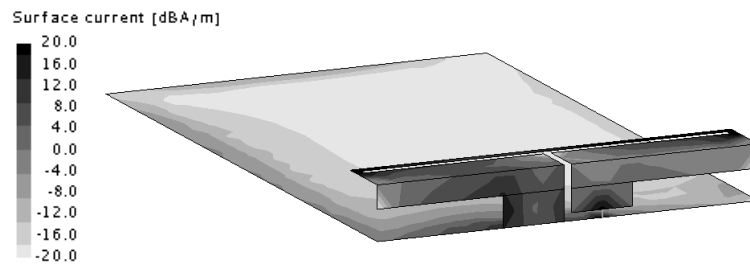


(a) 2.5 GHz

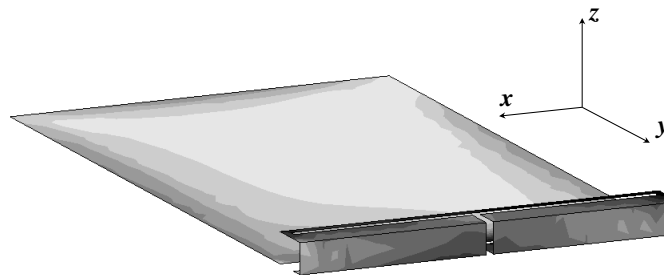


(b) 3.6 GHz

Figure 4.11: Radiation patterns (Model-B, $h=4$).



(a) Model-A ($h=7$)



(b) Model-B ($h=4$)

Figure 4.12: Current distributions at 2.5 GHz.

Figure 4.13 and 4.14 show the simulated 3D total radiation patterns of the three models at 2.5 GHz and 3.6 GHz. In Model-A ($h=7$), nulls are obviously improved especially in xy and yz directions compared to other two models at both frequencies. In Model-B ($h=4$), more nulls appear compared to Model-A, but better omnidirectional characteristic is obtained than Basic model at each frequency. Since this antenna system is assumed and designed for a small terminal such as mobile router for WiMAX, it is thought that omnidirectional radiation patterns and the high cross polarization level shown in Model-A are more favorable for multipath environment [87].

Figure 4.15 shows the variation of the peak gain in 3D (including impedance mismatch loss). In Model-A, the gains of $h=5$ mm and 6 mm are degraded to less than 1 dBi around 2.5 GHz due to the impedance mismatch loss as indicated in Fig. 4.5. In Model-B, more than 2 dBi is, however, observed through the both 2.5 GHz and 3.5 GHz bands of WiMAX at each antenna height. Table 4.3 shows the average peak gain from 1.5 GHz to 5.0 GHz. Since average peak gain of basic model is 2.90 dBi, the peak gain is enhanced except $h=5$ mm and 6 mm of Model-A and $h=1$ mm of Model-B. Therefore, the major degradation of gain is not generated by altering the antenna configuration from 2D to 3D model.

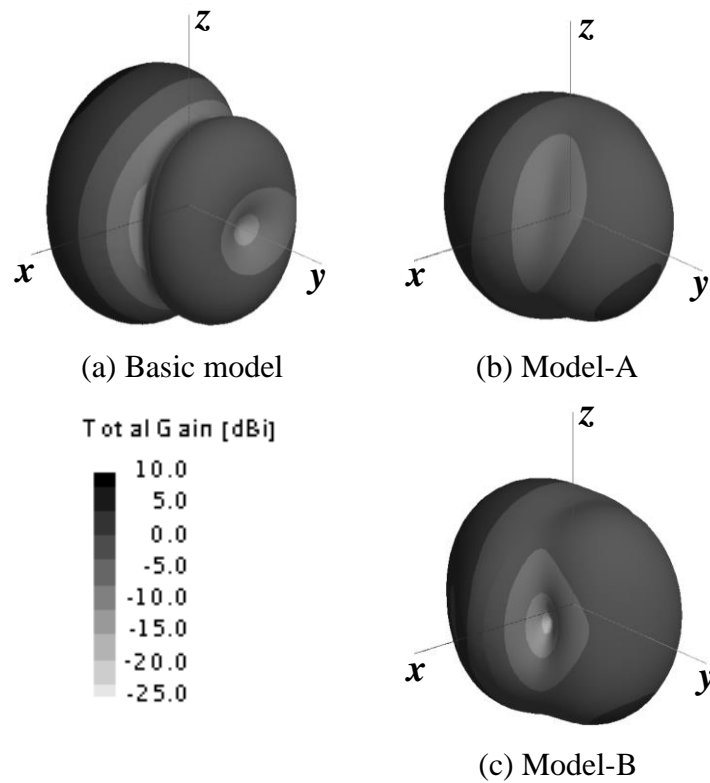


Figure 4.13: 3D radiation patterns at 2.5 GHz.

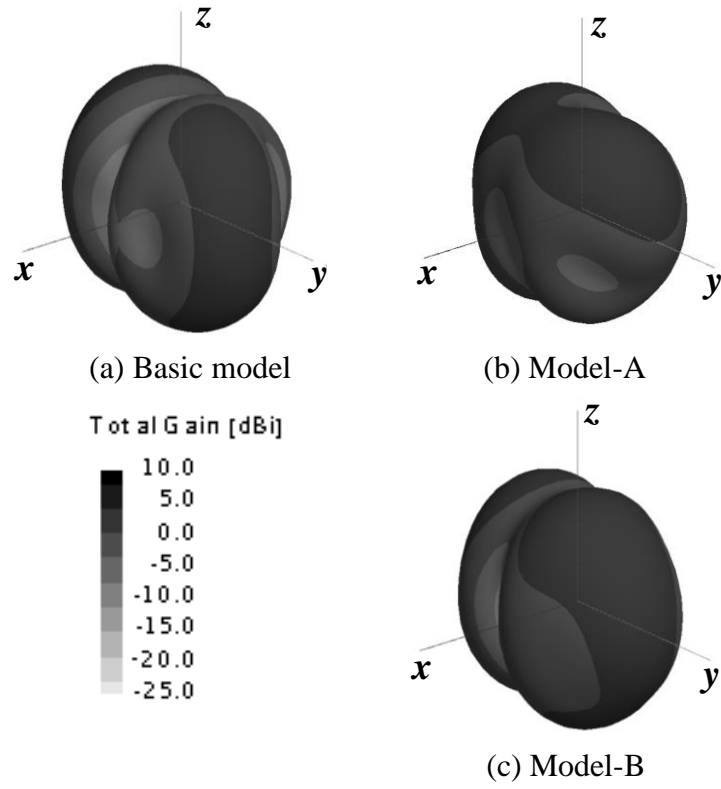
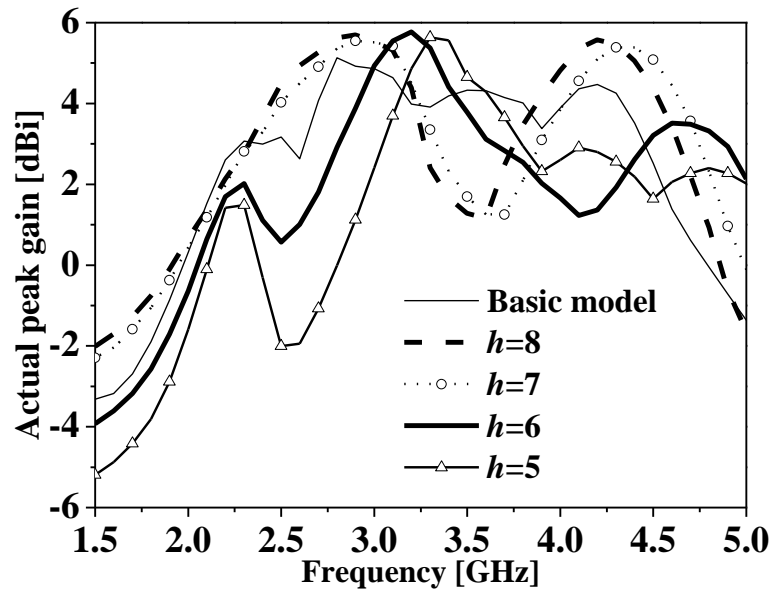
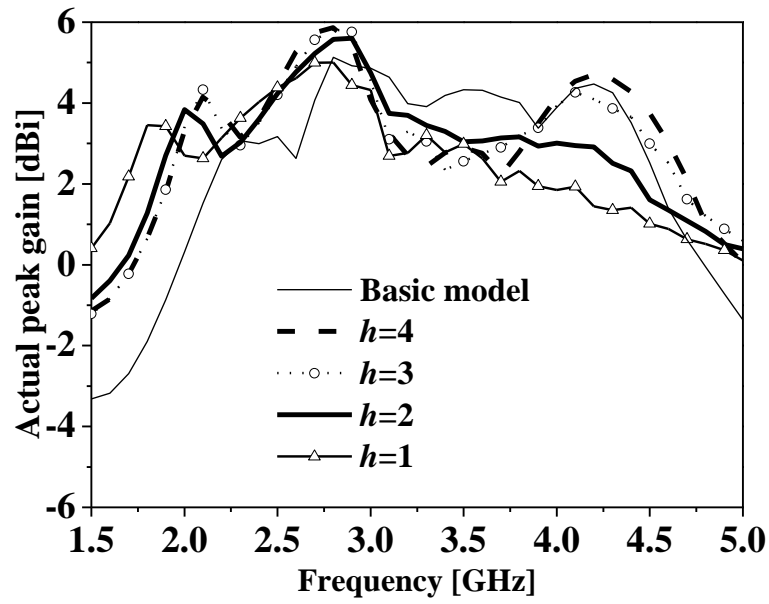


Figure 4.14: 3D radiation patterns at 3.6 GHz.



(a) Model-A



(b) Model-B

Figure 4.15: Simulated peak gain (ϕ -component).Table 4.3: Average peak gain from 1.5 GHz-5.0 GHz (ϕ -component).

h [mm]	Model-A [dBi]	h [mm]	Model-B [dBi]
8	3.32	4	3.31
7	3.26	3	3.22
6	2.45	2	3.02
5	1.96	1	2.70

4.7 Summary

In this chapter, the relative bandwidth, the VSWR characteristics and radiation characteristics of two 3D models of FDAFL have been investigated in order to minimize the prominence from the ground. Model-A is bent over the ground plane, and Model-B is bent outside of the ground plane.

As for Model-A, due to the effect of the ground plane, it is difficult to obtain a wider bandwidth at small values of h , while the antenna prominence from the ground plane is zero. However, since impedance transformation is possible by changing wa_2 and wf , the relative bandwidth over 74% is obtained when h is greater than 7 mm. Thus, more than 7 mm of h is required in order to obtain wider bandwidth than Basic model, which is about 65%. As for Model-B, very broadband characteristics over 86% were achieved even $h=1$ mm. Also, it was confirmed that w can be decreased from 12.5 mm to 6 mm with the bandwidth over 83% when $h=4$ mm. Therefore, at least 4 mm of h is required in order to reduce the prominence by half. In both cases, these 3D models can show wider bandwidth than Basic model.

Furthermore, by performing an experiment in both Model-A and Model-B, the analytical validity of the simulation could be confirmed. Parameter ranges for wideband operation are shown in detail, so it will help to design antennas for real application.

Chapter 5

MIMO Antenna Derived from FDAFL with Parasitic Element

5.1 Introduction

Due to the recent increase of high-speed large-capacity data transmission, MIMO system is the key technology to realize higher wireless communication speeds [34], [88]. MIMO system creates parallel data streams on a single channel, which increases the channel capacity and data throughput. Also, LTE/LTE-Advanced, WLAN (IEEE 802.11n/ac), and WiMAX/WiMAX2 introduce MIMO system. Thus, MIMO technology is necessary in today's wireless communication. In fact, many studies have addressed MIMO antennas [89]-[92]. The operational frequency bands of WiMAX and WLAN are 2.5/3.5/5.5 GHz bands (2.3-2.7/3.4-3.8/5.25-5.85 GHz) and 2.4/5 GHz bands (2.4-2.48/5.15-5.875 GHz), respectively [93]-[94].

On the other hand, since multi-antenna system takes more space in the small terminal, miniaturization of antenna elements is also necessary. Otherwise, the distance between the antenna elements becomes too close, which causes large pattern/spatial correlation and strong mutual coupling. Thus, radiation efficiency degrades, which eventually leads to the deterioration of effect of multi-antenna system. Thus, mutual coupling between the antenna elements should be carefully considered [37]-[39].

In Chapter 4, two types of 3D FDAFL are proposed for miniaturizing the antenna system. These 3D FDAFLs show wider bandwidth, 74% and 83% ($VSWR \leq 3$), than conventional planar FDAFL. However, since these FDAFLs cover only the lower frequency bands of WiMAX and WLAN applications, wideband or multiband operation of the antennas is highly required. Furthermore, consideration of MIMO systems for small terminals is indispensable in recent years. In this chapter, a wideband folded monopole antenna (FMA) is proposed as a variant of the 3D FDAFL, and suitable configuration of FMA array for the realization of WiMAX and WLAN MIMO antenna is investigated. Also, in order to present the wider bandwidth of FMA, the bandwidth of

FMA is compared with that of a planar inverted-F antenna (PIFA), which is widely used in wireless communication [94]-[97]. In addition, parasitic elements are applied in order to obtain one more resonance around 5 GHz, where the conventional FDAFL does not cover. Also, the basic characteristics, such as the S-parameter characteristics, antenna efficiencies, envelope correlation coefficients and radiation patterns are analyzed.

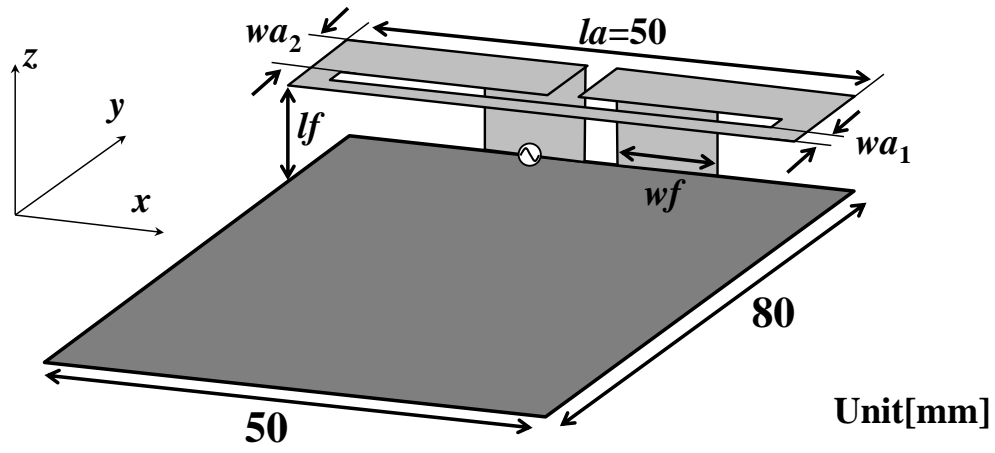
This chapter first presents the wideband characteristics of FMA in Sect. 5.2. In Sect. 5.3, suitable configuration for small terminal MIMO system is analyzed with four different FMA array models. Then, in Sect. 5.4 and 5.5, parasitic elements are introduced in the vicinity of FMA for covering the higher frequency bands of WiMAX and WLAN applications. Finally, conclusions of the chapter are given in Sect. 5.6.

5.2 Wideband Characteristic of FMA

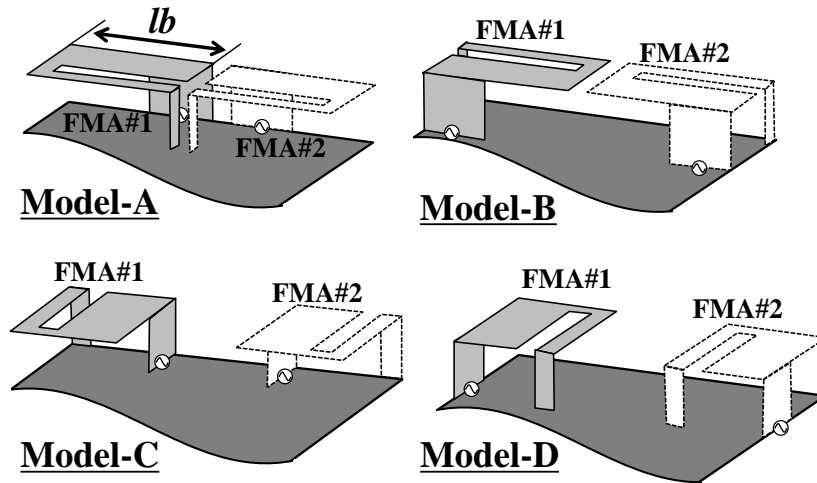
5.2.1 Antenna Configuration

Figure 5.1 shows the antenna configurations of the conventional 3D FDAFL and four different models of FMA (Model-A - Model-D). In Fig. 5.1(a), FDAFL is mounted over a rectangular ground plane of size $50 \times 80 \text{ mm}^2$. The antenna parameters are adjusted so that the VSWR becomes less than 3 in 2.5 and 3.5 GHz bands of WiMAX (2.3-3.8 GHz). The antenna length la , antenna element width wa_2 , feed line length lf and width wf are 50 mm, 10 mm, 9 mm and 10 mm, respectively. Other parameters are 1 mm. Figure 5.1(b) shows the four configurations of FMA which are derived from the FDAFL of Fig. 5.1 (a) by shorting the cut end of wa_1 to the ground plane. Antenna length lb is 23.5 mm, which is approximately half length of FDAFL, and the other parameters such as wa_2 , lf and wf are the same as the FDAFL. These four models are arranged so that each feed point, fed by a 50Ω coaxial cable in measurement, is located on a different side of the ground plane. Each antenna described by dash line in Fig. 5.1(b) is the case of FMA array, which is symmetric with respect to the centerline of the ground plane, and this is discussed in Sect. 5.3 and 5.5.

Figure 5.2 shows a PIFA for the comparison of relative bandwidth. It is composed of a 16.8 mm square, and the height is 9 mm. The parameters of the PIFA element are adjusted so that its minimum operational frequency is the same as FMA. Also, PIFA and FMA have almost the same physical volume ($\approx 2540 \text{ mm}^3$).



(a) Conventional 3D FDAFL



(b) Four types of FMA (FMA array-dash line)

Figure 5.1: Antenna configuration.

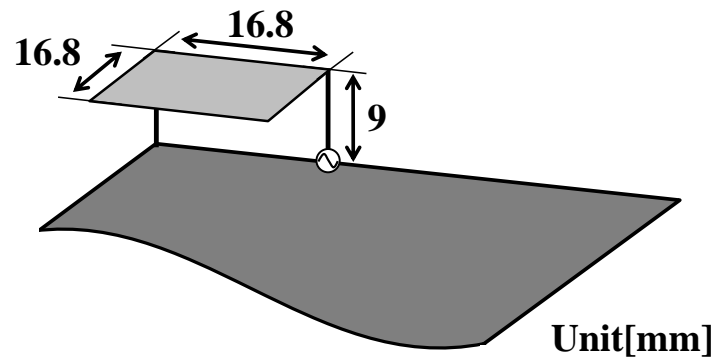


Figure 5.2: Configuration of PIFA used for the bandwidth comparison.

5.2.2 VSWR Characteristic and Current Distribution

Figure 5.3 shows the calculated VSWR characteristics of FDAFL and each model of FMA. In this case, only single FMA is placed on the ground plane as seen in Fig. 5.1(b). The VSWR characteristics are similar among the FMA models, but the bandwidth of FMAs is narrower than that of FDAFL. However, broadband characteristics are maintained, and WiMAX 2.5/3.5 GHz bands and WLAN 2.4 GHz band (2.3-3.8 GHz) are completely covered by FMAs except slight degradation of Model-A around 3.5 GHz. Also, each model of FMA has two resonant frequencies.

Figure 5.4 shows the current distributions of Model-A at each resonant frequency. The arrows in Fig. 5.4 show the vector of the current flow. Large current is observed on the element of wa_1 at 2.62 GHz and on the element of wa_2 at 3.86 GHz. In fact, the VSWR value of the second resonance changes significantly compared with the first one by altering the width of wa_2 , which is shown in Fig. 5.5. Also, the vector of the current flow is equivalent to the case of FDAFL, where the current distributions on the elements of wa_1 and wa_2 are dominant at the first and second resonant frequencies, respectively. Thus, the operating element of FMA is different at each resonant frequency, and the width of wa_2 contributes to the wideband characteristics of FMA

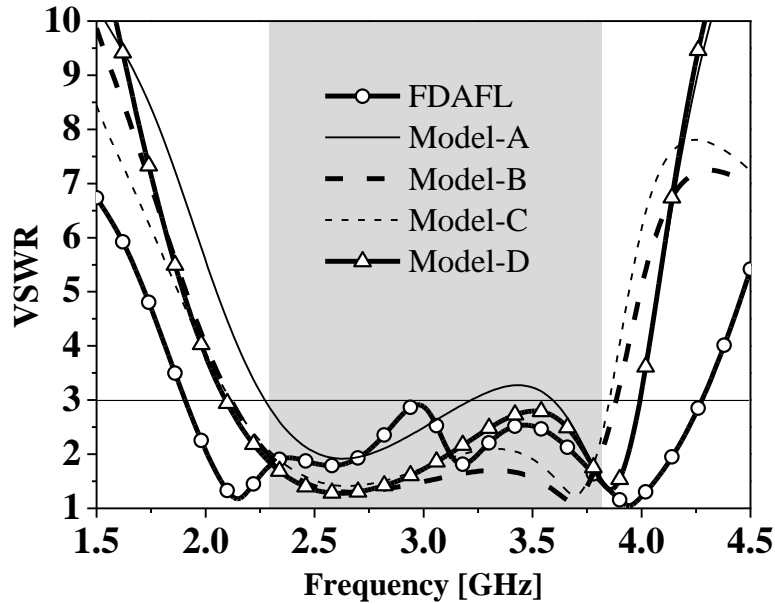


Figure 5.3: VSWR characteristics of FDAFL and FMAs.

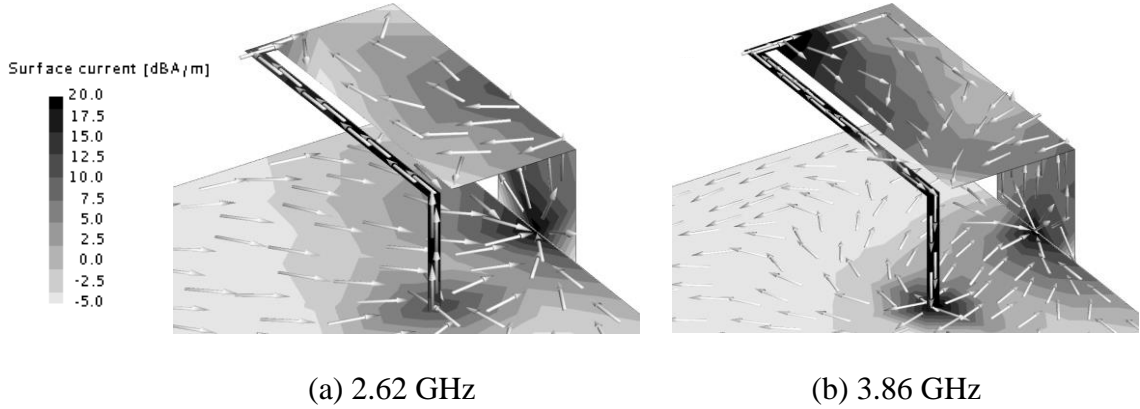
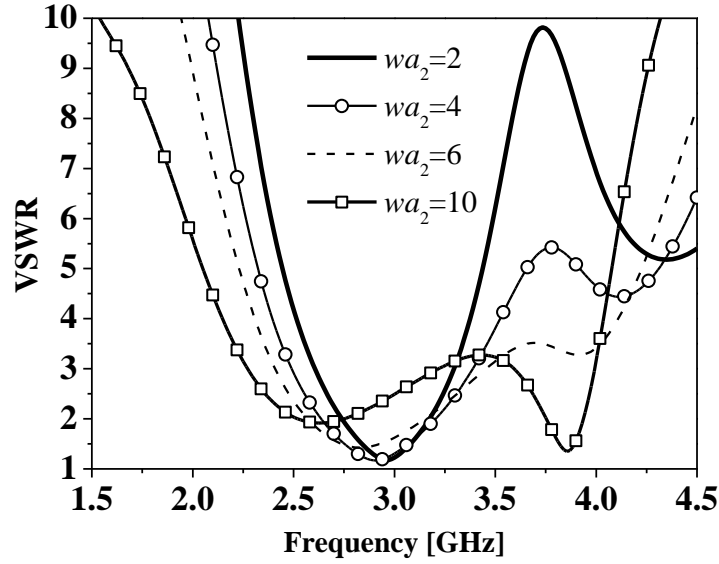


Figure 5.4: Current distributions of Model-A.

Figure 5.5: VSWR characteristics with respect to wa_2 .

5.2.3 Bandwidth Comparison with PIFA

Figure 5.6 shows the VSWR characteristics of FMA (Model-C) and PIFA. The minimum operational frequency, where the VSWR becomes 3, is around 2.11 GHz. However, the relative bandwidth of FMA (Model-C) and PIFA is respectively 58.0% and 34.8%, while the antenna height from the ground plane and physical volume are almost the same. Thus, FMA shows the wider bandwidth compared with the PIFA, which is realized by the structure producing the two resonant frequencies.

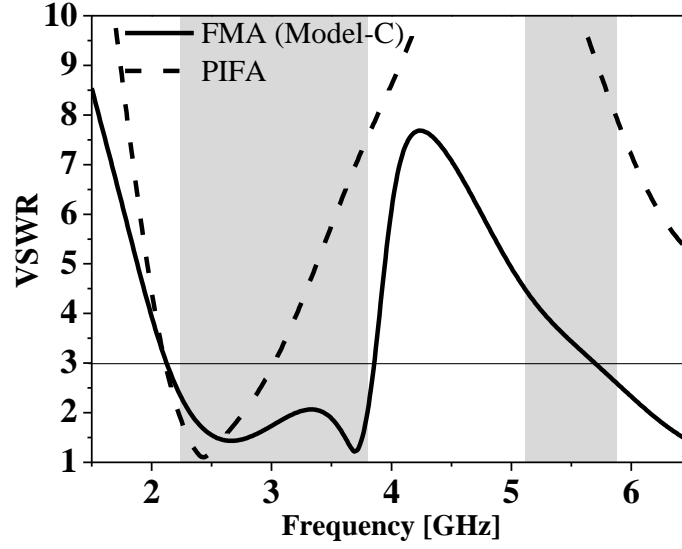


Figure 5.6: Comparison of VSWR between FMA (Model-C) and PIFA.

5.3 Suitable FMA Array for MIMO

5.3.1 S-parameter Characteristic and Electric Near-field Distribution

Figure 5.7 shows the S-parameter characteristics when two FMAs are placed on the ground plane as can be seen in Fig. 5.1(b) (dash-line). Also, Figure 5.8 shows the magnitude of electric near-field distributions of FMA array at 9.1 mm height from the ground plane. In this case, FMA#1 is excited, and FMA#2 is terminated with a terminal impedance of 50Ω , and the evaluated frequency is 2.97 GHz, where the mutual coupling of Model-C is the lowest in Figure 5.7(b).

For Model-B, the minimum operational frequency is lowered to approximately 1.75 GHz in Fig. 5.7(a), and this is the lowest value compared to other models. This is because when we see the configuration of Model-B, the folded parts of antenna, where usually the magnitude of electric near-field is the highest, are close to each other. Therefore, FMA array of Model-B operates like one bigger antenna due to the mutual coupling between the two FMAs. In fact, the relatively higher magnitude of mutual coupling in a wide range and near-field are observed in Fig. 5.7 (b) and in Fig. 5.8 (b), respectively. As for Model-C, $|S_{11}| < -6$ dB from 2.03 to 3.88 GHz and $|S_{21}| < -15$ dB from 2.33 GHz are satisfied, which covers WiMAX 2.5/3.5 GHz bands and WLAN 2.4 GHz

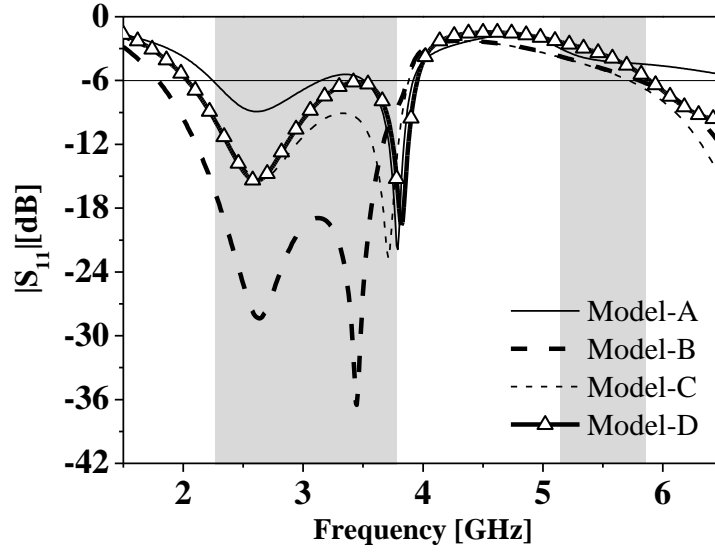
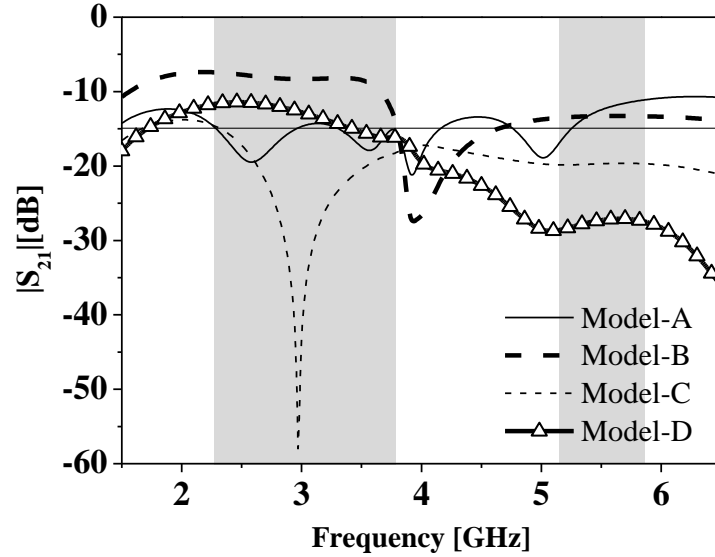
(a) S_{11} characteristics(b) S_{21} characteristics

Figure 5.7: S-parameter characteristics of FMA array.

band. Also, the physical distance of the folded parts between FMA#1 and FMA#2 is largest, then the magnitude of electric near-field is the lowest even though the feed points are relatively close to each other. The paper [98], which also analyses folded monopole antenna array, reaches the same result that the mutual coupling highly depends on the distance of the folded parts of the two folded elements rather than that of feed points.

For further understanding of the mechanism, the magnitude of electric near-field distributions at 0.1 mm height from the ground plane is shown in Fig. 5.9. Large magnitude of electric near-field can be observed at the edge of the ground plane and the area under the antenna elements. Also, there are several null points on the edge of the ground plane in each model. As for Model-C, the terminated port of FMA#2 locates around one of the nulls, and the magnitude of electric near-field is low. On the other hand, the terminated ports of other models are located at the place where the near-field is large. Thus, it is thought that the mutual coupling of Model-C is decreased compared with other models.

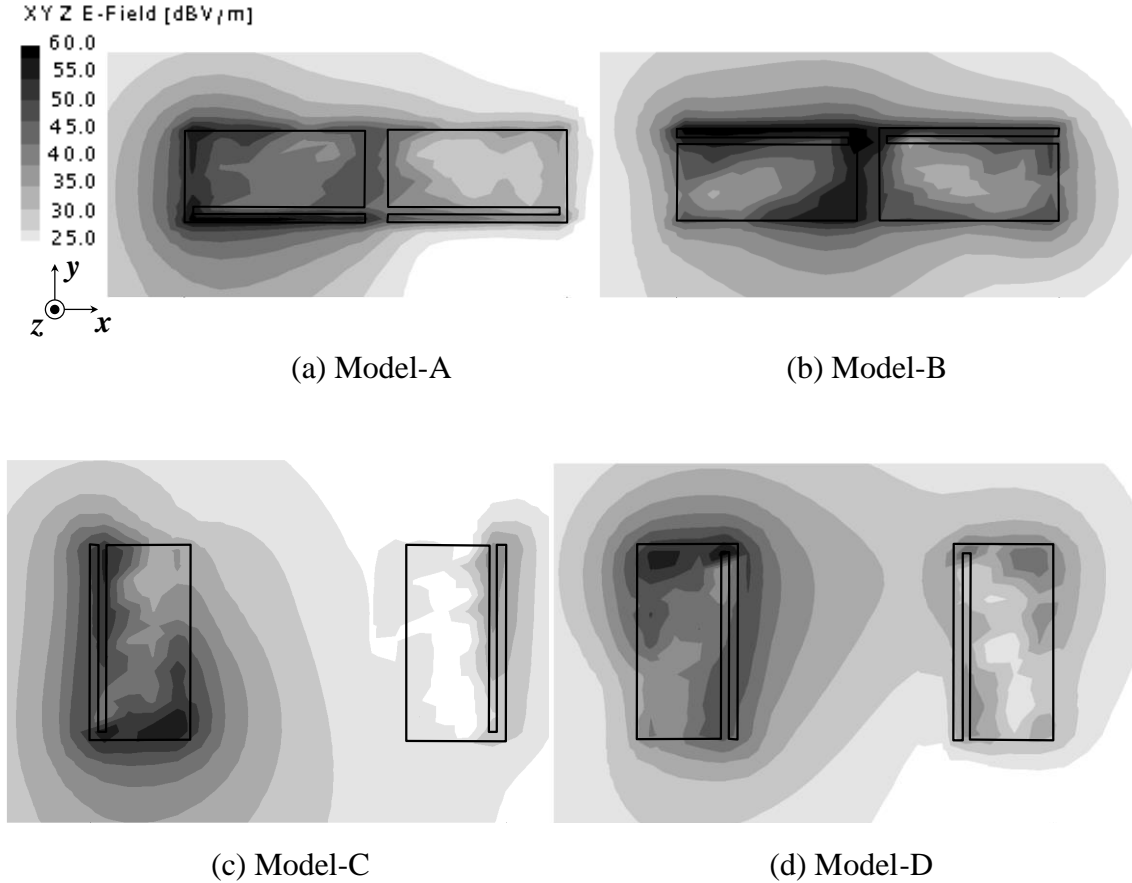


Figure 5.8: The magnitude of electric near-field distributions of FMA array at 2.97 GHz.

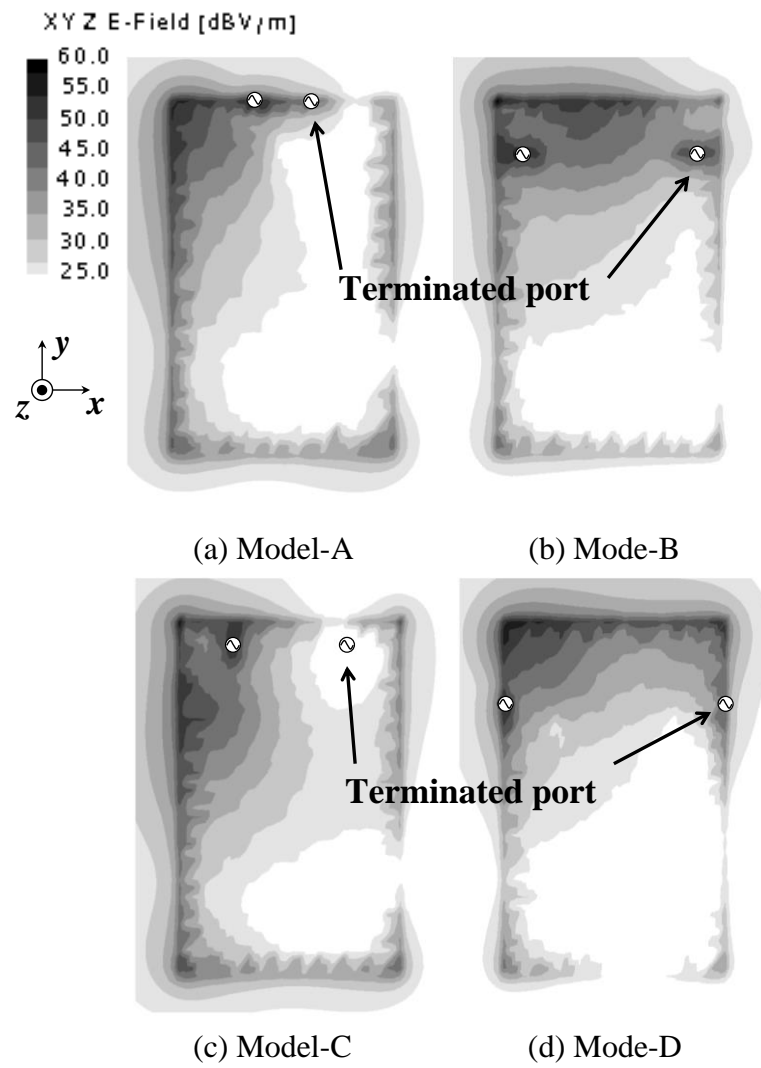


Figure 5.9: The magnitude of electric near-field distributions of ground plane at 2.97 GHz.

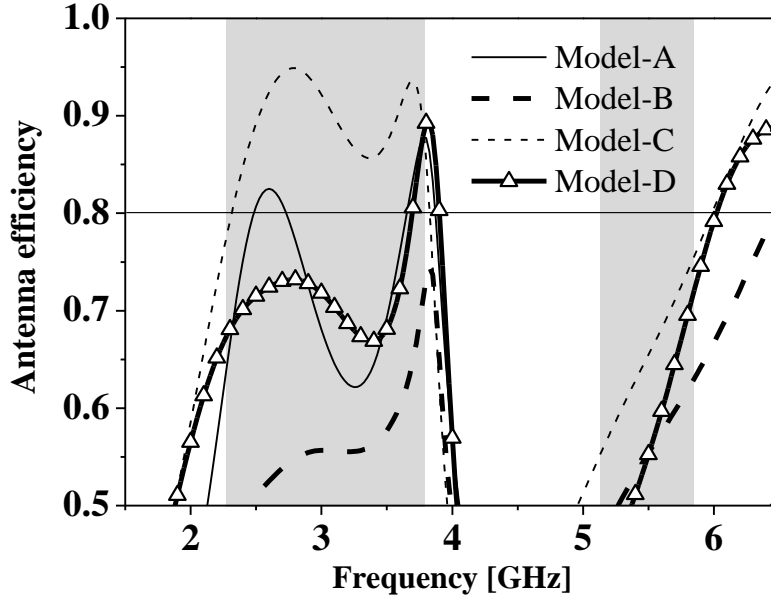


Figure 5.10: Antenna efficiency of FMA array.

5.3.2 Antenna Efficiency

Figure 5.10 shows the antenna efficiency of each FMA array model, which is calculated using Eq. (5.1) and according to the definition given in [99].

$$\eta_{ant} = \eta_{rad} (1 - |S_{11}|^2 - |S_{21}|^2) \quad (5.1)$$

where η_{rad} represents the radiation efficiency (=radiation power/input power). In the figure, the antenna efficiency of Model-C is more than 80% in the desired frequency band (2.3-3.8 GHz). However, the efficiencies of other models are mainly less than 80%. Since the radiation efficiencies of each model do not change so much, $|S_{21}|$ might be the important factor to decide the FMA array in this case. Thus, it is clear that Model-C is the most suitable configuration for MIMO application using the FMA.

5.4 Multiband FMA Employing Parasitic Element

It is shown that Model-C has suitable configuration for MIMO system in the lower frequency bands (2.3-3.8 GHz) from the analysis so far. However, the higher frequency band is not covered, and low efficiencies are observed in Fig. 5.10. In this section, a parasitic element is introduced in order to obtain one more resonant frequency around 5 GHz. The principle of operation for the parasitic element was already reported in [100], and the parasitic element was applied to L-shaped folded monopole antenna for the multiband antenna [101]. Therefore, it seems that the parasitic element operates very effectively in this analysis as well.

5.4.1 Antenna Configuration

Figure 5.11 shows the configuration of the parasitic elements (PE) and FMAs (Model-C). The width of PE is 1 mm. PE is located just under FMA in order to avoid the increase of the total antenna volume. The parameters of PE are defined that the height, length and the location are h , l , dx and dy , respectively. Since the central frequency of 5.5 GHz WiMAX band (5.25-5.85 GHz) and 5 GHz WLAN band (5.15-5.875 GHz) is about 5.5 GHz, the total length of PE ($l+h$) is initially selected to be 13.5 mm, which is quarter wavelength. In this section, single FMA and PE are mounted on the ground plane, and the case of FMA array will be analyzed in the next section.

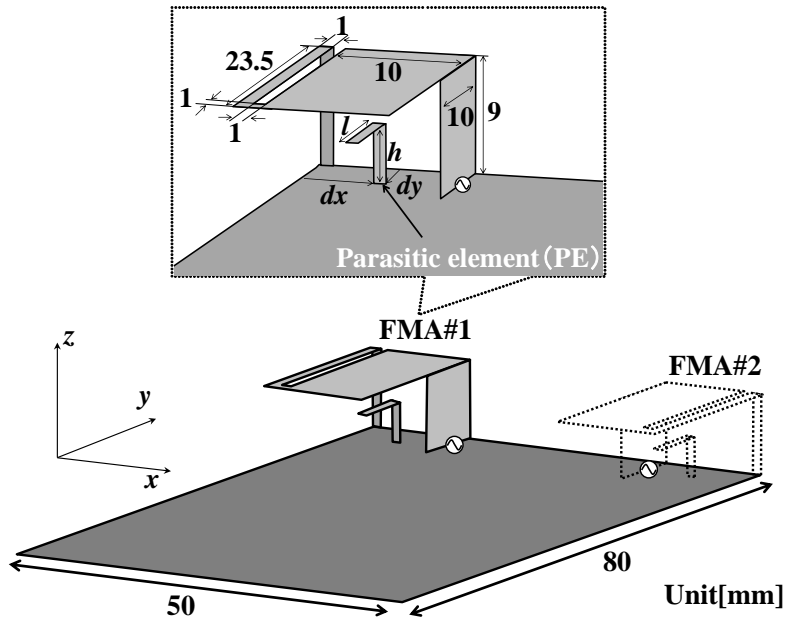
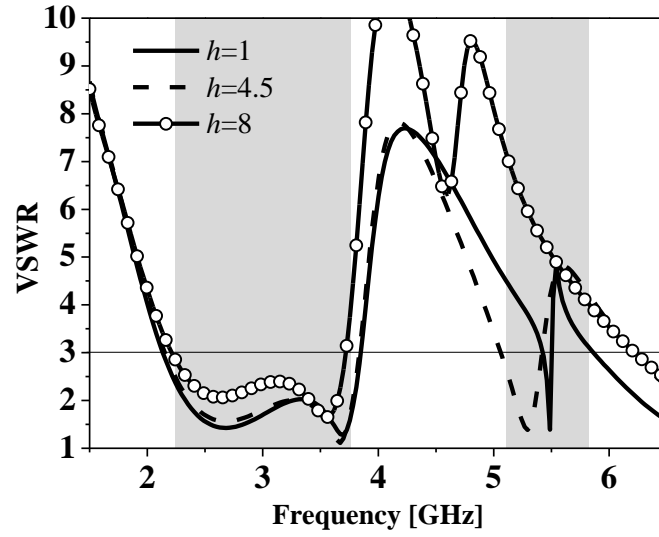


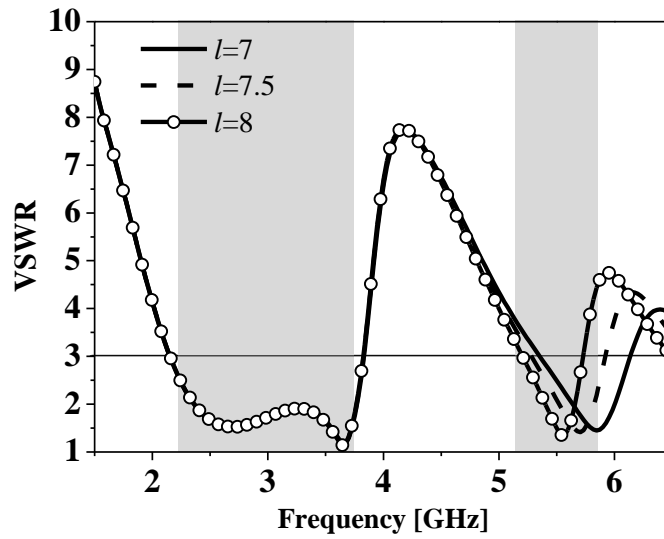
Figure 5.11: Configuration of PE and FMA (FMA array-dash line).

5.4.2 Parametric Analysis and Distribution of Cover Ratio

Figure 5.12(a) shows the VSWR characteristics when h is varied from 1 mm to 8 mm. In this case, the total length of PE ($l+h$) is 13.5 mm, and dx and dy is respectively 5.5 mm and 5 mm at this moment. In the figure, the 3rd resonant frequency is obtained by adding PE even just under FMA. When h is 4.5 mm, the midpoint between the antenna element and the ground plane, wider bandwidth is obtained. Then, Figure 5.12(b) shows the VSWR characteristics when l is changed from 7 mm to 8 mm so as to adjust the resonant frequency, while h is fixed to 4.5 mm. Thus, when l is 7.5 mm, the desired bandwidth is almost covered.



(a) With respect to h ($l+h=\text{const.}$)



(b) With respect to l ($h=4.5$)

Figure 5.12: VSWR characteristics.

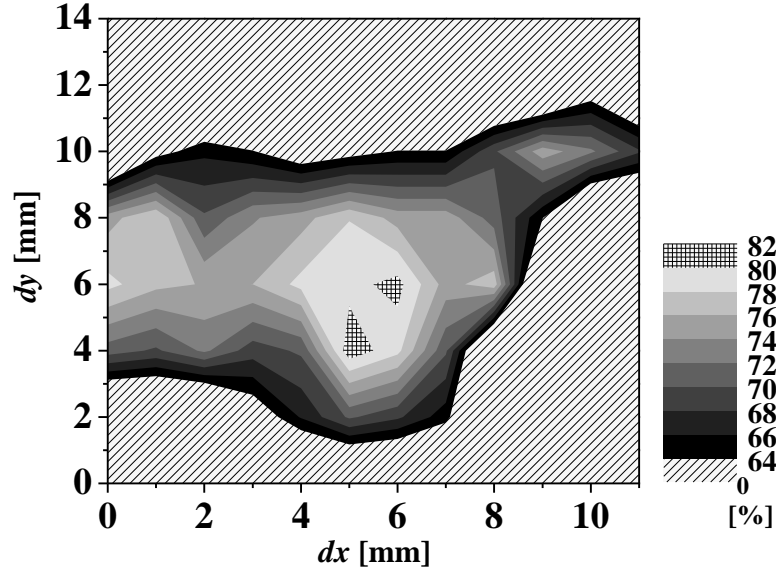
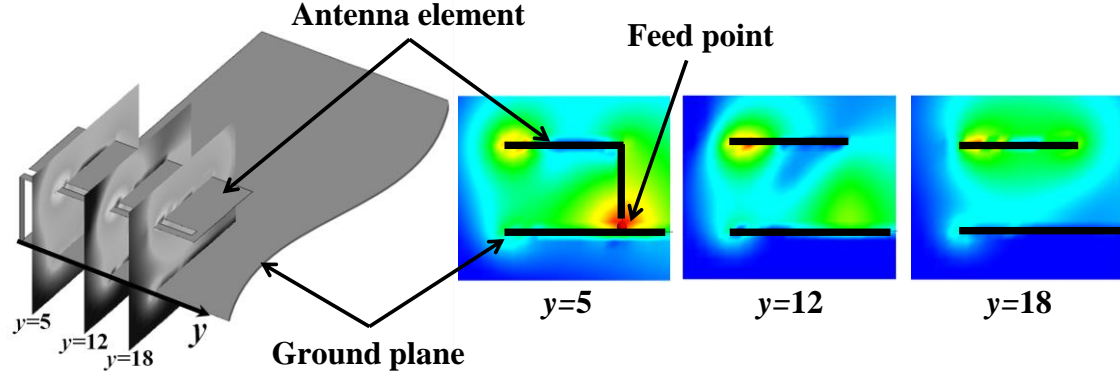


Figure 5.13: Cover ratio distributions of 5 GHz band.

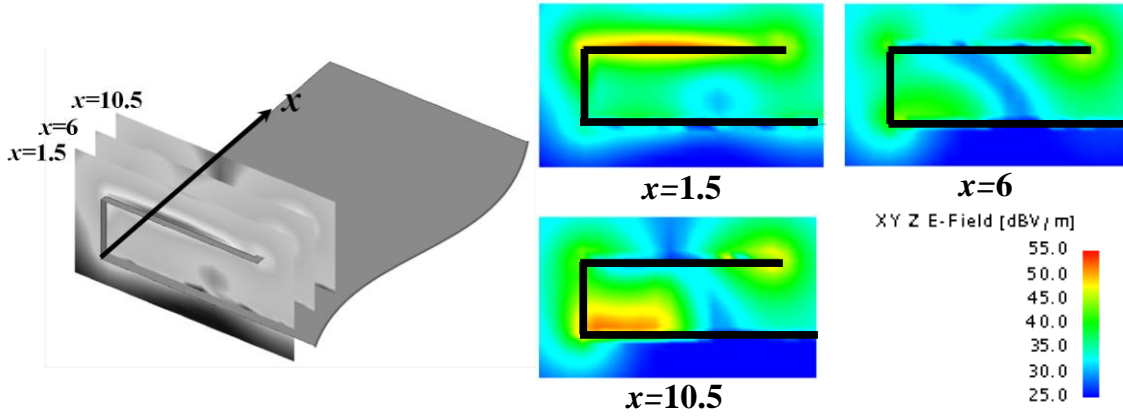
Figure 5.13 shows the cover ratio distribution of the 5 GHz band (5.15-5.875 GHz) with respect to the dx and dy . The cover ratio means the ratio of the covered frequency range by the PE to the whole frequency range of 5 GHz. From the parametric study above, h and l are 4.5 mm and 7.5 mm, respectively. Although it is very difficult to cover the entire 5 GHz band, more than 80% of the target band is covered. The maximum value is approximately 81.4% when $dx=5.5$ mm and $dy=5$ mm, where the PE is located around the central space of FMA.

Electric near-field distributions at 5.5 GHz around FMA are shown in Fig. 5.14, and there is no PE in this case. The distributions in Fig. 5.14 are observed from $+y$ direction and $-x$ direction, respectively. From the figure, it is found that the magnitude of electric near-field is small around the center of antenna space ($x=6$ mm, $y=12$ mm). In general, PE should be located in the vicinity of an antenna element where PE can effectively couple to electric and magnetic fields of the antenna. So, the area with the highest E field (near the end of the antenna) or the highest currents (near the feed and ground) are selected to the location of PE [48]. However, when PE is applied between an antenna element and ground plane, the influences from both antenna element and the ground plane have to be taken into consideration since the bandwidth is highly affected depending on the location as can be seen in Fig. 5.13. Figure 5.15 shows the composite view of electric near-field distributions ($x=6$ mm, $y=5$ mm) and PE ($dx=5.5$ mm, $dy=5$

mm) where the maximum cover ratio distribution is obtained in Fig. 5.13. It is clear that the tip of PE is located in which the electric near-field is relatively low, while the terminated part with ground of PE is located in which the electric near-field is high. Thus, the positions of tip and terminated part of PE have to be well considered in applying PE between antenna element and the ground plane.



(a) Observed from +y direction



(b) Observed from $-x$ direction

Figure 5.14: The magnitude of electric near-field distributions at 5.6 GHz.

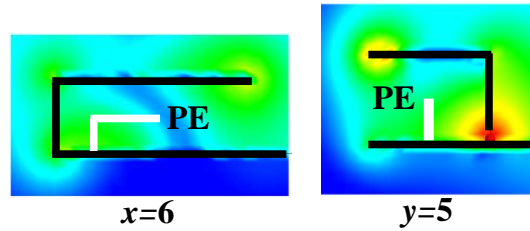


Figure 5.15: Composite view of electric near-field distributions ($x=6$, $y=5$) and PE ($dx=5.5$, $dy=5$).

5.4.3 Radiation Characteristic and Current Distribution

Figure 5.16 shows the comparison of radiation patterns between w/ and w/o PE at each resonant frequency. The radiation patterns hardly change at the 1st (2.68 GHz) and 2nd (3.68 GHz) resonant frequencies. So, the characteristic of FMA is maintained, and it is considered that the radiation from FMA is dominant at the 1st and 2nd resonant frequency. On the other hand, at the 3rd (5.70 GHz) resonance, the patterns between w/ and w/o PE are quite different. Thus, it seems that the operating element differ from each other at the 3rd resonance.

In fact, as for the current distributions, major change on FMA is not observed in Fig. 5.17(a) and 5.17(b). However, the current distribution on PE is much larger at the 3rd resonant frequency in Fig. 5.17(c). Thus, it can be confirmed that the radiation at the 1st and 2nd resonances are mostly from FMA, while the radiation of 3rd resonance is dominant from PE. (Actually, the gain is not degraded in case of w/ AE at 5.70 GHz. This is because the impedance mismatch loss is not so large, shown in Fig. 5.6.)

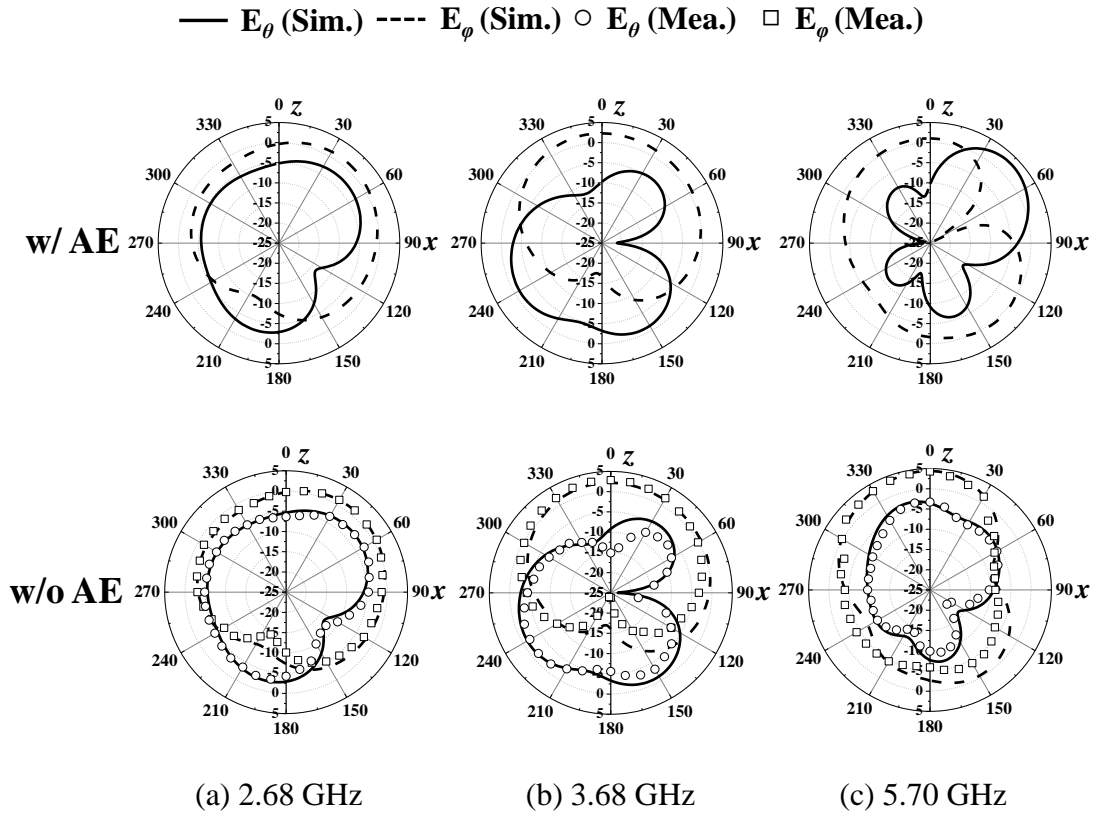


Figure 5.16: Comparison of radiation patterns between w/ and w/o PE at each resonant frequency.

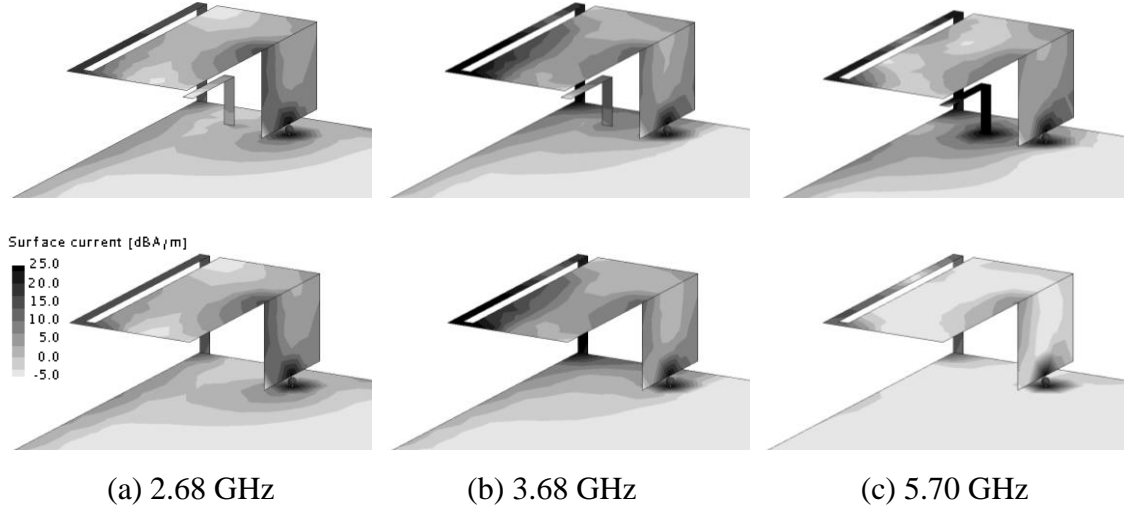


Figure 5.17: Comparison of current distributions between w/ and w/o PE at each resonant frequency.

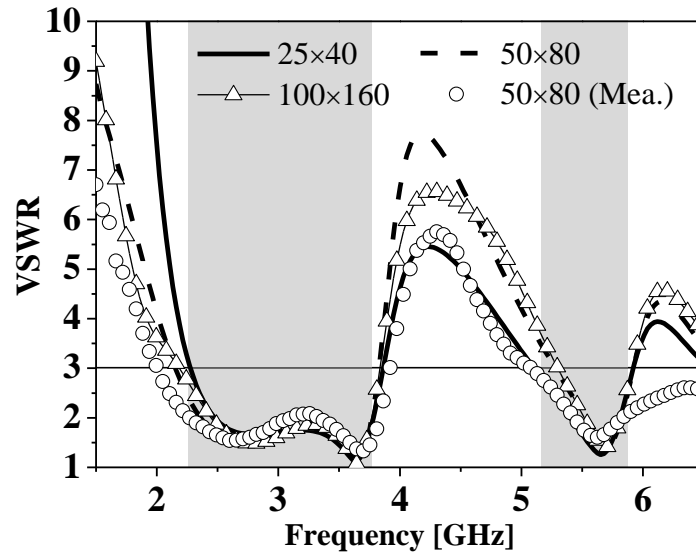


Figure 5.18: VSWR characteristics with respect to the size of the ground plane.

5.4.4 Characteristic Change with respect to Size of Ground Plane

Figure 5.18 shows the VSWR characteristics with respect to the size of the ground plane. In addition to $50 \times 80 \text{ mm}^2$ assuming a mobile phone or mobile router, $100 \times 160 \text{ mm}^2$ and $25 \times 40 \text{ mm}^2$ assuming a tablet and USB dongle is also analyzed. In the figure, it is found that the VSWR mostly remain less than 3 in the target frequency bands. Also, the variation of VSWR is relatively small regardless of the ground size.

5.5 Fundamental Characteristics of FMA Array with Parasitic Elements

In Sect. 5.4, single FMA with PE is analyzed on the location of PE and fundamental antenna characteristics. In this chapter, two FMA and PEs are mounted on the ground plane for MIMO antenna, then characteristics such as correlation coefficient and antenna efficiency are analyzed.

5.5.1 S-parameter Characteristic

Figure 5.19 shows the S-parameter characteristics when two FMAs and the parasitic elements are placed on the ground plane as can be seen in Fig. 5.11 (dash-line). Also, the comparison of S-parameter characteristics between the simulation and measurement is shown. In calculation, $|S_{11}| < -6$ dB from 2.05 to 3.87 GHz and from 5.27 to 5.90 GHz are observed, and $|S_{21}| < -15$ dB is satisfied in all the desired bands. Furthermore, the result shows good agreement in the target bands.

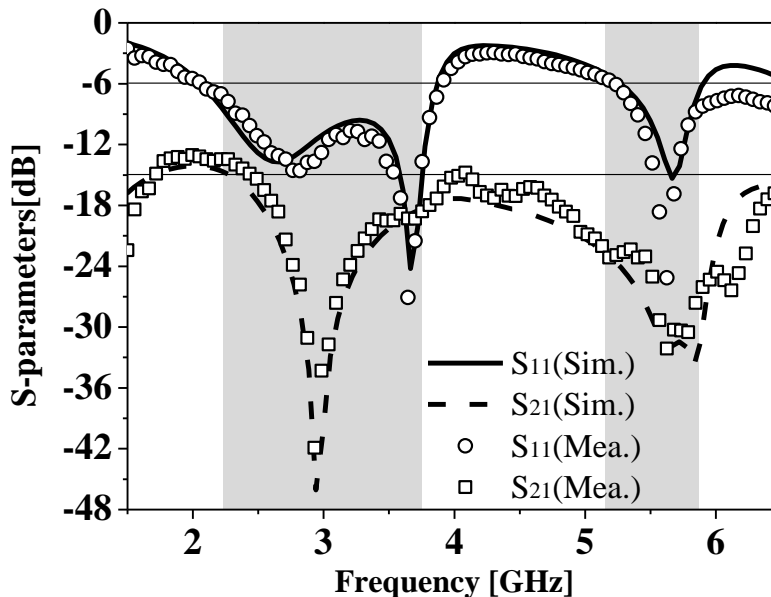


Figure 5.19: Comparison of S-parameter characteristics between simulation and measurement.

5.5.2 Envelope Correlation Coefficient and Antenna Efficiency

In MIMO antenna system, the mutual coupling between the two antennas must be low to preserve spatial diversity and channel independence. Envelope correlation coefficient (ECC), ρ , between the antennas is also one of the characteristics to measure the performance of MIMO systems. Figure 5.20 shows ECC of two antennas calculated from S-parameters. The ECC is given by Eq. (5.2) [102].

$$\rho = \frac{|S_{11}^* S_{12} + S_{21}^* S_{22}|^2}{(1 - |S_{11}|^2 - |S_{21}|^2)(1 - |S_{22}|^2 - |S_{12}|^2)} \quad (5.2)$$

In the figure, ECC in the desired bands becomes less than 0.02. It is considered that these values are sufficiently low for MIMO antenna since 0.5 is acceptable for mobile communication systems [103].

Figure 5.21 shows the antenna efficiency of FMA array comparing to the case of with/without PE, and they are obtained from Eq. (5.1). It is clear that the antenna efficiency is improved particularly in 5 GHz band because the magnitude of S_{11} and S_{21} are reduced by adding and adjusting the parameters of PE. Thus, efficiencies range from 70% to 96% in all the target frequency bands.

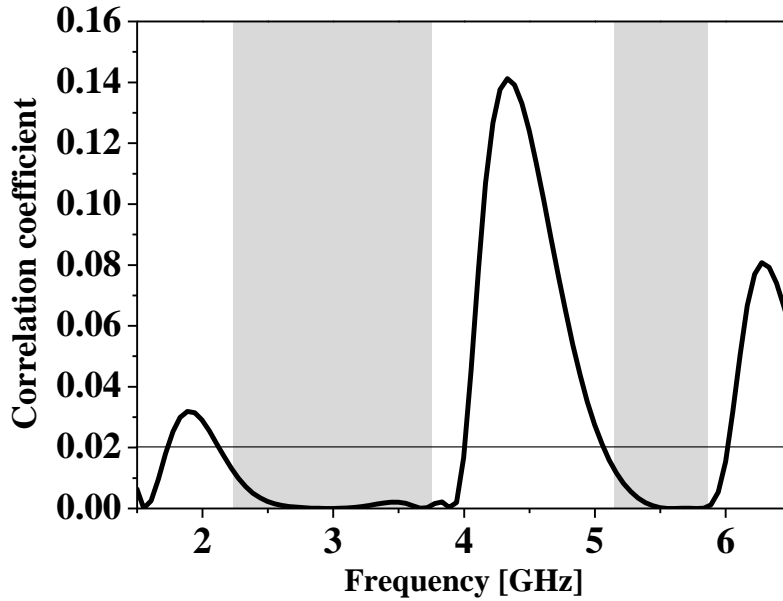


Figure 5.20: ECC of multiband FMA array.

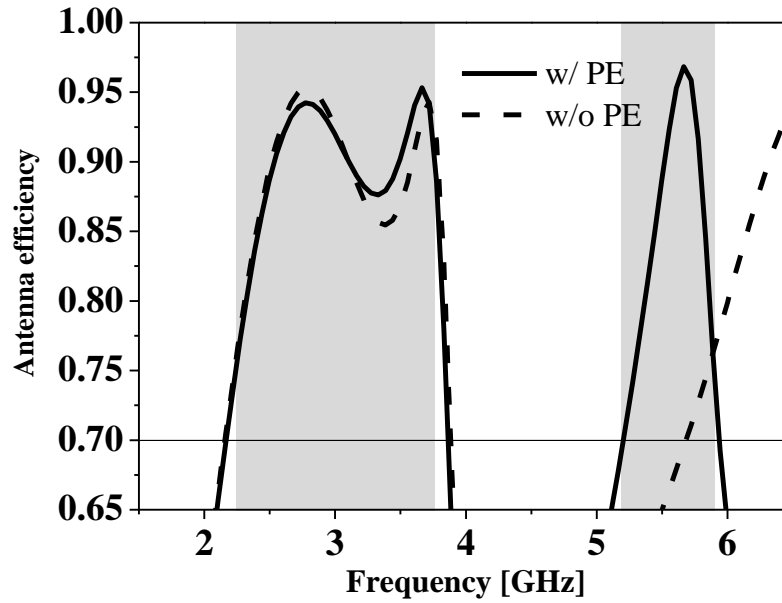


Figure 5.21: Comparison of antenna efficiency between w/ and w/o PE.

5.5.3 Radiation Characteristic

The simulated 3D total radiation patterns at resonant frequencies are shown in Fig. 5.22 and Fig. 5.23, where the excited antenna is different each other. In Figure 5.22, gain decreases and a null appears around $\varphi=300$ deg. and $\theta=90$ deg. at each resonant frequency when FMA#1 is excited. However, these are compensated by the patterns shown in Fig. 5.23, where FMA#2 is excited. Thus, the radiation patterns are mirror images by the change of excited feed points, and the antenna shows pattern diversity. Also, the simulated peak gains of each frequency are 4.1 dBi, 3.7 dBi and 6.3 dBi, respectively.

Figure 5.24 shows the comparison between simulated and measured results of 2D radiation patterns (xz -plane). This is also the case when the FMA#1 is excited and MFA#2 is terminated with impedance of 50Ω . Good agreement can be observed. Thus, we confirmed the analytical validity of the simulation.

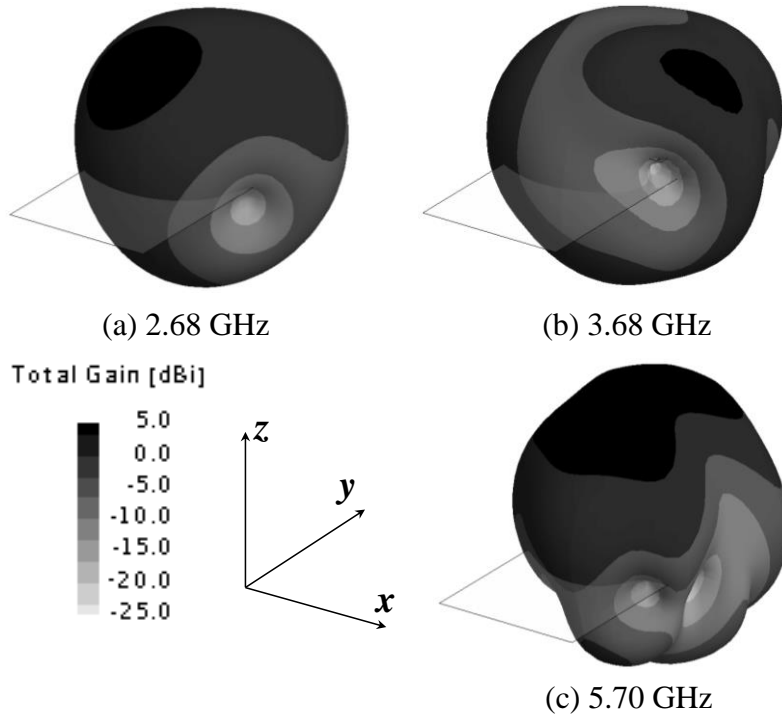


Figure 5.22: 3D radiation patterns when FMA#1 is excited.

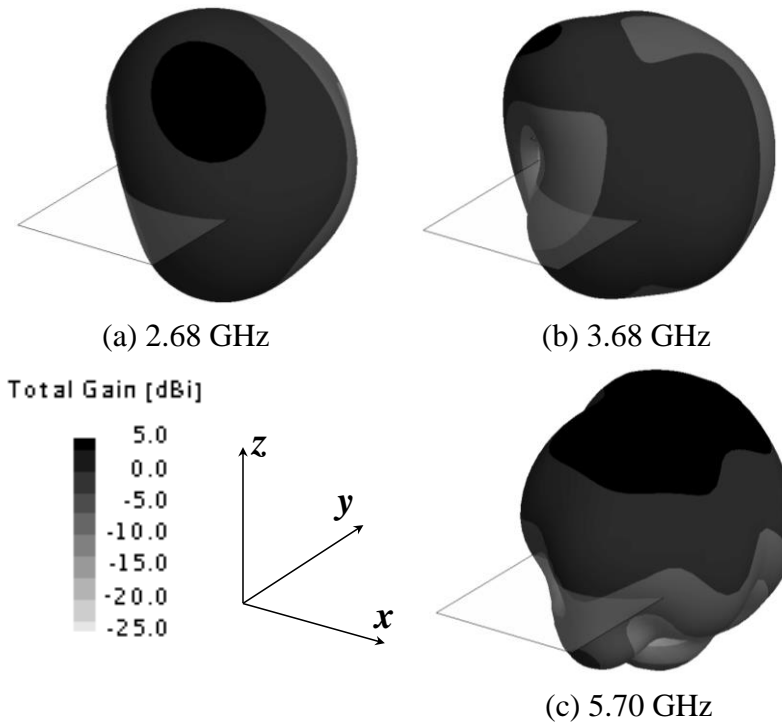


Figure 5.23: 3D radiation patterns when FMA#2 is excited.

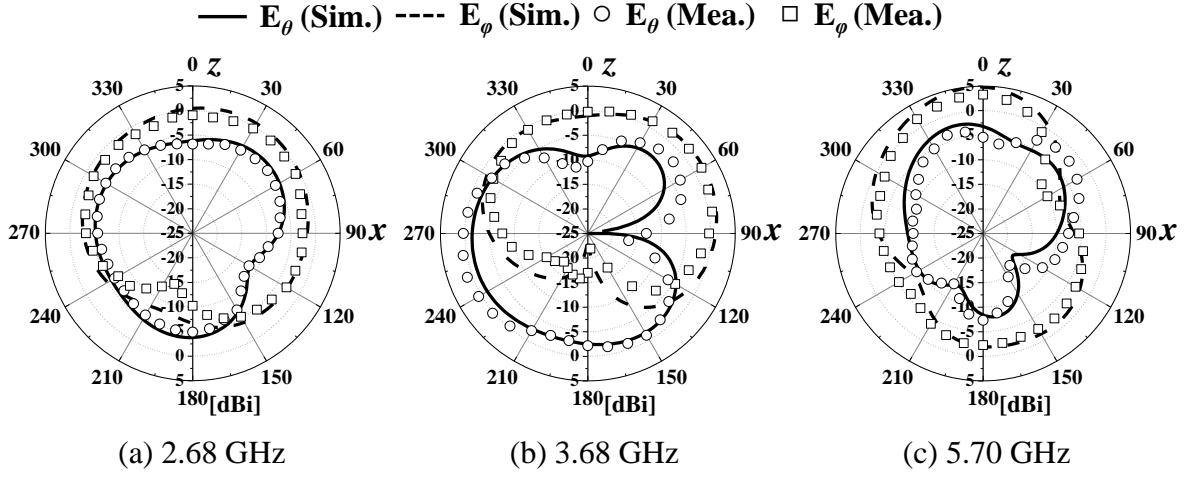


Figure 5.24: 2D radiation patterns when FMA#1 is excited.

5.6 Summary

In this chapter, FMA derived from FDAFL has been proposed, and its wideband characteristics and a suitable configuration for MIMO implementation are shown. Also, by using parasitic elements, multiband FMA is investigated regarding S-parameter characteristics, ECC, antenna efficiencies and radiation patterns.

FMA has wider bandwidth (58.0%) compared with PIFA (34.8%) which has the same physical volume. Analysis of several FMA array designs shows that Model-C is the most suitable configuration of those examined. Then, a parasitic element is introduced for multiband antenna. In order to avoid the increase of total antenna volume, the parasitic element is placed just under FMA. The location of PE is analyzed based on the cover ratio distribution and electric near-field distribution. From the analysis, it is found that the appropriate location of PE is the central space between FMA and the ground plane, where the electric near-field is relatively low.

In the proposal model, WiMAX 2.5/3.5/5.5 GHz bands and WLAN 2.4/5 GHz bands are almost covered. The antenna efficiency of between 70% to 96% and very low correlation coefficient of less than 0.02 are observed. Measurements were also conducted and showed good agreement with the simulation results.

Chapter 6

Current Reduction on the Ground Plane using Quarter-wavelength Additional Element

6.1 Introduction

It has been reported that the current on the conducting box contributes to the antenna characteristics such as radiation patterns and gain [47]. Also, antenna performances are degraded when the terminal is held by a hand since human hand absorbs the radiated power and current variation on the small terminal occurs, which cause the degradation of radiation efficiency, gain, and bandwidth. Thus, for the built-in type of antenna, many studies have proposed various methods to reduce the current on the ground plane, such as introduction of a slit on the ground plane [104]-[105], FDA which has self-balanced structure [42], [56], and use of a balun at the feed point. However, these techniques lead to the reduction of the ground plane area, complex antenna structure, increase of loss, narrow bandwidth, and so forth.

On the other hand, a quarter-wavelength additional element (AE) is employed in the vicinity of L-shaped folded monopole antenna element (LFMA) in order to reduce the terminal current [101]. To be more precise, the additional element is installed around a folded structure of LFMA, where the electric field is stronger. As a consequence, AE is strongly coupled with LFMA, resulting in acting as an antenna and contributing to radiation and current reduction on the ground plane. Thus, this method does not require a slit, specific antenna form, or a balun, which means that it is easy to introduce the element to the existing antenna system. However, the effectiveness of current suppression caused by AE has not clarified yet.

In Chapter 5, FMA array for the realization of WiMAX and WLAN MIMO antenna is investigated. Figure 6.1 shows the comparison of current distributions at 2.45 GHz between 3D-FDAFLs proposed in Chapter 4 and FMA array proposed in Chapter 5.

It is obvious that large current is observed on the ground plane of FMA array due to the monopole structure. Thus, in this chapter, the quarter-wavelength additional element is applied to FMA array in order to reduce the current on the ground plane. Then, the effect of the additional element with nearby object such as human hand is analyzed. In addition, the additional element is applied to a different type of antenna in order to confirm the effectiveness. In this study, wire inverted-F antenna (WIFA) is chosen, and antenna characteristics are analyzed.

This chapter first presents the parametric analysis contributing to current reduction on the ground plane in Sect. 5.2. In Sect. 5.3, the effect of a human hand on antenna characteristics is analyzed with a simplified one-layer hand model. Then, in Sect. 5.4, AE is applied to a different type of antenna. Finally, conclusions of this chapter are given in Sect. 5.5.

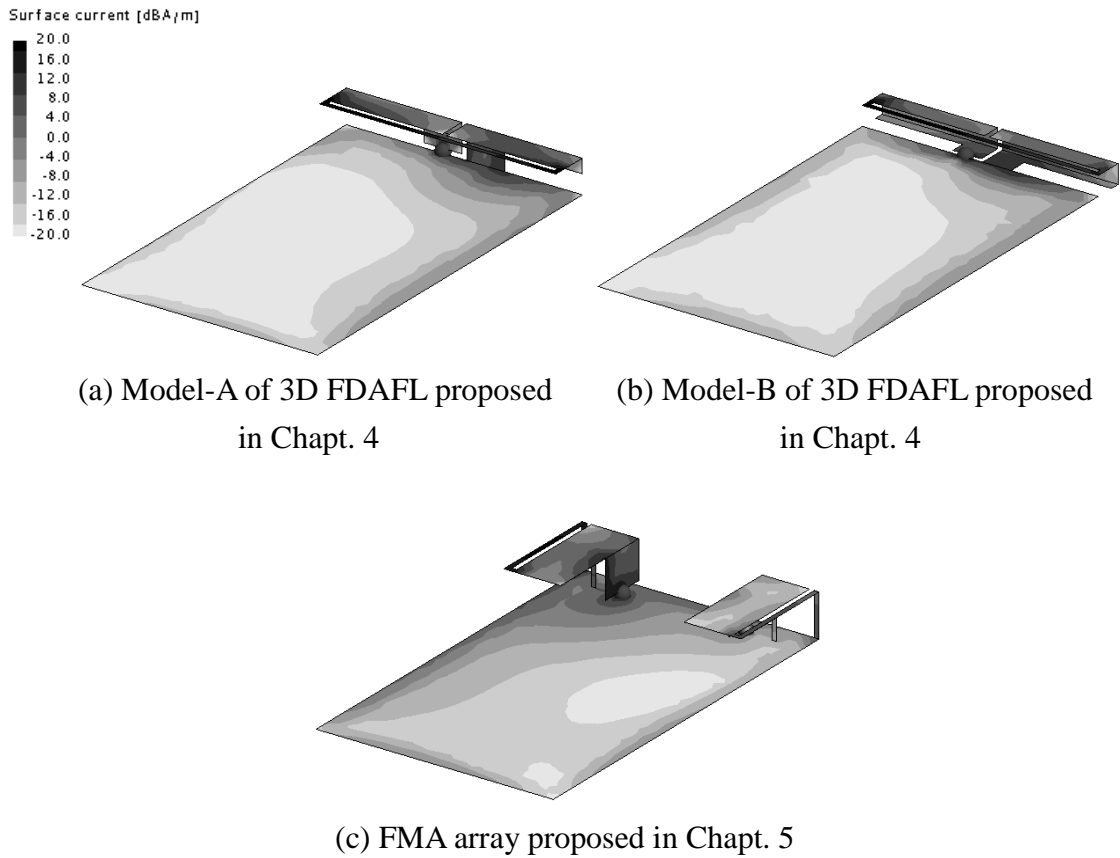


Figure 6.1: Current distributions at 2.45 GHz.

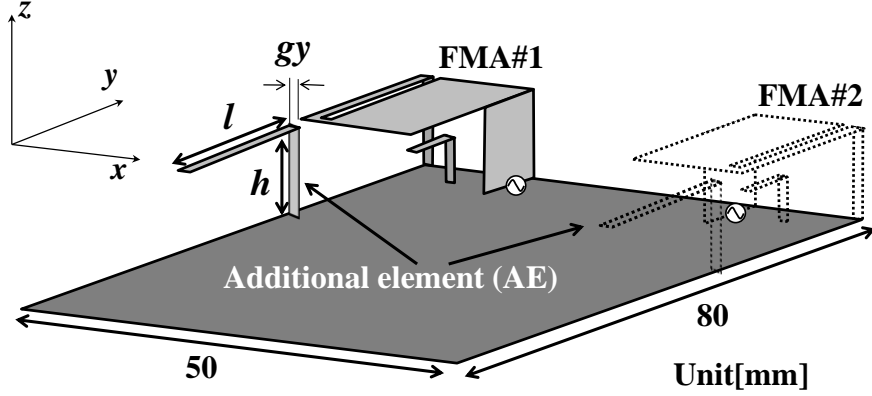


Figure 6.2: Antenna configuration.

6.2 Parametric Analysis Contributing to Current Reduction

6.2.1 Antenna Configuration

Figure 6.2 shows the configuration of the additional element (AE) and FMA proposed in Chapter 5, which are mounted on the rectangular ground plane of size $50 \times 80 \text{ mm}^2$. The antenna parameters of FMA are shown in the figure. Considering the antenna space, easiness of installation of AE, and study achievements in [101], the location of AE should be in the vicinity of the folded structure of FMA and along the edge of the ground plane. Also, AE has the width of 1 mm, and the other parameters of AE are defined that the distance between FMA and AE; g_y , the height; h , the length of the element bent in xy plane; l , and the total length; $L (=l+h)$. Since it is clarified that the large current flows on the ground plane especially at lower frequency, the target frequency is 2.45 GHz, which is the central frequency of 2.4 GHz band of WLAN, meaning that the initial total length of AE is set to be 30 mm ($\lambda/4$). In the case of FMA array, one more FMA and AE are considered as described by dash-line.

6.2.2 Length and Height of AE

Figure 6.3 shows the current distributions at 2.45 GHz when AE stands vertically ($L=h=\lambda/16, \lambda/8, \lambda/4, \lambda/2$) with $g_y=1 \text{ mm}$. In the figure, when $L=\lambda/4=30 \text{ mm}$, current reduction on the ground plane is the largest compared with the other cases including w/o AE. Especially, the current on the edge of the ground plane is suppressed. Figure 6.4

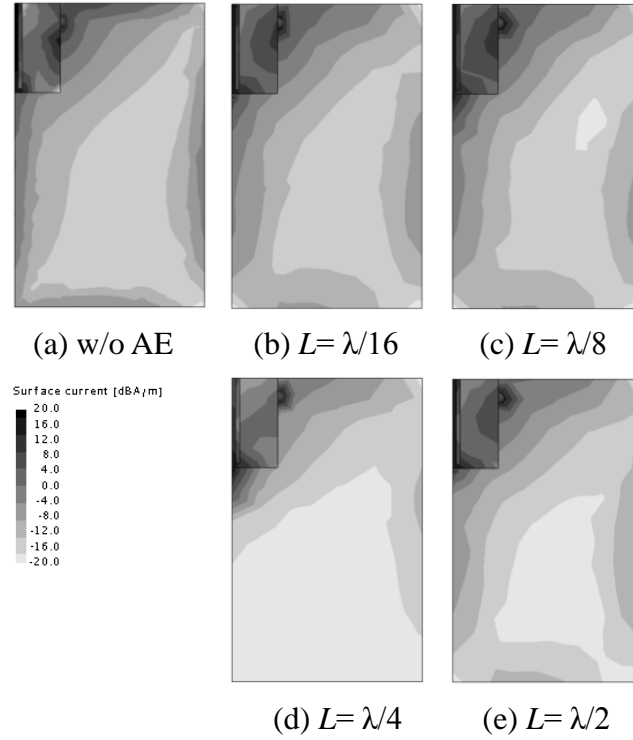


Figure 6.3: Current distributions at 2.45 GHz when AE stands vertically, and L is varied.

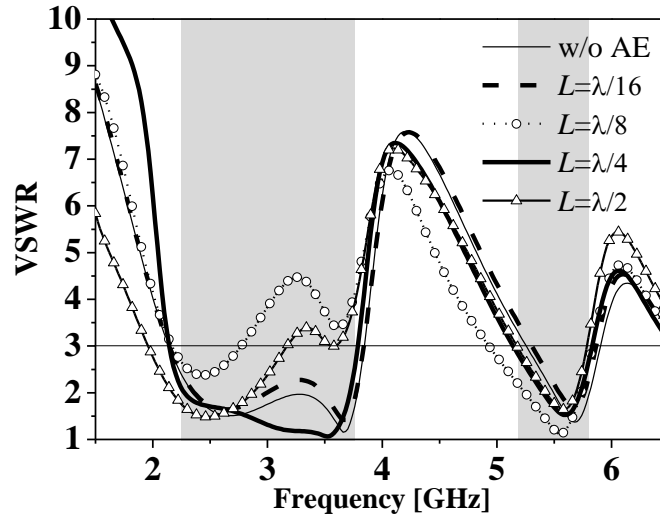


Figure 6.4: VSWR characteristics when AE stands vertically, and L is varied.

shows the VSWR characteristics corresponding to Fig. 6.3. Since the impedance characteristic is maintained when $L = \lambda/4$, and the characteristic is degraded when $L = \lambda/8$ and $\lambda/2$, thus the length of AE should be quarter-wavelength in order to reduce the current. However, this is the case when AE stands vertically along z -axis, and it's not realistic when AE is applied to a small terminal.

Figure 6.5 shows the current distributions at 2.45 GHz when h is changed from 3 mm to 12 mm ($L=l+h=30$ mm=const.) with $g_y=1$ mm. It can be seen that the effect of AE is maintained although AE is bent along y -axis. However, the current on the ground is more decreased with increasing h . Figure 6.6 shows the VSWR characteristics with respect to h . Although $VSWR \leq 3$ is maintained at 2.45 GHz in all the cases, the impedance matching is deteriorated with increasing h in lower frequency around 2.15 GHz. Figure 6.7 shows the current distributions of $h=3$ mm and $h=12$ mm at 2.15 GHz. Larger current is observed on both antenna element and ground plane when $h=12$ mm. Consequently, the VSWR degradation occurs due to the strong coupling between AE and FMA. Thus, the bandwidth of lower frequency band is barely narrowed by adding AE, but as a whole, the alternation of VSWR characteristics is not so large. In this study, in order to suppress the amount of current on the ground plane as much as possible and in order to aim for low-profile terminal, the parametric analysis is continued with $h=9$ mm since the height of FMA is 9 mm as well.

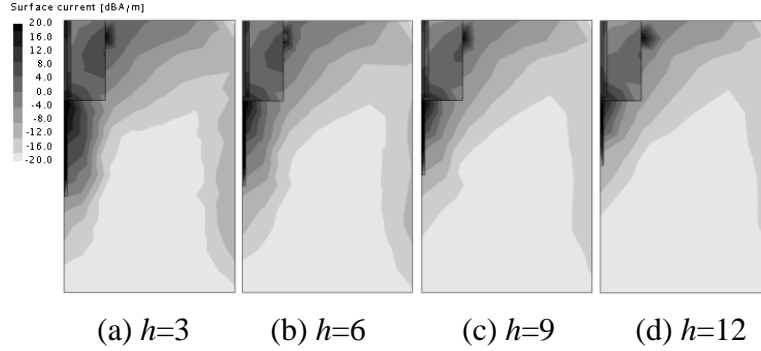


Figure 6.5: Current distributions at 2.45 GHz when h is varied ($l+h=\text{const.}$).

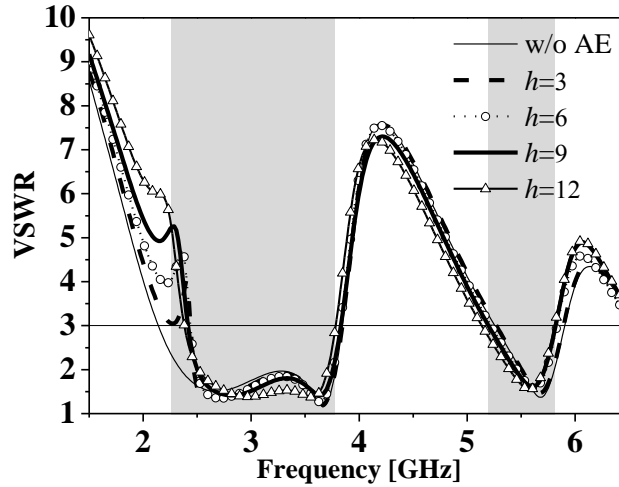


Figure 6.6: VSWR characteristics when h is varied ($l+h=\text{const.}$).

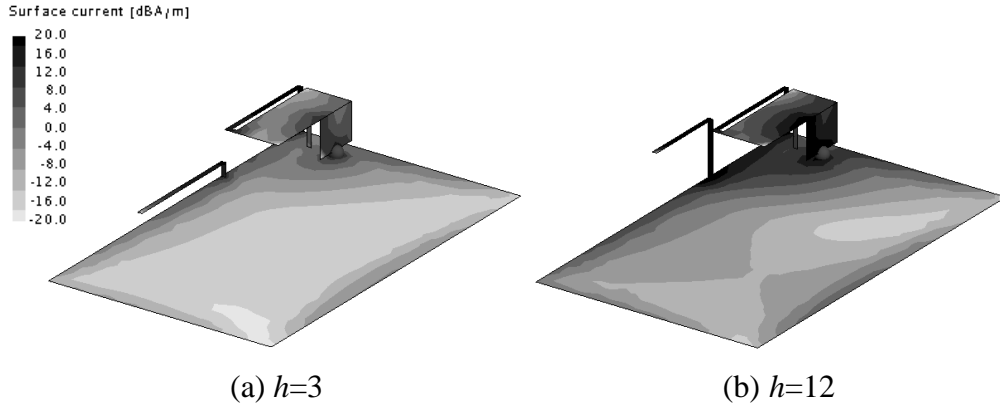


Figure 6.7: Current distributions at 2.15 GHz when h is varied ($l+h=\text{const.}$).

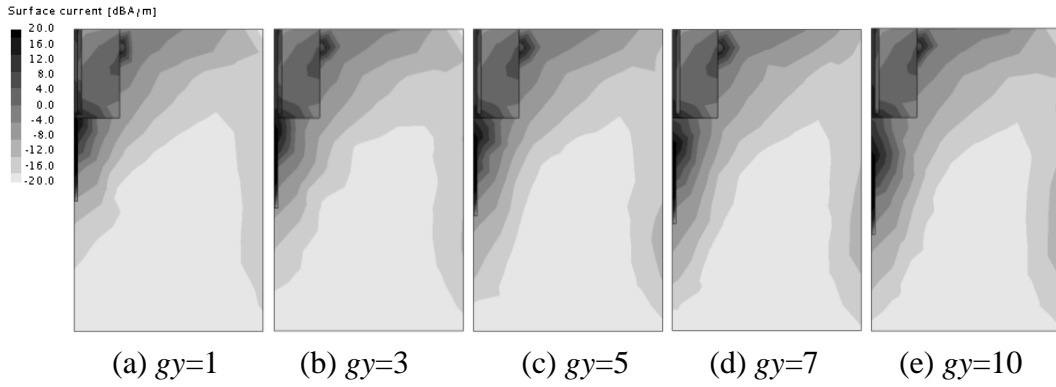


Figure 6.8: Current distributions at 2.45 GHz when g_y is varied with $h=9$ and $l=21$.

6.2.3 Location of AE

Figure 6.8 shows the current distributions at 2.45 GHz when g_y is altered from 1 mm to 10 mm with $h=9$ mm and $l=21$ mm. It is obvious that the distance between AE and FMA also contributes to current reduction on the ground plane, and the effect of AE on the current reduction becomes small with the increase of g_y . On the other hand, Figure 6.9 shows the VSWR characteristics corresponding to Fig. 6.8. $\text{VSWR} \leq 3$ is maintained at 2.45 GHz in all the cases. Also, the VSWR degradation in the lower frequency mitigates with larger g_y since the coupling effect between AE and FMA gradually disappears, while all the target frequency bands are covered when $g_y > 10$. Therefore, there is a trade-off between the current reduction and bandwidth in deciding the parameter g_y .

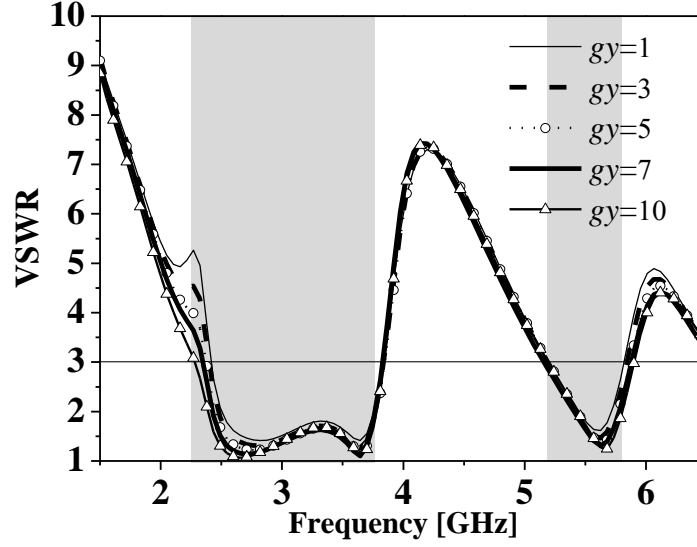
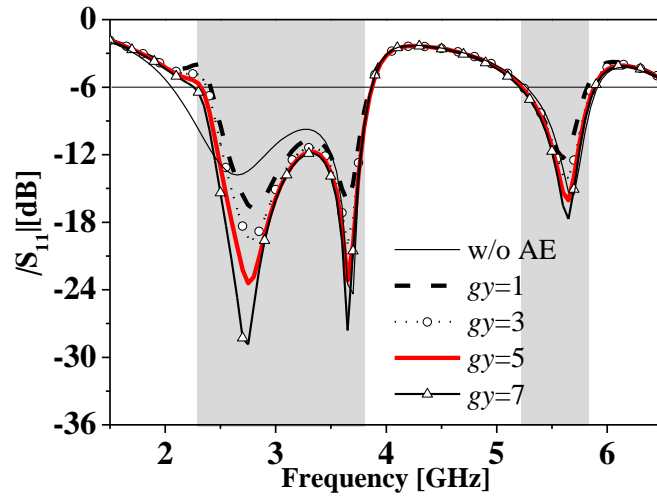
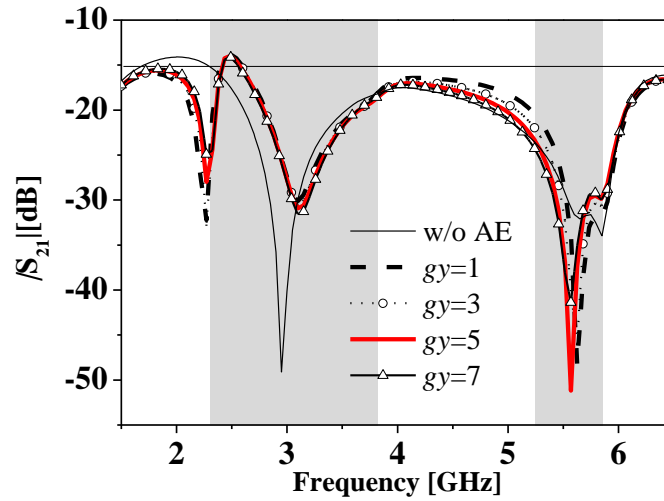
Figure 6.9: VSWR characteristics when g_y is varied.

Figure 6.10 shows the comparison of S-parameter characteristics for FMA array as can be seen in Fig. 6.2 (dash-line). The parameter g_y is changed from 1 mm to 7 mm. By applying AE, both S_{11} and S_{21} characteristics exhibit some changes compared with the case without AE, especially in the lower frequency band. As for the S_{11} characteristic, actually the bandwidth is narrowed, but $|S_{11}| < -6$ dB is obtained with $g_y > 5$ mm at 2.3 GHz, which is the minimum operational frequency of WiMAX. Similarly, AE affects the mutual coupling between AE and FMA. However, relatively high isolation is maintained, and it seems that S_{21} is independent from the parameter g_y in this case since the variation of S_{21} is quite small from $g_y = 1$ mm to 7 mm. The antenna efficiency is presented in Fig. 6.11. Due to the degradation of S-parameter characteristics, antenna efficiency is also deteriorated at 2.45 GHz by approximately 8.7%. However, more than 70% of efficiency is attained in the target frequency bands when $g_y > 5$ mm. Thus, g_y should be selected to 5 mm because of the trade-off between current reduction and bandwidth (or antenna efficiency).



(a) S_{11} characteristics



(b) S_{21} characteristics

Figure 6.10: S-parameter characteristics when gy is varied.

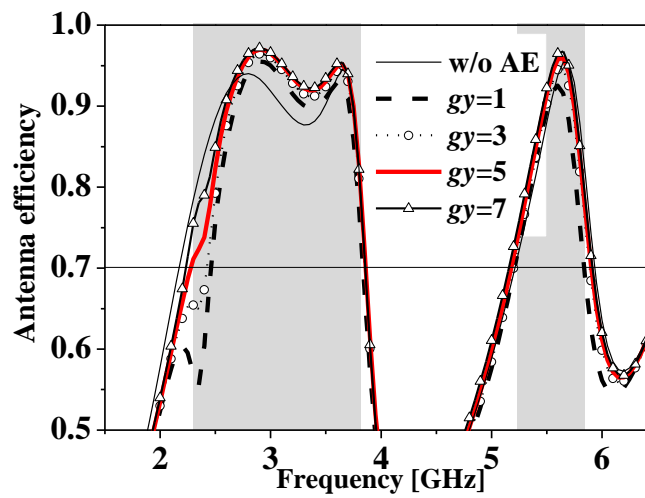


Figure 6.11: Antenna efficiency when gy is varied.

6.2.4 Current Distribution and Radiation Characteristic

Figure 6.12 shows the current distribution at 2.45 GHz with $h=9$ mm, $l=21$ mm, and $g_y=5$ mm. FMA#1 is excited, and FMA#2 is terminated with a terminal impedance of $50\ \Omega$. In comparing to FMA array without AE in Fig. 6.1(c), obviously the current on the ground plane is suppressed by applying AEs. Also, relatively large current can be seen flowing on AE. 3D total radiation patterns at 2.45 GHz are illustrated in Fig. 6.13. Due to the presence of AE and relatively large current on AE, the radiation patterns are different between w/ and w/o AE. Thus, the more power radiates toward $+y$ direction rather than $-y$ direction by adding AE, which means that AE acts as an inverted-L antenna. However, the peak gain of the model with/without AE is 4.2 dBi and 3.5 dBi, respectively. That is, the gain is slightly increased by applying AE.

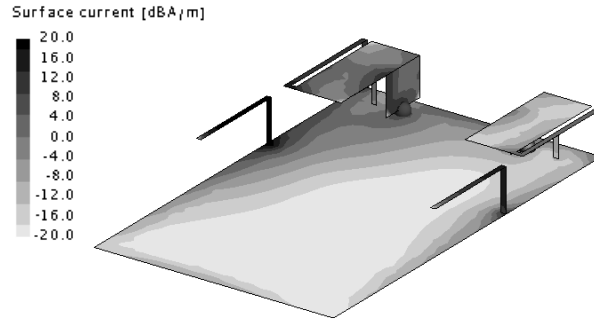


Figure 6.12: Current distributions at 2.45 GHz with $h=9$, $l=21$, and $g_y=5$.

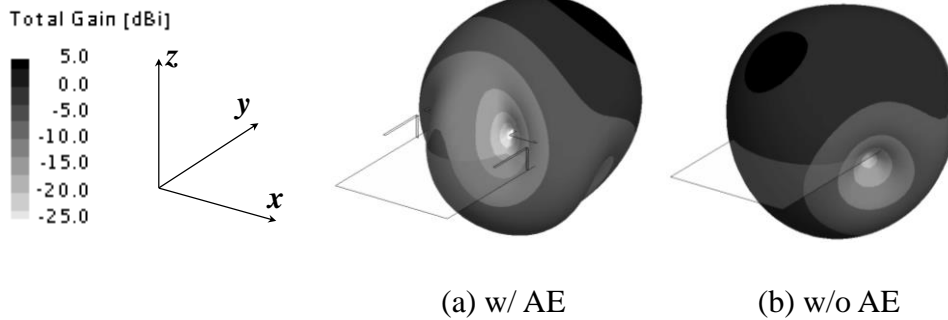


Figure 6.13: 3D radiation patterns at 2.45 GHz when FMA#1 is excited.

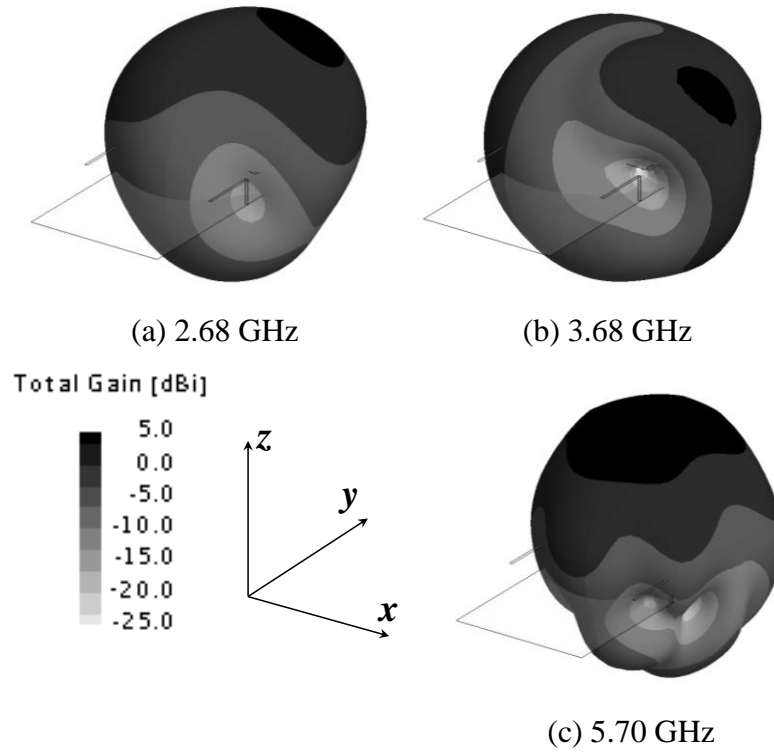


Figure 6.14: 3D radiation patterns when FMA#1 is excited for comparison with Fig. 5.22.

In addition, 3D total radiation patterns are shown in Fig. 6.14 in order to indicate that AE does not affect the radiation patterns at other resonant frequencies by comparing with Fig. 5.22. Actually, at the 1st resonance, 2.68 GHz, the patterns differ from each other since the target frequency of 2.45 GHz and 2.68 GHz are close. However, at the 2nd and 3rd resonance, 3.68 GHz and 5.70 GHz, the patterns are hardly varied regardless of the existence of AE. Thus, AE has the effect on radiation patterns around the operational frequency because AE itself acts as an antenna, while the gain is enhanced and the radiation patterns are maintained at the different frequency.

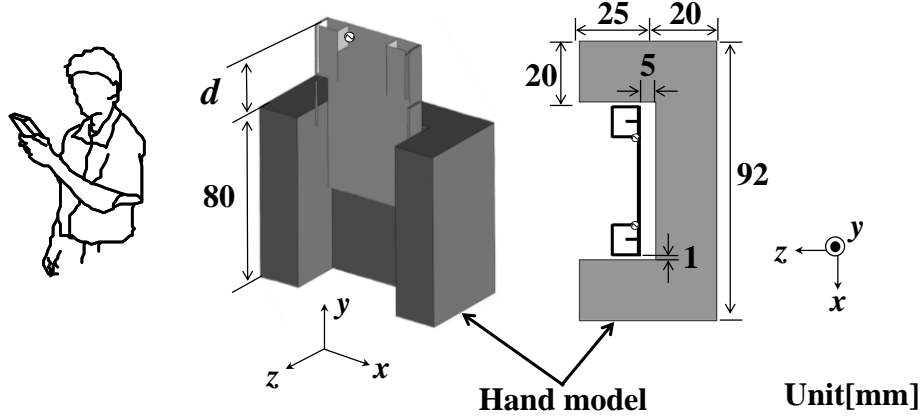


Figure 6.15: Hand model and terminal model in hand held condition.

6.3 Effect of a Human Hand on Antenna Characteristics

Parametric analysis has been conducted in Sect. 6.2, and the proper parameters of AE contributing to current reduction on the ground are determined. In this section, human hand will be considered assuming more practical usage, and the effect of AE will be analyzed employing a simulated hand model.

6.3.1 Antenna Configuration

Figure 6.15 shows the simulated hand model and terminal model in hand held condition. The hand model is based on COST 244 [106]. Also, the hand model has the relative permittivity (ϵ_r) of 54 and conductivity (σ) of 1.5 S/m corresponding to the electric constant of muscle at 2.45 GHz [107]. There are 1 mm and 5 mm spacings between the inner surface of hand model and the ground plane since the antenna is supposed to be surrounded by a handset case. The parameter d denotes the distance between the top of the terminal and the top of the hand model. Also, the parameters of AE are $h=9$ mm, $l=21$ mm, and $dy=5$ mm which are obtained in the previous section.

6.3.2 Antenna Efficiency and Current Distribution

Figure 6.16 shows the antenna efficiency at 2.45 GHz with respect to the parameter d . For the comparison, the model without AE is also presented in the figure. Due to the power absorption by the hand model, the efficiencies at $d=0$ decrease to less than 20% regardless of with/without AE, while the efficiencies are more than 75% when there is

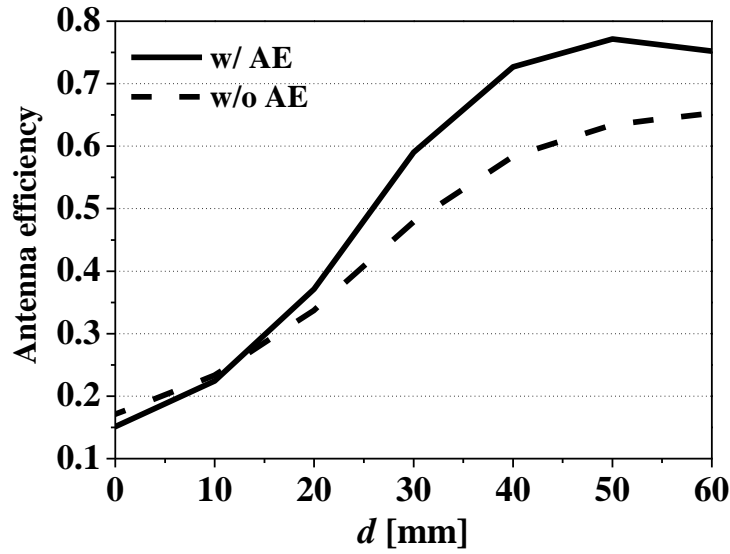
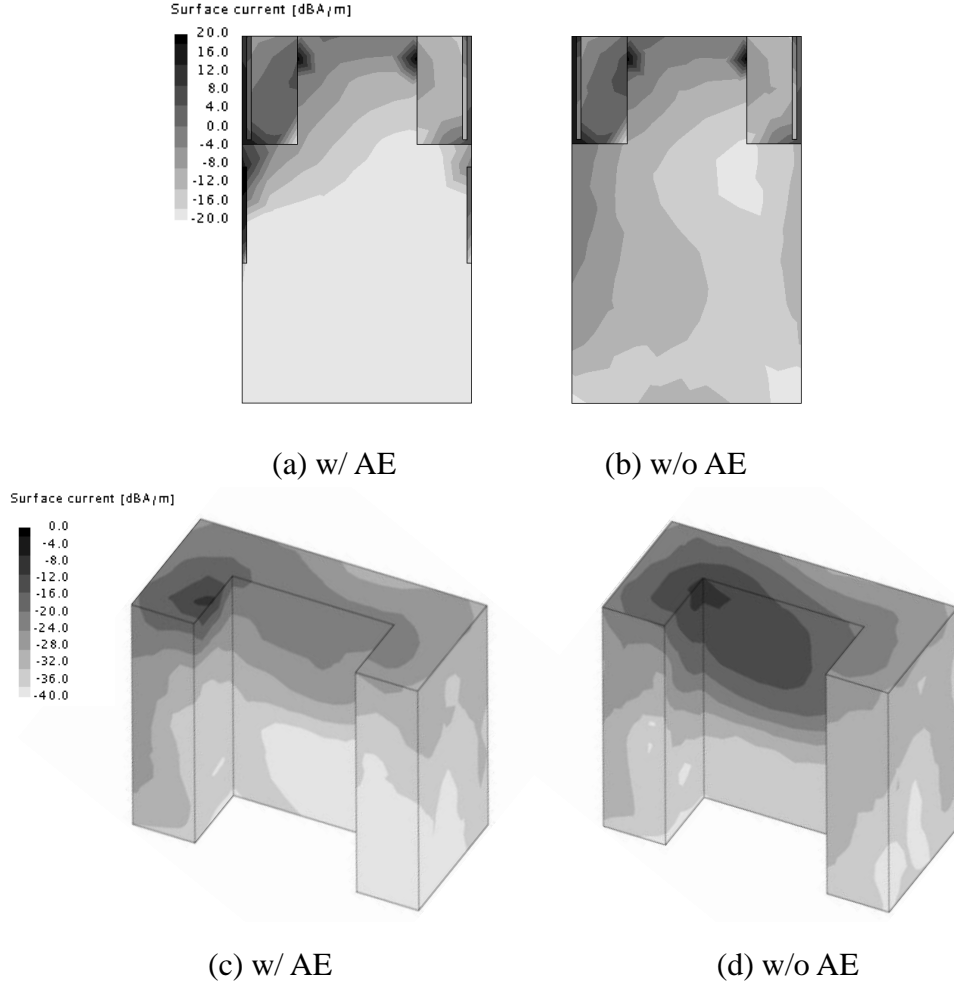


Figure 6.16: Antenna efficiency with respect to d .

no hand model in both cases (Fig. 6.11). However, higher improvement of the efficiency of the model with AE is achieved than that of the model without AE. At $d=40$ mm, the largest difference can be observed, which is approximately 14% improvement.

Figure 6.17 shows the current distributions at $d=40$ mm and 2.45 GHz. Current suppression on the ground plane is clearly observed in Fig. 6.17(a) and (b). Current is not only suppressed on the edge of the ground, but also inside area of the ground plane is significantly decreased. Furthermore, the current distributions on FMA element are quite similar between the two models, which mean that AE hardly affects the current on antenna element. On the other hand, when the surface current on the hand model is compared in Fig. 6.17(c) and (d), the current level is suppressed around the inner corner of the hand as well. Therefore, it is likely that the hand effect on antenna characteristics is alleviated by the application of AE.

Figure 6.17: Current distributions at $d=40$ and 2.45 GHz.

6.3.3 Radiation Characteristic

The variation of peak gain with respect to the distance d is shown in Fig. 6.18. As mentioned in Subsect. 6.2.4, the peak gain is enhanced by installing AE. In fact, the improvement of gain is confirmed from the simulation from $d=0$ to 60 mm. At $d=60$ mm, the gain ameliorates up to approximately 4.2 dBi, which is equivalent value when there is no hand. On the other hand, the model without AE remains low gain. This is caused by the variation of the current distributions on the ground plane. In addition, the human hand absorbs the radiated power, leading to degradation of antenna efficiency and gain. According to the simulation results at $d=60$, about 21.5% of power for radiated power is absorbed by the hand model in case of the model without AE. Meanwhile, the hand model absorbs only 5.8% of power for the model with AE.

Figure 6.19 and 6.20 shows the comparison of 3D radiation patterns between w/ and w/o hand model at 2.45 GHz and $d=40$ mm. Each polarization component and total component are illustrated in the figure. By applying AE, the variation of radiation patterns becomes small regardless of the presence of hand model, particularly E_ϕ component. It is considered that since the terminal current is suppressed, then current distributions on the ground have less influence from the body effect, resulting in maintain the gain and radiation patterns.

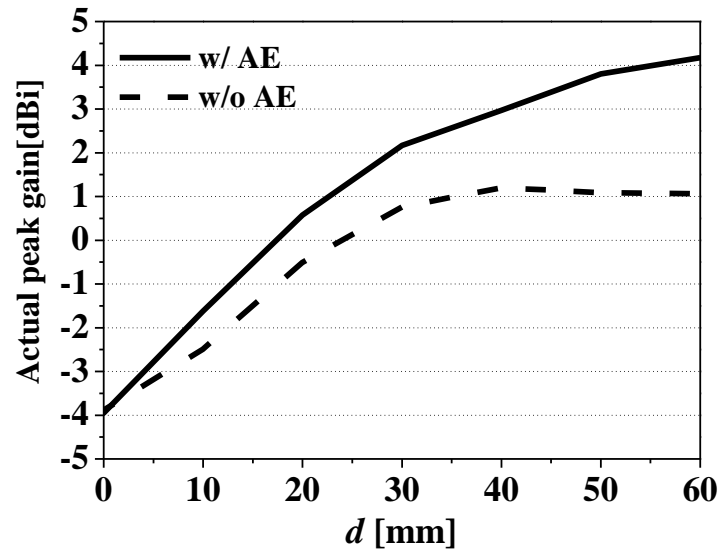


Figure 6.18: Peak gain (E_{tot}) with respect to d .

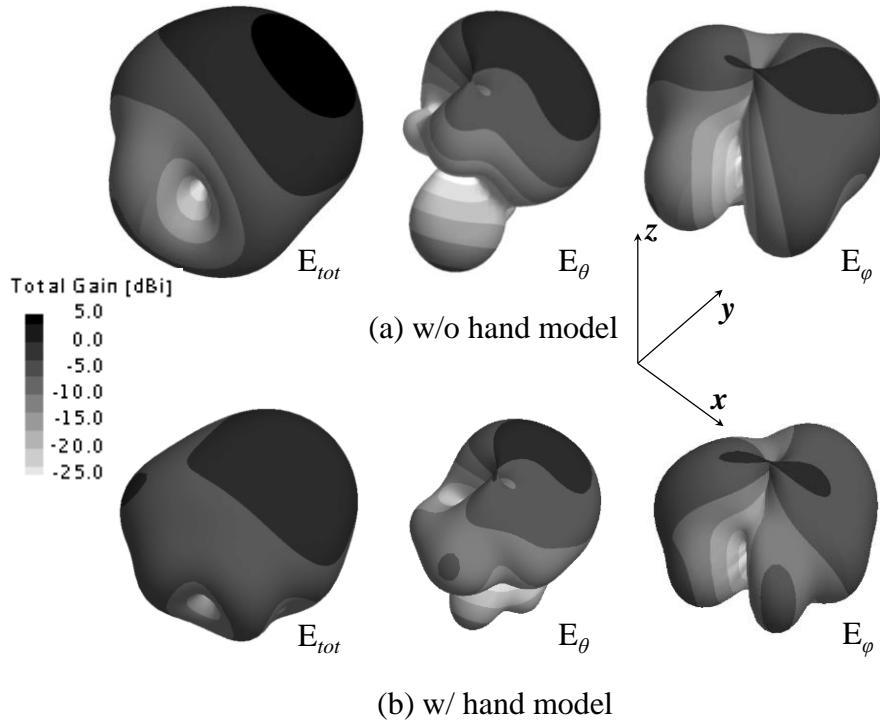


Figure 6.19: 3D radiation patterns w/ AE.

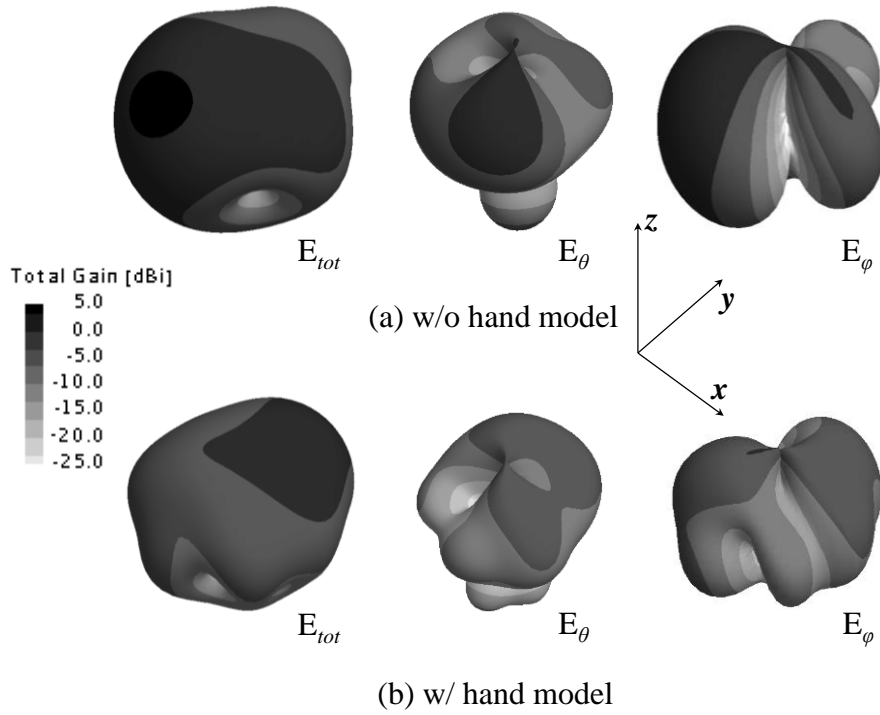


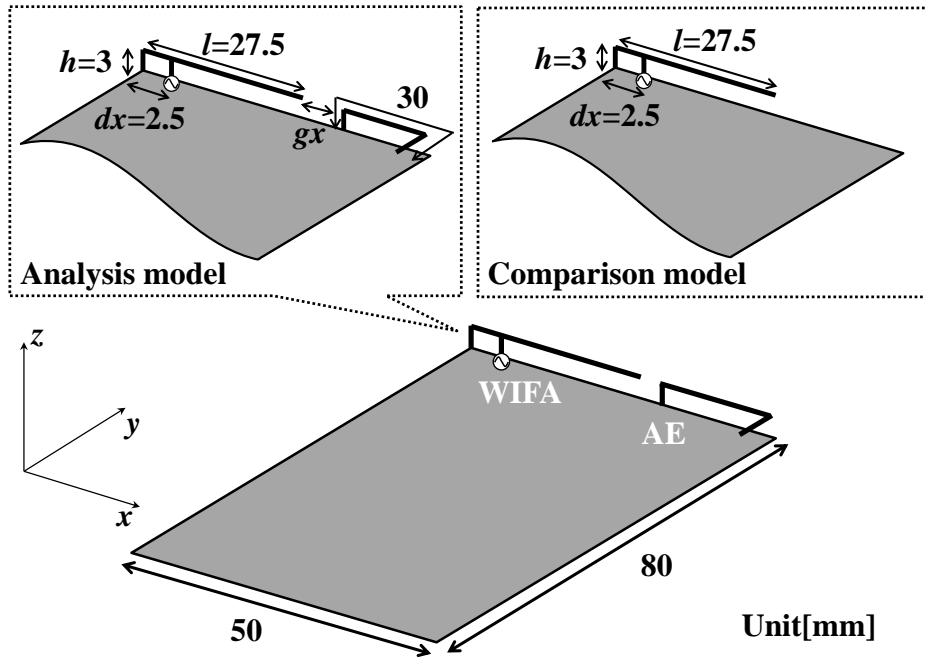
Figure 6.20: 3D radiation patterns w/o AE.

6.4 Application of AE to a Different Antenna

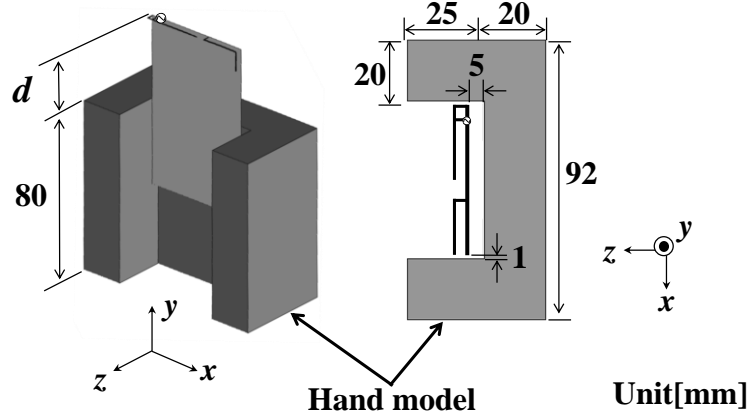
In this section, AE is applied to a different type of antenna. Here, wire inverted-F antenna, which is commonly used in wireless communication, is selected.

6.4.1 Antenna Configuration

Figure 6.21 shows the antenna configuration of wire inverted-F antenna (WIFA) with AE, which is mounted on the same size ground plane of $50 \times 80 \text{ mm}^2$, and simulated hand model. Analysis model and comparison model are presented in Fig. 6.21(a). In the analysis model, AE is placed around the tip of WIFA, where the electric near-field is strong, and it is defined that AE is separated from WIFA by gx . For considering low-profile antenna configuration, the height of AE is equivalent to WIFA, that is, 3 mm. The target frequency is 2.45 GHz, so the total length of AE is 30 mm ($\lambda/4$). AE and WIFA are composed of wire element whose radius is 0.25 mm. As can be seen in Fig. 6.21(b), the same hand model is utilized in order to analyze the effect of AE, and the hand-held condition is presented as well.

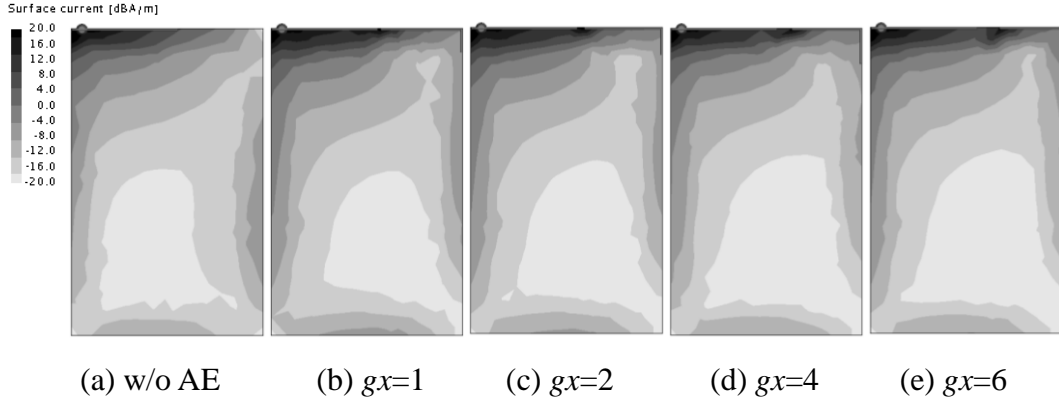


(a) Structure of WIFA and AE



(b) Hand model and terminal model in hand held condition

Figure 6.21: Antenna configuration.

Figure 6.22: Current distributions at 2.45 GHz when g_x is varied.

6.4.2 Location of AE

Figure 6.22 shows the current distributions at 2.45 GHz when the distance g_x between WIFA and AE is varied. The height and length of AE are fixed. It is true that the current around the edge on the ground, particularly right side edge where AE is located, is suppressed by placing AE. However, the amount of current reduction is not so large even though g_x is changed. The VSWR characteristics are shown in Fig. 6.23 with respect to g_x . The resonant frequencies hardly shift, and bandwidths are almost the same. Thus, in the case of WIFA, the distance between WIFA and AE does not strongly affect the current reduction and impedance characteristic. Figure 6.24 shows antenna efficiency corresponding to the variation of g_x . When g_x is 4 mm, the efficiency is the largest. Therefore, g_x is set to 4 mm in the following analysis.

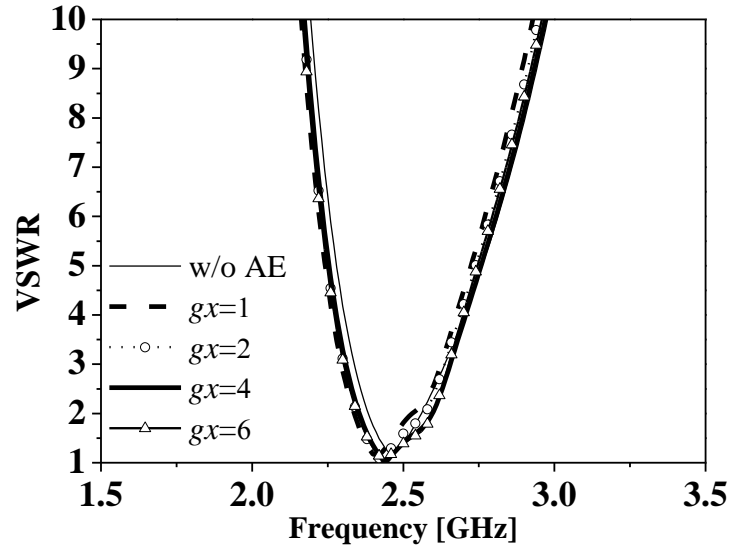


Figure 6.23: VSWR characteristics when g_x is varied.

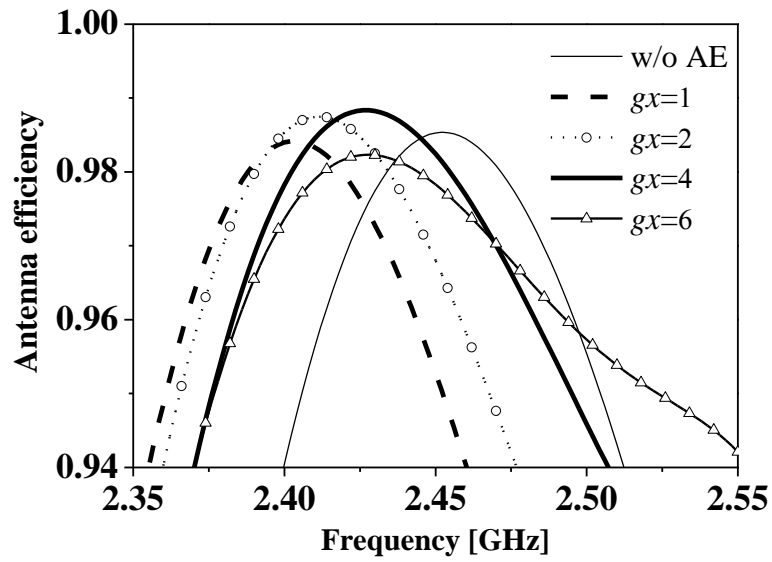


Figure 6.24: Antenna efficiency when g_x is varied.

6.4.3 Fundamental Characteristics

Figure 6.25 shows antenna efficiency at 2.45 GHz when sliding the hand model by the distance d as presented in Fig. 6.21(b). For the comparison, the model without AE is also presented in the figure. It is obvious that the efficiency is increased all the way from 0 mm to 60 mm. The maximum improvement is about 7.2% at $d=30$ mm, which is a smaller value compared to the case FMA array discussed above. This is because the amount of current reduction on the ground plane remains small despite the installation of AE.

Figure 6.26 shows the current distributions at $d=30$ mm and 2.45 GHz. Similarly, the current on both the ground and hand model of analysis model can be suppressed compared with the comparison model (w/o AE). Consequently, the gain is also remedied as presented in Fig. 6.27. The similar results are obtained, which means that the peak gain is also enhanced since the power absorption by hand model is mitigated. Thus, AE is applied to WIFA, then improvements of various properties are confirmed by the simulation.

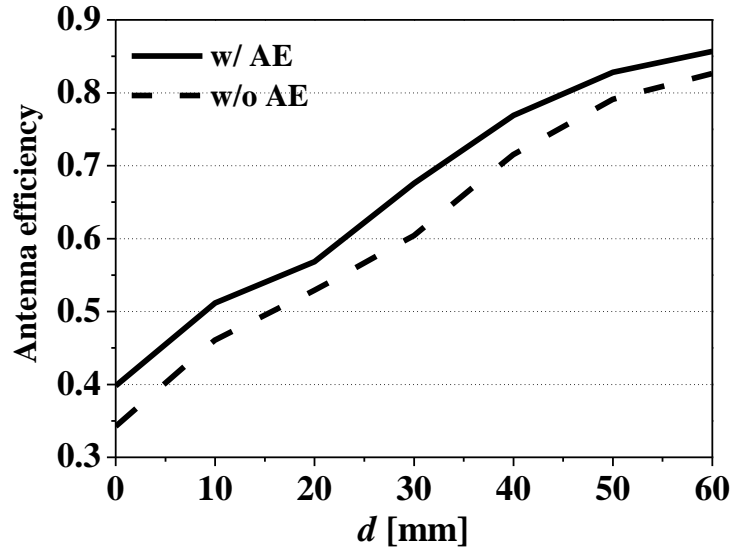


Figure 6.25: Antenna efficiency with respect to d .

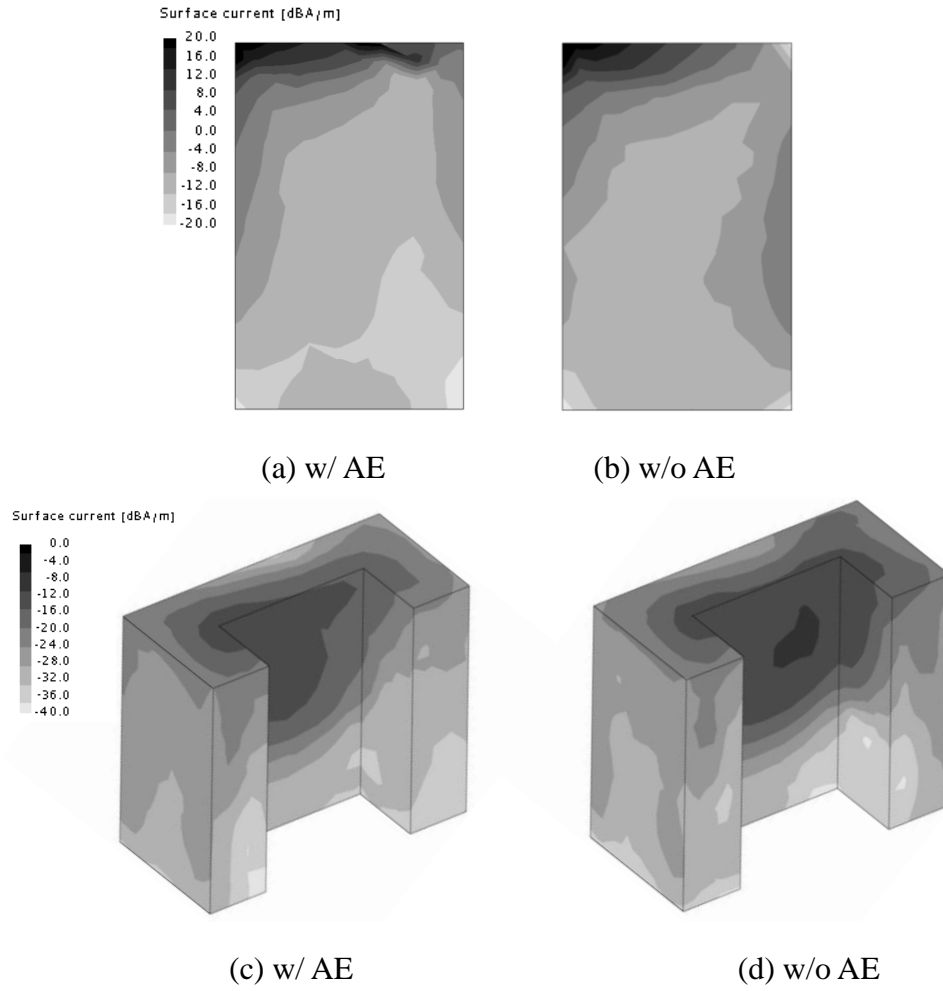


Figure 6.26: Current distributions at $d=30$ and 2.45 GHz.

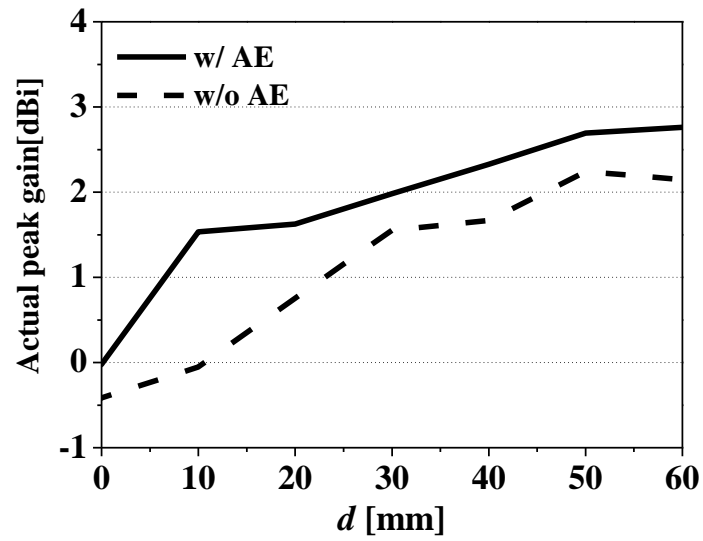


Figure 6.27: Peak gain (E_{tot}) with respect to d .

6.5 Summary

In this chapter, the quarter-wavelength additional element (AE) has been applied to FMA array and WIFA in order to reduce the current on the ground plane. Then, the effect of AE on a human hand is analyzed utilizing simplified one-layer hand model.

First of all, the length, height, and location of AE are analyzed based on current distribution, impedance characteristic, and antenna efficiency. It is confirmed from the simulation results that $\lambda/4$ and higher structure of AE from the ground are more effective for current suppression. Also, there is a trade-off between current reduction and bandwidth in deciding the location of AE. In addition, the hand model is taken into consideration. Due to the application of AE, antenna efficiency and radiation characteristics are improved. AE is applied to WIFA as well, and similar effects are confirmed, such as current reduction on the ground plane and hand model, improvement of antenna efficiency, and enhancement of gain.

Thus, AE is very effective to reduce the current on the ground plane and enhance antenna performances with user's hand in hand-held condition. Also, it is considered that AE can work with other different antennas.

Chapter 7

Conclusion

This dissertation has focused on FDAFL, and the objective was to apply FDAFL to a small terminal and to present indications for enhancing antenna performances with consideration of requirements for a terminal antenna.

Chapter 2 presented an overview of FDAFL as well as fundamental characteristics and operation principle of FDA. FDA was the most fundamental antenna with folded structure, consisting of two parallel dipoles. Due to the structure, the current flow on the antenna element was varied, which generates distinctive antenna properties. On the other hand, FDAFL showed wider bandwidth than FDA, led by two resonant operation, while current distribution and radiation characteristic were equivalent between FDAFL and FDA. Also, the equivalent circuit of the feed lines was clarified.

Chapter 3 presented the way to miniaturize the feed line of FDAFL without utilizing meandered structure, then FDAFL was applied to a small terminal. Impedance matching of FDAFL could be obtained by altering the width of wa_2 and wf , which resulted in low-profile antenna configuration and broadband property of FDAFL. In addition, FDAFL was applied to various sizes of the ground plane, but wideband characteristics were maintained despite of the different ground sizes. When the antenna parameters were $(lf, wa_2, wf) = (4 \text{ mm}, 6 \text{ mm}, 10 \text{ mm})$ on the ground plane of $50 \times 80 \text{ mm}^2$, H was reduced to 12 mm, which was 43% compared with the initial length. Relative bandwidth ($VSWR \leq 3$) was about 65%. Thus, FDAFL could be applied to a small terminal with wideband characteristic.

In Chapter 4, two different 3D FDAFL were proposed for miniaturizing the antenna system, and fundamental characteristics were analyzed. Model-A was bent over the ground plane, and Model-B was bent outside of the ground plane. In both cases, since impedance transformation was possible by changing wa_2 and wf , the relative bandwidth over 74% was obtained when antenna height h was greater than 7 mm in Model-A. As for Model-B, very broadband characteristics over 86% were achieved

even $h=1$ mm. It was also confirmed that the prominence w could be decreased from 12 mm to 6 mm with the bandwidth over 83% when $h=4$ mm. Thus, these 3D models could show wider bandwidth than planar FDAFL proposed in Chapter 3. Parameter ranges for wideband operation were shown in detail, so it will help to design antennas for real application.

In Chapter 5, multiband FMA array derived from FDAFL was proposed, and its wideband characteristics and a suitable configuration for MIMO antenna were presented. FMA had wider bandwidth (58.0%) compared with PIFA (34.8%) which had the same physical volume. In order to obtain a frequency resonance, a parasitic element was introduced for multiband antenna. Proposed antenna could almost cover WiMAX 2.5/3.5/5.5 GHz bands and WLAN 2.4/5 GHz bands. The antenna efficiency of between 70% to 96% and very low correlation coefficient of less than 0.02 were observed in the target frequency bands.

Chapter 6 presented the application of a quarter-wavelength additional element to multiband FMA array and WIFA in order to reduce the current on the ground plane. Then, the effect of AE on a human hand was analyzed in hand-held condition. First of all, it was confirmed from the simulation results that $\lambda/4$ and higher structure of AE from the ground were more effective for current suppression. Also, there was a trade-off between current reduction and bandwidth in deciding the location of AE. In addition, the hand model was taken into consideration, then antenna efficiency and radiation characteristics were improved by the installation of AE. Thus, AE was very effective to reduce the current on the ground plane and enhance antenna performances with user's hand. Also, it was found that AE could work with other different antennas.

From these results, it has been confirmed that FDAFL has high versatility for various types of applications, such as a USB dongle, handset, Wi-Fi router, and tablet. Also, MIMO application and multiband operation derived from FDAFL showed good antenna performances, then further improvement was achieved by AE. Thus, FDAFL has high availability for the real application as well. Finally, it is desired that this dissertation will contribute to antenna design.

Acknowledgments

First of all, I am extremely grateful to my supervisor, Professor Hisashi Morishita for his invaluable advice and concern. He gave me a lot of opportunities for various things, then I could meet many people, which was irreplaceable experience in my life. In addition, I would like to express my sincere gratitude to Dr. Shingo Tanaka of Yazaki Corp. for great advice and comments on this work.

Also, I would like to express appreciation to Professor Hiroyuki Arai of Yokohama National University, Professor Toru Uno of Tokyo University of Agriculture and Technology, Professor Hiroshi Moritake and Associate professor Naobumi Michishita of National Defense Academy for the discussions and critical reading of manuscript.

I am also very grateful to Mr. Tsuneto Kimura, Mr. Youichi Ido, Dr. Tatsuo Toba, and Mr. Yuta Nakagawa of Yazaki Corp., Dr. Satoru Kurokawa, Dr. Masanobu Hirose, Dr. Michitaka Ameiya of National Institute of Advanced Industrial Science and Technology, Mr. Masao Sakuma of Sakuma Antenna Co., Ltd., Professor Yoshihide Yamada of Malaysia-Japan International Institute of Technology, Mr. Toshiro Shibushita of Mitsubishi Electric Corp. and many other professors, company researchers, and students who have joined various conference activities.

I would like to give a special thanks to my colleagues in Morishita Laboratory, Dr. Ichikawa (JASDF), Dr. Hayashida (Sangikyo Corp.), Dr. Kim Yong Ho (Republic of Korean Army), Dr. Itoh (Harada Industry Co., Ltd.), Dr. Miyamoto (JASDF), Mr. Tuan Hung Nguyen (Vietnamese Army), Mr. Matsuzaki (JASDF), Mr. Komuro (JASDF), Mr. Tenma (JASDF), Mr. Hirayama (JASDF), Mr. Miyamoto (JASDF), Mr. Yamano (JASDF), Mr. Franck Pacaud (French Army), Mr. Kim Jun Myeoung (Republic of Korean Army), Mr. Watanabe (JASDF), Mr. Nakao (JASDF), Mr. Suzuki (JASDF), Mr. Kobayashi (JASDF), Mr. Simon Condette (French Army), Mr. Iwata (JASDF), Mr. Kagiya (JGSDF), Mr. Ohara (JASDF), Mr. Julien Banasiak (French Army), Mr. Saita (JGSDF), Mr. Agung Susetio (Indonesian Navy), Mr. Murata, Mr. Oki (JGSDF), Mr. Nishiyama, Mr. Benjamin Giordani (French Army), other bachelor students, and all the people I met in the academy during my Ph.D. course.

This work was not accomplished without help of my family. I would like to thank my wife and adorable daughters.

Bibliography

- [1] H. Hojo, "Trends in wireless access system technology toward expanded broadband based on optical and wireless systems," NTT Technical Review, vol.6, no.5, May 2008.
- [2] S. Uno, "Seamless communication service in ubiquitous environment and its realization techniques," IEICE Trans. Commun. (Japanese Edition), vol.J89-B, no.8, pp.1334-1346, Aug. 2006.
- [3] V. Nair "Heterogeneous wireless communication devices-present and future," in Proc. IEEE Int. Conf. of Recent Advances in Microwave Theory and Applications, Nov. 2008.
- [4] Ministry of Internal Affairs and Communications (in Japanese). [Online] Available: <http://www.soumu.go.jp/johotsusintokei/index.html>
- [5] K. Ogawa, "IEEE 802.11ah based M2M networks employing virtual grouping and power saving methods," IEICE Trans. Commun., vol.E96-B, no.12, pp.2976-2985, Dec. 2013.
- [6] T. Ohya, K. Cho, and S. Narahashi, "Key wireless technologies for future high-speed and large-capacity communications," NTT DOCOMO Technical Journal, vol.10, no.2, pp.23-30, Sept. 2008.
- [7] International Telecommunication Union. [Online] Available: http://www.itu.int/net/newsroom/wrc/2012/reports/imt_advanced.aspx
- [8] S. Konishi, "Comprehensive analysis of heterogeneous networks with pico cells in LTE-Advanced systems," IEICE Trans. Commun., vol.E96-B, no.6, pp.2976-2985, June 2013.
- [9] ITU-R Report M.2134: "Requirements related to technical performance for IMT-Advanced radio interface(s)," 2008.
- [10] S. Nomoto, "A consideration on future wireless communication systems for smarter society," IEICE Trans. Commun. (Japanese Edition), vol.J97-B, no.9, pp.731-737, Sept. 2014.
- [11] European Telecommunications Standards Institute (ETSI), Future Mobile Summit, France, Nov. 2013. [Online] Available: <http://www.etsi.org/news-events/events/682-2013-etsi-future-mobile-summit>
- [12] ARIB News, no.912, Dec. 2013. [Online] Available: <http://www.arib.or.jp/osirase/news.pdf>

- [13] K. S. So, "The CJK triangle-formation leads the 1,000 times faster 5G...", Korea IT News, Dec. 2013. [Online] Available: <http://english.etnews.com/news/article.html?id=20131203200004>
- [14] T. A. Levanen, J. Pirskanen, T. Koskela, J. Talvitie, and M. Valkama, "Radio interface evolution towards 5G and Enhanced local area communications," IEEE Access, vol.2, pp.1005-1029, Sept. 2014.
- [15] K. Hiramatsu, T. Oisumi, and D. Imamura, "Radio communication technology evolution in terminals," in Proc. IEICE Society Conference, BP-2-4, Sept. 2010 (in Japanese).
- [16] S. Abeta, "Requirements for LTE/LTE-Advanced," IEICE Journal, vol.96, no.3, pp.144-149, March 2013 (in Japanese).
- [17] R. Kohno, and S. Haruyama, "Current status and the future of software radio," IEICE Trans. Commun. (Japanese Edition), vol.J84-B, no.7, pp.1112-1119, July 2001.
- [18] T. Ueda, S. Bandyopadhyay, and K. Hasuiki, "An adaptive media access control protocol and system performance of wireless ad hoc network using smart antenna," IEICE Trans. Commun. (Japanese Edition), vol.J85-B, no.12, pp.2189-2197, Dec. 2002.
- [19] W. Yu, and T. Lan, "Transmitter optimization for the multi-antenna downlink with per-antenna power constraints," IEEE Trans. Signal Process., vol.55, no.6, pp.2646-2660, June 2007.
- [20] H. Arai, and K. Cho, "Cellular and PHS base station antenna systems," IEICE Trans. Commun., vol.E86-B, no.3, pp.980-992, March 2003.
- [21] K. Ogawa, "Assessment, analysis and high-performance technologies for handset antenna systems," IEICE Trans. Commun. (Japanese Edition), vol.J93-B, no.9, pp.1100-1114, Sept. 2010.
- [22] K. Cho, R. Yamaguchi, and H. Jiang, "Base station and terminal antenna technologies required for next generation mobile communication systems," IEICE Trans. Commun. (Japanese Edition), vol.J91-B, no.9, pp.886-900, Sept. 2008.
- [23] H. Arai, and D. Uchida, "Design of MIMO antennas for indoor base station and mobile terminal," IEICE Trans. Commun., vol.E95-B, no.1, pp.10-17, Jan. 2012.
- [24] K. Ogawa, "High-performance technologies for portable radio antennas: Toward the harmony of antenna, propagation, human body and system," IEICE Journal, vol.84, no.11, pp.775-781, Nov. 2001 (in Japanese).
- [25] T. Hori, "Broadband/multiband printed antennas," IEICE Trans. Commun. (Japanese Edition), vol.J87-B, no.9, pp.1130-1139, Sept. 2004.

-
- [26] Federal Communications Commision: "In the matter of revision of part15 of the commission's rules regarding ultra-wideband transmission systems," First report and order, ET Docket 98-153, April 2002.
- [27] Ministry of Internal Affairs and Communications (in Japanese). [Online] Available: <http://www.tele.soumu.go.jp/j/adm/freq/search/share/index.htm>
- [28] H. Morishita, "Small mobile terminal antennas: From design concept to fugure perspective," IEICE Trans. Commun. (Japanese Edition), vol.J88-B, no.9, pp.1601-1612, Sept. 2005.
- [29] A. Cihangir, W. G. Whittow, C. J. Panagamuwa, F. Fabien, G. Jacquemod, F. Ganesello, and C. Luxey, "Feasibility study of 4G cellular antennas for eyewear communicating devices," IEEE Antennas Wireless Propagat. Lett., vol.12, pp. 1704-1707, Oct. 2013.
- [30] D. Gaspar, and A. A. Moreira, "Belt antenna for wearable applications," in Proc. IEEE Antennas and Propagation Society International Symposium, July 2009.
- [31] H. Horie, and H. Iwasaki, "Wearable finger ring type antenna made of fabric cloth for BAN use at UHF and ISM bands," in Proc. IEEE MTT-S IMWS-BIO, Dec. 2013.
- [32] G. J. Foschini, and M. J. Gans, "On limits of wireless communications in a fading environment when using multiple antennas," Wireless Personal Commun., vol.6, no.3, pp.311-335, March 1998.
- [33] D. Gesbert, M. Shafi, D. S. Shiu, P. Smith, and A. Naguib, "From theory to practice: An overview of MIMO space- time coded wireless systems," IEEE J. Sel. Areas Commun., vol.21, no.3, pp.281-302, April 2003.
- [34] Y. Asai, K. Ishihara, T. Murakami, R. Kudo, T. Ichikawa, Y. Takatori, and M. Mizoguchi, "Overview of very high throughput wireless LAN standard IEEE 802.11ac and experimental evaluation of multiuser-MIMO transmission," IEICE Trans. Commun. (Japanese Edition), vol.J97-B, no.1, pp.1-18, Jan. 2014.
- [35] Q. Li, X. Lin, J. Zhang, and W. Roh, "Advancement of MIMO technology in WiMAX: from IEEE 802.16d/e/j to 802.16m," IEEE Communication Magazine, vol.47, no.6, pp.100-107, June 2009.
- [36] Q. Li, G. Li, W. Lee, M. Lee, D. Mazzarese, B. Clerckx, and Z. Li, "MIMO techniques in WiMAX and LTE: A feature overview," IEEE Communication Magazine, vol.48, no.5, pp.86-92, May 2010.
- [37] M. A. Jensen, J. W. Wallace, "A review of antennas and propagation for MIMO wireless communications," IEEE Trans. Antennas Propagat., vol.52, no.11, pp.2810-2824, Nov. 2004.
- [38] L. Zhao, L. K. Yeung, and K. Wu, "A coupled resonator decoupling network for two-element compact antenna arrays in mobile terminals," IEEE Trans. Antennas Propagat., vol.62, no.5, pp.2767-2776, May 2014.

- [39] C. A. Balanis, *Antenna Theory: Analysis and Design*, 3rd ed., John Wiley & Sons, 2005.
- [40] K. Sato, K. Nishikawa, N. Suzuki, and A. Ogawa, "Analysis of antennas mounted on the portable equipment near human body," *IEICE Trans. Commun. (Japanese Edition)*, vol.J79-B-II, no.11, pp.892-900, Nov. 1996.
- [41] H. Morishita, Y. Kim, and K. Fujimoto, "Analysis of handset antennas in the vicinity of the human body by the electromagnetic simulator," *IEICE Trans. Electron.*, vol.E84-C, no.7, pp.937-947, July 2001.
- [42] H. Morishita, S. Hayashida, J. Ito, and K. Fujimoto, "Analysis of built-in antennas for handset using human (head, hand and finger) model," *IEICE Trans. Commun. (Japanese Edition)*, vol.J85-B, no.5, pp.687-697, May 2002.
- [43] K. Ogawa, H. Iwai, and N. Hatakenaka, "A high-precision real human phantom for EM evaluation of handheld terminal antennas in a talk situation," *IEICE Trans. Commun. (Japanese Edition)*, vol.J85-B, no.5, pp.676-686, May 2002.
- [44] H. Hatamoto, N. Nakamoto, H. Kikuchi, S. Shimizu, "A study on patch antenna design for wireless networks in ICT equipment," in *Proc. IEICE General Conference*, B-1-134, March 2012 (in Japanese).
- [45] M. Ohira, "Development of small antenna for in-machine wireless harness and its robustness evaluation," in *Proc. IEICE General Conference*, B-1-193, March 2013 (in Japanese).
- [46] A. Yamada, S. Sekine, M. Higaki, S. Obayashi, H. Shoki, and H. Arai, "Mechanism of H-shaped antenna using parallel resonance mode with unidirectional radiation pattern," *IEICE Technical Report*, AP2009-49, pp.29-34, July 2009 (in Japanese).
- [47] K. Hirasawa, and K. Fujimoto, "Characteristics of wire antennas on a rectangular conducting body," *IEICE Trans. Commun. (Japanese Edition)*, vol.J56-B, no.9, pp.1133-1139, Sept. 1982.
- [48] C. Rowell, and E. Y. Lam, "Mobile-phone antenna design," *IEEE Antennas Propagation Magazine*, vol.54, no.4, pp.14-34, Aug. 2012.
- [49] S. Hayashida, H. Morishita, and K. Fujimoto, "A wideband folded loop antenna for handsets," *IEICE Trans. Commun. (Japanese Edition)*, vol.J86-B, no.9, pp.1799-1805, Sept. 2003.
- [50] S. Hayashida, T. Tanaka, H. Morishita, Y. Koyanagi, and K. Fujimoto, "Characteristics of built-in folded monopole antenna for handsets," *IEICE Trans. Commun.*, vol.E88-B, no.6, pp.2275-2283, June 2005.
- [51] K. Ishiyama, J. Takada, "Multi-band folded dipole antenna for mobile phone," in *Proc. IEEE International Workshop on Antenna Technology*, pp.275-278, March 2007.

-
- [52] I. Szini, C. D. Nallo, and A. Faraone, "The enhanced bandwidth folded inverted conformal antenna (EB FICA) for multi-band cellular handsets," in Proc. Int. Symp. on Antenna Propagat., pp.4697-4700, June 2007.
- [53] Y. Kim, T. Hayashi, Y. Koyanagi, and H. Morishita, "Compact built-in handset MIMO antenna using L-shaped folded monopole antenna," IEICE Trans. Commun., vol.E91-B, no.6, pp.1743-1751, June 2008.
- [54] M. Hirayama, T. Yamano, Y. Kim, and H. Morishita, "A study on wideband characteristics of folded dipole antenna by using a electromagnetic simulator," IEICE Technical Report, MW2008-129, pp.61-65, Nov. 2008 (in Japanese).
- [55] Y. Chi, and K. Wong, "Compact multiband folded loop chip antenna for small-size mobile phone," IEEE Trans. Antennas Propagat., vol.56, no.12, pp.3797-3803, Dec. 2008.
- [56] A. Kajitani, Y. Kim, H. Morishita, and Y. Koyanagi, "Characteristics of U-shaped folded dipole antenna for handsets," IEICE Trans. Commun. (Japanese Edition), vol.J92-B, no.3, pp.567-575, March 2009.
- [57] Y. Yu, and J. Tarng, "A novel modified multiband planar inverted-F antenna," IEEE Antennas Wireless Propagat. Lett., vol.8, pp.189-192, April 2009.
- [58] Y. Chi, and K. Wong, "Quarter-wavelength printed loop antenna with an internal printed matching circuit for GSM/DCS/PCS/UMTS operation in the mobile phone," IEEE Trans. Antennas Propagat., vol.57, no.9, pp.2541-2547, Sept. 2009.
- [59] M. Hirayama, J. Itou, and H. Morishita, "Compact balanced-fed folded dipole antenna," IEICE Technical Report, AP2009-155, pp.1-6, Jan. 2010 (in Japanese).
- [60] J. Itoh, N. T. Hung, and H. Morishita, "The mutual coupling reduction between two J-shaped folded monopole antennas for handset," IEICE Trans. Commun., vol.E94-B, no.5, pp.1161-1167, May 2011.
- [61] G. Augustin, B. P. Chacko, and T. A. Denidni, "Printed folded monopole antenna for portable devices operating in LTE/GSM/UMTS/WiFi bands," in Proc. Int. Symp. on Antenna Technology and Applied Electromagnetics, July 2014.
- [62] M. Nagatoshi, S. Tanaka, S. Horiuchi, and H. Morishita, "Broadband characteristics of a planar folded dipole antenna with a feed line," IEICE Trans. Commun., vol.E94-B, no.5, pp.1168-1173, May 2011.
- [63] FEKO User's Manual Suite 6.2.2, Feb. 2013.
- [64] H. Uchida, and Y. Mushiaki, VHF-Antenna, Corona Publishing Co., LTD, 1961.
- [65] Y. Kim, H. Morishita, Y. Koyanagi, and K. Fujimoto, "A folded loop antenna system for handsets developed and based on the advanced design concept," IEICE Trans. Commun., vol.E84-B, no.9, pp.2468-2475, Sept. 2001.

- [66] S. Hayashida, H. Morishita, and K. Fujimoto, "Self-balanced wideband folded loop antenna," *IEE Proc.-Microw. Antennas Propagat.*, vol.153, no.1, pp.7-12, Feb. 2006.
- [67] S. Tanaka, Y. Kim, H. Morishita, S. Horiuchi, Y. Atsumi, and Y. Ido, "Wideband planar folded dipole antenna with self-balanced impedance property," *IEEE Trans. Antennas Propagat.*, vol.56, no.5, pp.1223-1228, May 2008.
- [68] J. D. Kraus, and R. J. Marhefka, *Antennas for All Applications*, 3rd ed., McGraw-Hill, Chapt. 16, and Chapt. 23, 2002.
- [69] W. L. Stutzman, and G. A. Thiele, *Antenna Theory and Design*, 2nd ed., John Wiley & Sons, Chapt. 5, 1998.
- [70] R. W. Lampe, "Design Formulas for an asymmetric coplanar strip folded dipole," *IEEE Trans. Antennas Propagat.*, vol.33, no.9, pp.1028-1031, Sept. 1985.
- [71] R. C. Johnson, *Antenna Engineering Handbook*, 3rd ed., McGraw-Hill, Chapt. 4, 1961.
- [72] G. A. Thiele, E. P. Ekelman, Jr., and L. W. Henderson, "On the accuracy of the transmission line model of the folded dipole," *IEEE Trans. Antennas Propagat.*, vol.28, no.5, pp.700-703, Sept. 1980.
- [73] G. Ruvio, and M. J. Ammann, "A novel wideband semi-planar miniaturized antenna," *IEEE Trans. Antennas Propagat.*, vol.55, no.10, pp.2679-2685, Oct. 2007.
- [74] R. E. Collin, *Foundations for Microwave Engineering*, 2nd ed., John Wiley & Sons, 2001.
- [75] J. Huang, S. Wu, "Planar T-shaped monopole antenna for WLAN/WiMAX applications," *IEICE Trans. Electron.*, vol.E91-C, no.4, pp.625-630, April 2008.
- [76] N. Michishita, H. Kitahara, and Y. Yamada, "Small broadband handset antenna using composite right/left-handed transmission line," *IEICE Trans. Commun. (Japanese Edition)*, vol.J95-B, no.9, pp.1060-1068, Sept. 2012.
- [77] N. Takemura, "Self-complementary inverted-FL antenna using electromagnetic coupling feed for mobile phone," *IEICE Trans. Commun.*, vol.E95-B, no.4, pp.1329-1337, April 2012.
- [78] K. Nishimoto, T. Fukasawa, H. Miyashita, and Y. Konishi, "Bandwidth enhancement method using the resonance of a slide structure in a small terminal antenna," *IEICE Trans. Commun. (Japanese Edition)*, vol.J96-B, no.9, pp.1019-1027, Sept. 2012.
- [79] Y. Yu, and J. Tarng, "A novel modified multiband planar inverted-F antenna," *IEEE Antennas Wireless Propagat. Lett.*, vol.8, pp. 189-192, April Oct. 2009.
- [80] J. Lee, Y. Liu, and H. Kim, "Mobile antenna using multi-resonance feed structure for wideband operation," *IEEE Trans. Antennas Propagat.*, vol.62, no.11, pp.5851-5855, Nov. 2014.

-
- [81] F. Chu, and K. Wong, "Internal coupled-fed dual-loop antenna integrated with a USB connector for WWAN/LTE mobile handset," *IEEE Trans. Antennas Propagat.*, vol.59, no.11, pp.4215-4221, Nov. 2011.
 - [82] B. Tlili, "Design of double C-slot microstrip patch antenna for WiMax application," in *Proc. IEEE Antennas and Propagation Society International Symposium*, 303.8, July 2010.
 - [83] L. Chou, K. Wong, M. Hsu, C. Wang, and R. Lee, "Compact coupling-type antenna for WLAN/WiMAX operatio in the laptop computer," in *Proc. IEEE Antennas and Propagation Society International Symposium*, IF517.6, July 2010.
 - [84] N. Oomura, T. Hori, and M. Fujimoto, "Structure of TV reception antenna suitable for car window installation," *IEICE Technical Report*, AP2005-73, pp.49-52, Sept. 2005 (in Japanese).
 - [85] H. Arai, "Small antennas: Downsizing Techniques and its index factor," *IEICE Trans. Commun.*, vol.E88-B, no.5, pp.1801-1808, May 2005.
 - [86] N. T. Hung, S. Watanabe, and H. Morishita, "Broadband characteristic of U-shaped folded dipole antenna for WiMAX with considering ground plane," *IEICE Trans. Commun.(Japanese Edition)*, vol.J95-B, no.2, pp.371-374, Feb. 2012.
 - [87] J. Kim, S. Kim, and J. Choi, "Design of a compact and wideband printed monopole antenna," *IEICE Trans. Commun.*, vol.E87-B, no.12, pp.3820-3823, Dec. 2004.
 - [88] T. Ohgane, "Base and element technology of MIMO system," *IEICE Workshop*, no.29/30, 2004 (in Japanese).
 - [89] T. Suzuki, N. Miyazaki, and S. Konishi, "Testbed development for IMT-Advanced radio experiments," *IEICE Trans. Commun.(Japanese Edition)*, vol.J93-B, no.7, pp.854-867, July 2010.
 - [90] Y. Ren, "Ceramic based small LTE MIMO handset antenna," *IEEE Trans. Antennas Propagat.*, vol.61, no.2, pp.934-938, Feb. 2013.
 - [91] R. Karimian, H. Oraizi, S. Fakhte, and M. Farahani, "Novel F-shaped quad-band printed slot antenna for WLAN and WiMAX MIMO systems," *IEEE Antennas Wireless Propagat. Lett.*, vol.12, pp.405-408, April 2013.
 - [92] M. U. Khan, and M. S. Sharawi, "A compact 8-element MIMO antenna system for 802.11ac WLAN applications," in *Proc. IEEE International Workshop on Antenna Technology*, pp.91-94, March 2013.
 - [93] G. Kim, and T. Yun, "Compact ultrawideband monopole antenna with an inverted-L-shaped coupled strip," *IEEE Antennas Wireless Propagat. Lett.*, vol.12, pp.1291-1294, Oct. 2013.
 - [94] C. Lee, and K. Wong, "Uniplanar printed coupled-fed PIFA with a band-notching slit for WLAN/WiMAX operation in the laptop computer," *IEEE Trans. Antennas Propagat.*, vol.57, no.4, pp.1252-1258, April 2009.

- [95] D. Kearney, M. John, and M. J. Ammann, "Miniature ceramic dual-PIFA antenna to support band group 1 UBW functionality in mobile handset," *IEEE Trans. Antennas Propagat.*, vol.59, no.1, pp.336-339, Jan. 2011.
- [96] J. Yeom, S. Jeon, H. Choi, and H. Kim, "Compact hybrid DRA combined with PIFA," *IEICE Trans. Commun.*, vol.E93-B, no.10, pp.2781-2783, Oct. 2010.
- [97] A. Diallo, C. Luxey, P. L. Thuc, R. Staraj, and G. Kossiavas "Study and reduction of the mutual coupling between two mobile phone PIFAs operating in the DCS1800 and UMTS bands," *IEEE Trans. Antennas Propagat.*, vol.54, no.11, pp.3063-3074, Nov. 2006.
- [98] J. Itoh, N. T. Hung, and H. Morishita, "The mutual coupling reduction between two J-shaped folded monopole antennas for handset," *IEICE Trans. Commun.*, vol.E94-B, no.5, pp.1161-1167, May 2011.
- [99] P. Hallbjorner, "The significance of radiation efficiencies when using S-parameters to calculate the received signal correlation from two antennas," *IEEE Antennas Wireless Propagat. Lett.*, vol.4, pp.97-99, June 2005.
- [100] Y. Ebine, and K. Kagoshima, "Multi-frequency dipole antenna with closed-spaced parasitic elements," *IEICE Trans. Commun. (Japanese Edition)*, vol.J71-B, no.11, pp.1252-1258, Nov. 1988.
- [101] S. Watanabe, N. T. Hung, and H. Morishita, "Characteristics of L-shaped folded monopole antenna with parasitic elements," *IEICE Technical Report, AP2010-133*, pp.1-6, Jan. 2011 (in Japanese).
- [102] S. Blanch, J. Romeu, and I. Corbella, "Exact representation of antenna system diversity performance from input parameter description," *IET Electronics Lett.* vol.39, no.9, pp.705-707, May 2003.
- [103] H. Zhang, Z. Wang, J. Yu and J. Huang, "A compact MIMO antenna for wireless communication," *IEEE Antennas and Propagation Magazine*, vol.50, no.6, pp.104-107, Dec. 2008.
- [104] S. Sekine, H. Shoki, A. Tsujimura, T. Maeda, and K. Sawaya, "A study of current control in dual resonance antenna mounted on a conducting board that has two notches," *IEICE Trans. Commun. (Japanese Edition)*, vol.J88-B, no.9, pp.1700-1709, Sept. 2005.
- [105] T. Ohishi, N. Odachi, S. Sekine, and H. Shoki, "Low pattern correlation and low mutual coupling diversity antenna with a slit," *IEICE Trans. Commun. (Japanese Edition)*, vol.J90-B, no.9, pp.844-853, Sept. 2007.
- [106] G. D'Inzeo, "Proposal for numerical canonical models in mobile communications," in *Proc. COST 244 Meeting on Reference Models for Bioelectro-magnetic Test of Mobile Communication Systems*, Nov. 1994.
- [107] [Online] Available: <http://transition.fcc.gov/oet/rfsafety/dielectric.html> (FCC web site)

List of Publications and Awards

Journal Papers

1. T. Ito, M. Nagatoshi, S. Tanaka, and H. Morishita, "Characteristics of wideband folded dipole antenna with feed line for mounting to small terminal," IEICE Trans. Commun. (Japanese edition), vol.J96-B, no.2, pp.124-132, Feb. 2013.
2. T. Ito, S. Tanaka, and H. Morishita, "A study on wideband L-shaped folded monopole antenna with parasitic element," IEICE Commun. Express, vol.2, no.5, pp.200-204, May 2013.
3. T. Ito, M. Nagatoshi, S. Tanaka, and H. Morishita, "Wideband 3D folded dipole antenna with feed line for small terminal," IEICE Trans. Commun., vol.E96-B, no.10, pp.2410-2416, Oct. 2013.
4. T. Ito, M. Nagatoshi, S. Tanaka, and H. Morishita, "Folded monopole antenna with parasitic element in small terminal for WiMAX and WLAN MIMO systems," IEICE Trans. Commun., vol.E97-B, no.10, pp.2042-2049, Oct. 2014.

International Conferences

1. T. Ito, M. Nagatoshi, and H. Morishita, "A study of planar folded dipole antenna with feed line for MIMO," IEEE Antennas and Propagation Society International Symposium (AP-S 2012), IF46.7, Chicago, USA, July 2012.
2. T. Nakao, T. Ito, and H. Morishita, "Fundamental study on the radiation restraint from helmet antenna to the human head direction," Joint Conference of Electrical Electronics and Engineers (JCEEE 2012), 02-1A-03, pp. 3, Nagasaki, Japan, Sept. 2012.
3. T. Ito, M. Nagatoshi, S. Tanaka, and H. Morishita, "Application of planar folded dipole antenna with feed line to small terminal for WiMAX," International Symposium on Antennas and Propagation (ISAP 2012), POS2-3, pp.1039-1042, Nagoya, Japan, Nov. 2012.
4. T. Ito, M. Nagatoshi, S. Tanaka, and H. Morishita, "Fundamental characteristics of folded monopole antennas with parasitic element for triple

- band MIMO antenna,” The 29th International Review of Progress in Applied Computational Electromagnetics Society (ACES 2013), pp.599-603, Monterey, USA, Mar. 2013.
5. T. Ito, S. Tanaka, and H. Morishita, “Triple band MIMO antenna for WiMAX using electromagnetic simulator,” The 32nd JSST International Conference on Simulation Technology, OS4, Tokyo, Japan, Sept. 2013.
 6. T. Ito, M. Nagatoshi, S. Tanaka, and H. Morishita, “Fundamental characteristics of L-shaped and U-shaped folded monopole antennas with parasitic elements for WiMAX/MIMO antenna,” International Conference on Advanced Technology for Communications (ATC 2013), M2.5, pp.207-210, Ho Chi Minh, Vietnam, Oct. 2013.
 7. N. Kagiya, Y. Saita, T. Ito, and H. Morishita, “Fundamental characteristics of a combined folded dipole antenna with a feed line,” International Conference on Advanced Technology for Communications (ATC 2013), M1.2, pp.70-73, Ho Chi Minh, Vietnam, Oct. 2013.
 8. T. Ito, S. Tanaka, and H. Morishita, “Design and performance comparison of folded dipole antenna with feed line for mobile terminal,” The 30th International Review of Progress in Applied Computational Electromagnetics Society (ACES 2014), pp.134-138, Jacksonville, USA, Mar. 2014.
 9. Y. Saita, N. Kagiya, T. Ito, and H. Morishita, “Fundamental characteristics of a circular combined folded dipole antenna with a feed line,” Asian Workshop on Antennas and Propagation (AWAP 2014), POS1-7, Kanazawa, Japan, May 2014.
 10. T. Ito, T. Oki, Y. Nakagawa, T. Kimura, S. Tanaka, and H. Morishita, “Effect of nearby object on the characteristics of folded monopole antenna with parasitic element for WiMAX/WLAN applications,” IEEE Antennas and Propagation Society International Symposium (AP-S 2014), 228.9, pp.587-588, Memphis, USA, July 2014.
 11. Y. Saita, N. Kagiya, T. Ito, and H. Morishita, “Fundamental characteristics of a circular combined folded dipole antenna with a feed line,” IEEE Antennas and Propagation Society International Symposium (AP-S 2014), 327.8, pp.1011-1012, Memphis, USA, July 2014.

12. T. Ito, T. Oki, S. Tanaka, and H. Morishita, "Current reduction on the ground plane using additional element for WiMAX/WLAN folded monopole antenna," IEEE International Workshop on Electromagnetics; Applications and Student Innovation Competition (iWEM 2014), POS2.11, pp.153-154, Sapporo, Japan, Aug. 2014.
13. T. Ito, T. Oki, and H. Morishita, "Current reduction on the ground plane using quarter-wavelength element," International Symposium on Antennas and Propagation (ISAP 2014), Kaohsiung, Taiwan, Dec. 2014.
14. Y. Saita, T. Ito, N. Michishita, and H. Morishita, "Low-frequency inverted-F antenna on hemispherical ground plane," International Symposium on Antennas and Propagation (ISAP 2014), Kaohsiung, Taiwan, Dec. 2014.

Technical Reports and Other Conferences

1. M. Nagatoshi, T. Ito, M. Sakuma, and H. Morishita, "Application of a planar folded dipole antenna with a feed line to a small terminal for WiMAX," IEICE Technical Report, AP2011-76, pp.65-70, Osaka, Sept. 2011 (in Japanese).
2. T. Ito, M. Nagatoshi, and H. Morishita, "Study of planar folded dipole antenna with feed line for MIMO," IEICE General Conference, B-1-84, Okayama, Mar. 2012 (in Japanese).
3. T. Ito, M. Nagatoshi, S. Tanaka, and H. Morishita, "Characteristics of wideband folded dipole antenna with feed line for mounting to small terminal," IEICE Technical Report, AP2012-43, pp.75-80, Sapporo, July 2012 (in Japanese).
4. T. Ito, H. Ohara, N. Kagiya, S. Tanaka, and H. Morishita, "Study on folded dipole antenna with feed line for lower profile configuration," IEICE Society Conference, B-1-156, Toyama, Sept. 2012 (in Japanese).
5. N. Kagiya, T. Nakao, T. Ito, and H. Morishita, "Fundamental characteristics of a combined folded dipole antenna with a feed line," IEICE Society Conference, B-1-152, Toyama, Sept. 2012 (in Japanese).
6. N. Kagiya, T. Ito, H. Morishita, M. Ameya, M. Hirose, and S. Kurokawa, "Radiation characteristics of the helmet antenna (150MHz/2.4GHz) for disaster prevention," IEICE Technical Report, AMT2012-7, pp.1-6, Naha, Dec. 2012 (in Japanese).

7. T. Nakao, T. Ito, N. Kagiyaama, and H. Morishita, "Study on the helmet antenna for disaster," IEICE Technical Report, AP2012-134, pp.69-74, Miyazaki, Jan. 2013 (in Japanese).
8. T. Ito, M. Nagatoshi, S. Tanaka, and H. Morishita, "Fundamental characteristics of folded monopole antennas with parasitic elements for triple band MIMO antenna," IEICE General Conference, B-1-185, Gifu, Mar. 2013 (in Japanese).
9. N. Kagiyaama, T. Ito, and H. Morishita, "Fundamental study on the helmet antenna (150MHz/2.4GHz) for disaster prevention," IEICE General Conference, B-1-105, Gifu, Mar. 2013 (in Japanese).
10. N. Kagiyaama, Y. Saita, T. Ito, and H. Morishita, "Fundamental study of the helmet antenna for disaster prevention (2)," Technical Report of Japan Society of Simulation Technology, JSST-MDMC2013-1-05, pp.26-31, Tokyo, June 2013 (in Japanese).
11. N. Kagiyaama, Y. Saita, T. Ito, and H. Morishita, "Fundamental study of the helmet antenna for disaster prevention," ITE Technical Report, BCT2013-74, vol.37, no.34, pp.29-32, Otaru, July 2013 (in Japanese).
12. T. Ito, N. Michishita, S. Tanaka, and H. Morishita, "Left-handed folded dipole antenna," IEICE Society Conference, B-1-111, Fukuoka, Sept. 2013 (in Japanese).
13. N. Kagiyaama, Y. Saita, T. Ito, and H. Morishita, "Study on the helmet antenna (150MHz/2.4GHz) for disaster prevention," IEICE Society Conference, B-1-153, Fukuoka, Sept. 2013 (in Japanese).
14. Y. Saita, N. Kagiyaama, T. Ito, and H. Morishita, "A study on radiation restraint from helmet antenna to the human head direction," IEICE Society Conference, B-1-187, Fukuoka, Sept. 2013 (in Japanese).
15. N. Kagiyaama, Y. Saita, T. Ito, H. Morishita, M. Ameya, M. Hirose, and S. Kurokawa, "Study of the helmet antenna (150MHz/2.4GHz) for disaster prevention," IEICE Technical Report, AMT2013-14, pp.12-17, Ishigaki, Dec. 2013 (in Japanese).
16. T. Ito, S. Tanaka, and H. Morishita, "Folded dipole antenna with feed line for communication application of small terminal," ITE Technical Report,

- BCT2014-13, vol.38, no.5, pp.49-52, Nagasaki, Jan. 2014 (in Japanese).
17. N. Kagiya, Y. Saita, T. Ito, and H. Morishita, "Fundamental study of the two resonances helmet antenna for disaster prevention," ITE Technical Report, BCT2014-12, vol.38, no.5, pp.45-48, Nagasaki, Jan. 2014 (in Japanese).
 18. T. Ito, Y. Nakagawa, T. Kimura, S. Tanaka, and H. Morishita, "Characteristic change of folded monopole antenna with parasitic elements by nearby object," IEICE General Conference, B-1-180, Niigata, Mar. 2014 (in Japanese).
 19. Y. Saita, N. Kagiya, T. Ito, and H. Morishita, "A study on radiation restraint from helmet antenna to the human head direction (2)," IEICE General Conference, B-1-178, Niigata, Mar. 2014 (in Japanese).
 20. H. Morishita, and T. Ito, "Wide bandwidth of antennas with folded structure," IEICE Technical Report, AP2014-18, pp.95-100, Kyoto, April 2014 (in Japanese).
 21. T. Ito, T. Oki, Y. Nakagawa, S. Tanaka T. Kimura, K. Shirasu, and H. Morishita, "Current reduction on the ground plane using quarter-wavelength element," IEICE Society Conference, B-1-80, Tokushima, Sept. 2014 (in Japanese).
 22. Y. Saita, T. Ito, N. Michishita, and H. Morishita, "Low-frequency inverted-F antenna on hemispherical ground plane," IEICE Society Conference, B-1-81, Tokushima, Sept. 2014 (in Japanese).
 23. S. Tanaka, Y. Nakagawa, T. Kimura, K. Shirasu, T. Ito, T. Oki, and H. Morishita, "A fundamental study on metal insensitive antenna (1): UFMA with higher impedance," IEICE Society Conference, B-1-29, Tokushima, Sept. 2014 (in Japanese).
 24. Y. Nakagawa, S. Tanaka, T. Kimura, K. Shirasu, T. Ito, T. Oki, and H. Morishita, "A fundamental study on metal insensitive antenna (2): WIFA with higher impedance," IEICE Society Conference, B-1-30, Tokushima, Sept. 2014 (in Japanese).
 25. Y. Saita, T. Ito, N. Michishita, H. Morishita, M. Ameya, M. Hirose, and S. Kurokawa, "A study of low-frequency inverted-F antenna on hemispherical ground plane," IEICE Technical Report, AMT2014-13, pp.7-12, Miyakojima, Dec. 2014 (in Japanese).

26. Y. Nakagawa, T. Toba, S. Tanaka, T. Kimura, K. Shirasu, T. Ito, T. Oki, and H. Morishita, “A study on miniaturization of U-shaped folded monopole antenna,” IEICE General Conference, Mar. 2015 (in Japanese).

Awards

1. Traveling Expense Support of the Telecommunications Advancement Foundation (電気通信普及財団, 渡航旅費援助), Tokyo, Feb. 2013.
2. T. Ito, S. Tanaka, and H. Morishita, “Triple band MIMO antenna for WiMAX using electromagnetic simulator,” The 32nd JSST International Conference on Simulation Technology, Outstanding Presentation Award, Tokyo, Sept. 2013.
3. T. Ito, S. Tanaka, and H. Morishita, “Design and performance comparison of folded dipole antenna with feed line for mobile terminal,” The 30th International Review of Progress in Applied Computational Electromagnetics Society (ACES 2014), Honorable Mention of the Student Paper Competition, Jacksonville, USA, Mar. 2014.
4. N. Kagiya, Y. Saita, T. Ito, and H. Morishita, “Fundamental study of the two resonances helmet antenna for disaster prevention,” ITE Outstanding Presentation Award (優秀研究発表賞), Tokyo, Dec. 2014.

Other Research Activities

Internship

Centre de recherche des ecoles de Saint-Cyr Coetquidan (CREC), France, Sept. 3rd – Sept. 28th, 2012.

Technical Presentation

T. Ito, and H. Morishita, “小型端末用アンテナの設計事例,” Japan Altair Technology Conference, July 2014.